Evidence-Based Complementary and Alternative Medicine

Gut Microbiome and Chronic Diseases: Does a Natural Product-Rich Diet Matter?

Lead Guest Editor: Célia Cabral
Guest Editors: Flávio Reis, Claudia Carbone, Jose Boga, and Maria Rosaria Lauro

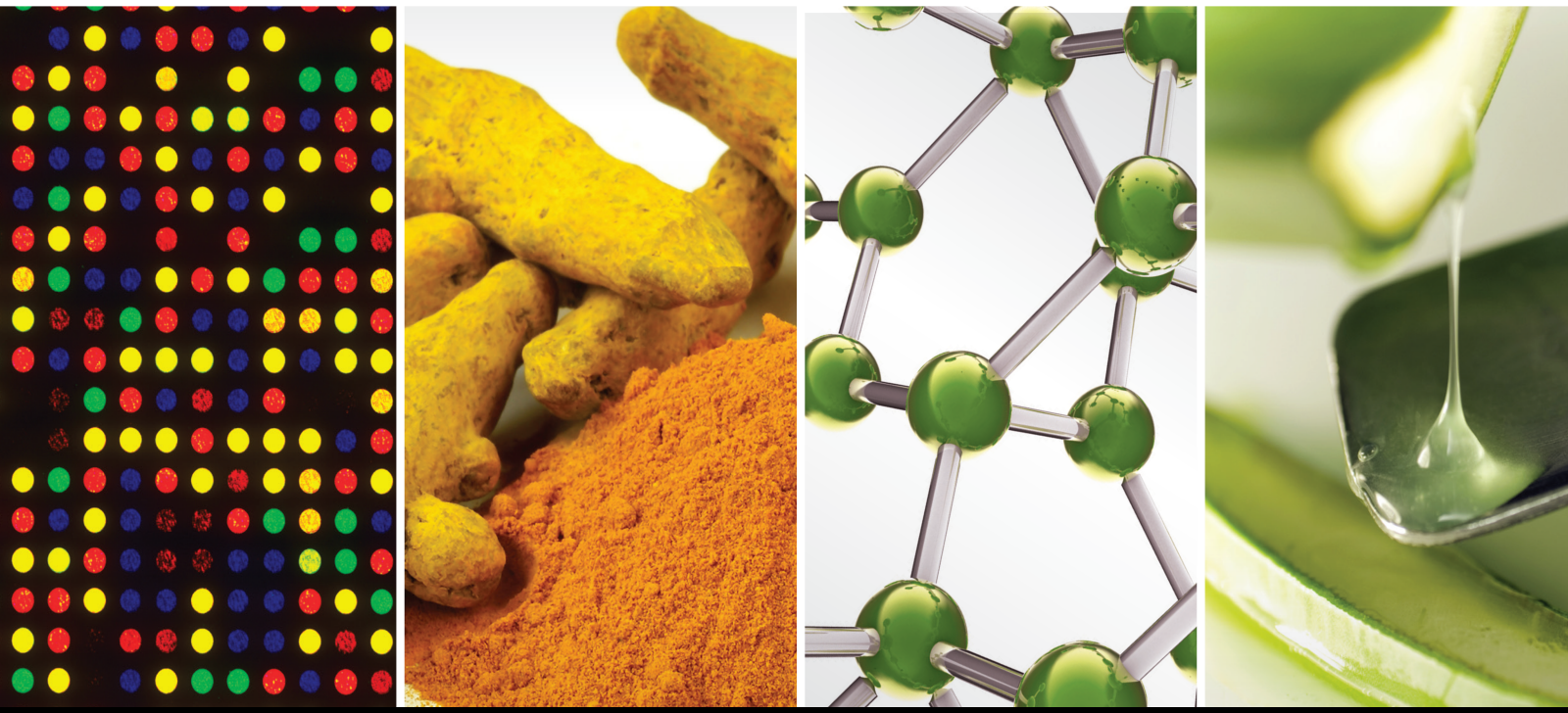

Gut Microbiome and Chronic Diseases: Does a Natural Product-Rich Diet Matter?

Evidence-Based Complementary and Alternative Medicine

Gut Microbiome and Chronic Diseases: Does a Natural Product-Rich Diet Matter?

Lead Guest Editor: Célia Cabral
Guest Editors: Flávio Reis, Claudia Carbone, Jose Boga, and Maria Rosaria Lauro

Chief Editor

Associate Editors

Academic Editors

Contents

Hindawi
Evidence-Based Complementary and Alternative Medicine
Volume 2019, Article ID 3907915, 16 pages
https://doi.org/10.1155/2019/3907915

Research Article

Design, Preparation, and Characterization of Dioscin Nanosuspensions and Evaluation of Their Protective Effect against Carbon Tetrachloride-Induced Acute Liver Injury in Mice

Hong-Ye JU, Kun-Xia Hu, Guo-Wang Zhao, Zhi-Shu Tang, and Xiao Song

School of Pharmacy, Shaanxi University of Chinese Medicine, Xianyang 712046, China

Correspondence should be addressed to Xiao Song; song-xiaoyao@163.com

Received 11 October 2018; Revised 20 December 2018; Accepted 17 July 2019; Published 14 November 2019

Guest Editor: Maria Rosaria Lauro

The purpose of this study was to prepare a dioscin nanosuspension (Dio-NS) that has a better distance and high solubility for oral administration and to evaluate its hepatoprotective effects. Optimal primary manufacture parameters, including shear time, shear speed, emulation temperature, pressure, and cycles of homogenization, were determined by single-factor experiments. The concentrations of dioscin, SDS, and soybean lecithin were optimized using the central composite design-response surface method, and their effects on the mean particle size (MPS) and particle size distribution of Dio-NS were investigated. Characterization of the Dio-NS formulations included examinations of the surface morphology and physical status of dioscin in Dio-NS, the stability of Dio-NS at different temperatures, *in vitro* solubility, and liver protective effect *in vivo*. Under optimal conditions, Dio-NS had an MPS of 106.72 nm, polydispersity index of 0.221, and zeta potential of −34.27 mV. Furthermore, the proportion of dioscin in Dio-NS was approximately 21.26%. The observation of particles with a spherical shape and the disappearance of crystalline peaks indicated that the physical and chemical properties of Dio-NS were altered. Furthermore, we observed that the dissolution of Dio-NS was superior to that of a physical mixture and Dio-GZF. Moreover, Dio-NS was demonstrated to have a protective effect against CCl_4-induced acute liver damage in mice that was equivalent to that of silymarin (a positive control drug) at the same dose. The good hepatoprotective effect of our Dio-NS preparation can provide a theoretical basis for investigating its absorption mechanisms in the body.

1. Introduction

Dioscin (Figure 1), also known as *Paris polyphylla* saponin III, is a steroidal saponin [1]that can be extracted from the Chinese yam (*Dioscorea paniculata*) and other plants in the Dioscoreaceae family [2]. Dioscin has several important pharmacological activities, including antitumor [3], anti-inflammatory [4], antiliver damnification [5], antihepatic fibrosis [6, 7], antihyperlipidemic, and antioxidative properties. Furthermore, the compound has therapeutic potential in metabolic diseases and can also be decomposed into diosgenin, which has been an important basic raw material for the production of steroid hormone drugs [8].Meanwhile, it has also been established that there is potential to develop the pharmaceutic value of dioscin. In addition, some reports have been found on dioscin toxicology. It has no adverse effect on the acute toxicological studies at a dose of 562.5 mg/kg/d in mice [9, 10]. However, on the subchronic toxicological assessment, it was verified as the NOAEL (no-observed-adverse-effect level) at a dose of 300 mg/kg/day in female rats and in male rats was marked as the LOAEL (lowest-observed-adverse-effect level) at the same dose [11]. So, rational drug use is the key to lower ADR.

In fact, dioscin has a notable disadvantage, in that when the valid route fails, the probability of a new established route occurring via secondary chain scission is large. Its poor solubility and slow dissolution rate limit its absorption, thus affecting its efficacy.

Poor solubilities and dissolution rates are key factors affecting the absorption of drugs in the body. Thus, several techniques have been devised in order to overcome these undesirable properties, including micronization [12],

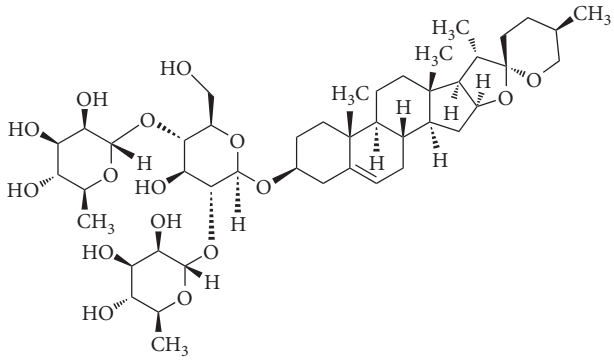

Figure 1: The chemical structure of dioscin.

solubilization, and salt formation [13]. However, these techniques are only partially effective. The advent of nanotechnology, which can produce nanoscale particles with novel functional properties, offers a potential solution to the aforementioned drawbacks. Nanotechnology has, for example, been used to enhance the bioavailability of certain antibiotics [14] and has also been applied to produce different targeted drugs for the treatment of different diseases [15–17], and various nanosuspensions have been successfully applied [18, 19]. Nanoparticles can also be prepared using a variety of different processes, including reverse solvent, homogenization pressure, milling, and the production of self-nanoemulsifying self-nanosuspensions [20].

Diseases of the liver, including hepatitis, hepatapostema, hepatocirrhosis, and liver cancer, are common and often life-threatening. Carbon tetrachloride (CCl_4) [21, 22], paracetamol [23, 24], lipopolysaccharide [25, 26], and certain other chemicals can also cause acute liver damage, and consequently, a large number of drugs are used for the treatment of hepatic disorders [27]. It was confirmed that dioscin has significant hepatoprotective effect against CCl4-induced liver injury in mice, and the cellular mechanisms of this effect are likely to be associated with inhibition of lipid peroxidation, inflammatory cytokines, necrosis, and apoptosis. Thus, in the present study, we formulated a dioscin nanosuspension (Dio-NS) using reverse solvent precipitation combined with high-pressure homogenization and compared its efficacy with that of the commercial drug silymarin in protecting mice from acute hepatic damage induced by CCl_4. We assumed that the Dio-NS formulation would enhance the solubility of dioscin and thus increase the efficacy of this compound in protecting against liver injury.

2. Methods

2.1. Materials. Dioscin was purchased from Nanjing Spring and Autumn Biological Engineering (Nanjing, China) with the purity of >99%. Soybean lecithin, mannitol, poloxamer-188, Tween-80, PVP K30, sodium cholate, sodium alkyl sulfate twelve (SDS), anhydrous ethanol, lactose, glucose, sucrose, D-sorbitol, silymarin, 4% paraformaldehyde solution, methanol, and acetonitrile were all of chromatographic grade, and the other reagents were all of analytical grade. AST and ALT kits were purchased from Nanjing Jiancheng Institute of Biotechnology (Nanjing, China). TNF-α, IL-1β, IL-6, MDA, SOD, and GSH-Px kits were purchased from Shanghai Elisa Biotech Co., Ltd.

2.2. Preparation of Dio-NS. Dioscin was dissolved in ethanol as a solvent and dispersed for 15 min in a KQ-3-DE ultrasonic bath (Kunshan, China). In the next emulsification process, ethanol was used as the organic phase of the emulsion. The solution was rapidly added dropwise to double-distilled water-saturated ethanol together with sodium alkyl sulfate twelve and soybean lecithin as excipients that can be used to improve the stability of emulsions, commixing using magnetic stirrer (HJ-6B, Changzhou, China). A microemulsion was obtained by high-speed shearing (FJ-200, ShenZhen, China). The microemulsion preparation was then homogenized to produce a nanoemulsion via high-pressure homogenization (AH-BASICI, ATS Engineering Inc., Canada). An EYELA N-1300 rotary evaporator was used to remove the ethanol (LangYi, Shanghai, China) at an evaporation temperature of 40°C, thereby yielding the Dio-NS preparation. In this study, the optimal process conditions were determined on the basis of single-factor experimental results. All the preparation steps are shown in Figure 2.

2.3. Preparation of a Physical Mixture. The desired dosage of Dio-NS was obtained by dissolving in water and freeze-drying for 12 h to yield an NS-A physical mixture.

2.4. Screening of Excipients. Eleven groups were examined to select the best accessories that have a minimum size and powder dispersion index.

2.5. Single-Factor Experiment. In the single-factor experiment, particle size and multiple dispersion index were taken as indicators to determine optimal preparation parameters, including shear time, shear speed, emulation temperature, pressure, and cycles of homogenization.

2.6. Optimization of the Response Surface of the Star Design. On the basis of the results of the single-factor experiment and the feasibility of preparing nanosuspensions at the highest or lowest level, we selected the level of each factor and the star response surface design software and determined the best experimental results.

2.7. Lyophilization. The Dio-NS preparation was lyophilized using a VaCo-5 freeze-drying apparatus (Zirbus, Germany) to obtain dry powder with good physicochemical stability. In this study, a single-factor method was used to select optimal conditions, and the best freeze-drying protectant was selected. The results are shown in Table 1. The content of freeze-drying protectant ranged from 2% to 10%. The levels are shown in Table 2.

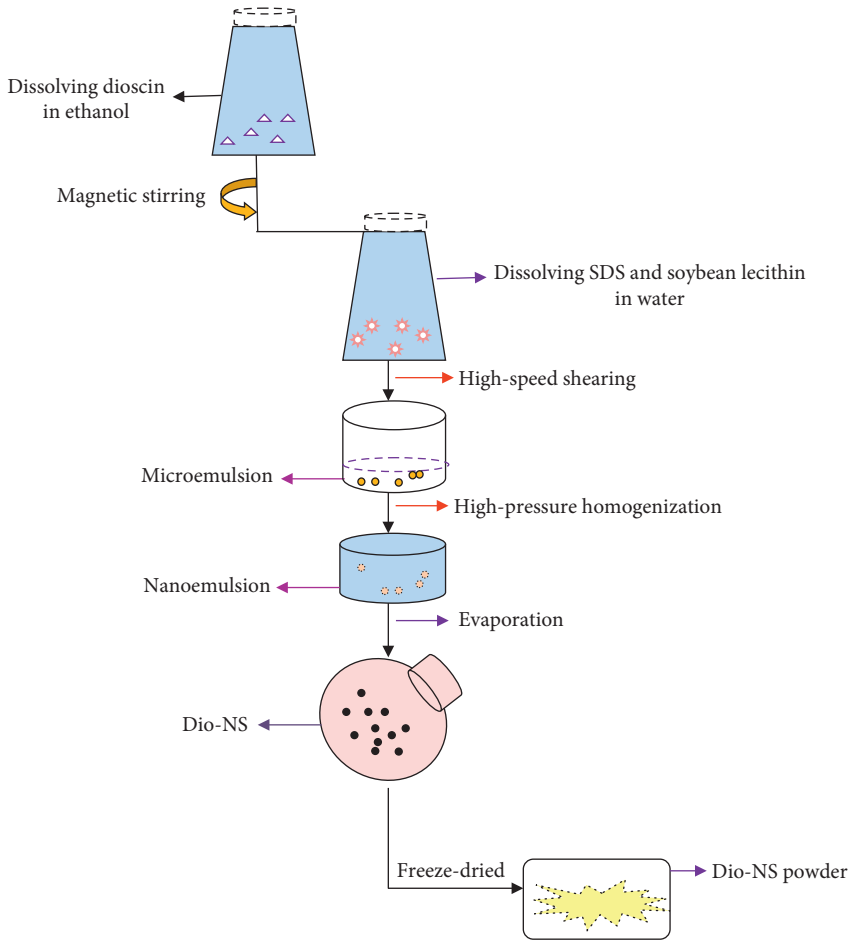

Figure 2: A flow diagram showing the steps involved in the preparation of Dio-NS.

Table 1: Screening of freeze-drying protectants.

Type	Sensory evaluation	Size (nm)	PDI	Zeta (mv)
Lactose	White powder: shows collapse and shrinkage, uneven color, and poor dispersion.	123.5 ± 0.61	0.278 ± 0.003	−23.2 ± 2.25
Glucose	White powder: shows collapse and shrinkage, uneven color, and poor dispersion	2200 ± 521.85	1 ± 0.001	−42.3 ± 1.86
Sucrose	White powder: shows collapse and shrinkage, uneven color, and poor dispersion.	1195.7 ± 382.27	0.586 ± 0.075	−51.4 ± 5.41
D-sorbitol	White powder: shows collapse and shrinkage, uneven color, and poor dispersion.	172.4 ± 6.99	0.271 ± 0.023	−52.6 ± 2.68
Mannitol	White powder: shows no collapse or shrinkage, uniform color, and good dispersion.	223 ± 1.56	0.273 ± 0.055	−59.1 ± 0.38

($n = 3$, Mean ± SEM).

2.8. Particle Size and Zeta Potential. The mean particle size (MPS), particle size distribution (PSD), and zeta potential of the formulation were determined using a Malvern particle size meter. Samples were prepared by dissolution of Dio-NS in deionized water, and each property was measured 3 times.

2.9. Morphological Observations (SEM). The morphology of particles was determined by scanning electron microscopy (SEM) (MERLIN Compact, German). Samples were affixed to aluminum stubs using a double-sided carbon tape and sputter-coated with gold under an argon atmosphere.

2.10. Transmission Electron Microscopy (TEM). After 4 types of samples had been vortexed for 2 min, they were dripped onto a copper sheet of a transmission electron microscope (JEOL, Japan), and the excess moisture was dried using a filter paper. Images of the samples were observed on the perspective electron microscope.

2.11. X-Ray Powder Diffraction. The crystalline state of substances was typically determined by X-ray powder diffraction. Diffraction patterns of the Dio-NS and other auxiliary material were determined using a Bruker D8

Table 2: Screening for the dosage of freeze-drying protectants.

Ratio (%)	Size (nm)	PDI	Zeta (mv)
	433.4	0.620	−40.8
2	463.2	0.553	−41.8
	441.3	0.540	−42.8
	229.2	0.391	−53.4
3	231.6	0.402	−58.5
	229.5	0.416	−57.4
	196.4	0.285	−35.3
5	194.8	0.275	−36.9
	194.9	0.285	−36.2
	173.8	0.234	−53.6
7	173.1	0.245	−57.3
	172.7	0.239	−58.0
	187.4	0.223	−58.0
8	182.6	0.245	−57.1
	184.3	0.248	−56.0
	205.5	0.242	−53.9
10	201.6	0.263	−54.2
	207.1	0.272	−56.3

advance X-ray diffractometer (Bruker, Germany). A Cu line was used as the source of radiation, and standard runs were performed at a voltage of 40 kV, step length of 0.01°, current of 40 mA, and a scanning rate of 0.1 s/step over a 2 theta range of 5–90°.

2.12. Thermal Analysis. Individual samples were placed in different aluminum differential scanning calorimeter (DSC) pans (214 Polyma, Netzsch, Germany), which were heated to 200°C and 150°C for approximately 15 min. Thereafter, the samples were quench-cooled in liquid nitrogen externally to the DSC instrument. DSC was implemented by returning the samples to a prerefrigerating room (−50°C), and thermograms were recorded.

2.13. In Vitro Dissolution of Dio-NS. The Dio-NS powder and physical mixture were loaded into dialysis membranes, which were placed in constant-speed oscillators at constant temperature and oscillated for different times. Samples of Dio-NS obtained at different time points were analyzed by HPLC (Waters e2695, USA). The cumulative release rate was determined using the following equation:

$$Q\%\,(\text{cumulative release rate}) = \frac{(Qt_1 + Qt_2 + \cdots + Qt_n)}{Q} \times 100\%, \quad (1)$$

where Qt_1,Qt_2,. . .,Qt_n is the content of dioscin dissolved in Dio-NS between time t_0 and $t_{1,2,\ldots,n}$.

2.14. Stability Study. The stability of the dioscin nanoscale suspension at temperatures of 4°C and 25°C was investigated over a period of 1 month, and the results are shown in Table 3.

Table 3: Stability of Dio-NS freeze-dried powder over a period of 2 months ($n = 3$).

Time (d)	Size (nm)	PDI	Zeta (mV)
0	173.2 ± 0.56	0.235 ± 0.01	−56.3 ± 2.36
15	173.7 ± 0.63	0.237 ± 0.21	−56.54 ± 2.66
30	173.9 ± 0.75	0.237 ± 0.56	−56.73 ± 2.86
60	174.9 ± 0.85	0.239 ± 0.46	−63.43 ± 1.26

2.15. The Effects of Dio-NS on Liver Preservation

2.15.1. Animals and Treatment. Kunming male mice (18–22 g) were purchased from Chengdu Dashuo Biotechnology Co., Ltd. (Chendu, China.). The mice were acclimated for 1 week in a controlled environment at 25 ± 2°C under a 12 h dark/light photoperiod. They were subsequently randomly divided into the following 6 groups each containing 8 animals: group 1 (normal control) and group 2 (model control) were orally administered water for 7 days; group 3 (positive control) received silymarin (50 mg/kg) for 7 days; and groups 4 to 6 (low-, medium-, and high-dose groups, respectively) were administered Dio-NS (25, 50, and 100 mg/kg, respectively) intragastrically. Two hours after the final administration, the animals in group 1 were injected intraperitoneally with pure olive oil, whereas mice in the other groups were treated with 0.2% (v/v) CCl_4 (10 mL/kg body weight, i.p.; dissolved in olive oil) [28]. Thereafter, the mice were maintained with free access to water and were sacrificed 24 h later, at which time blood was collected for the preparation of serum. After killing the animals, the livers were immediately isolated and weighed to determine the liver index (liver index = liver weight/body weight × 100%). A portion of each liver was fixed in 4% paraformaldehyde solution for pathological study, and the remainder along with the acquired serum samples were stored at −80°C for subsequent studies. The entire process was performed on ice.

2.15.2. Serum Biochemistry Assays. The activities of ALT, AST, TNF-α, IL-1β, and IL-6 in the serum were measured using commercial kits following the manufacturer's instructions.

2.15.3. Liver Lipid Peroxidation Assay. After saline was added to the appropriate liver tissue, the sample was placed into an automated tissue homogenizer (SCIENTZ-48, Ningbo, China) to prepare a 10% hepatic homogenate. Samples were processed using commercial kits according the manufacturer's instructions, and the levels of MDA, GSH-Px, and SOD in the liver homogenate were evaluated using a microplate reader.

2.15.4. Histopathological Examination. Fixed liver tissues were embedded in paraffin, from which 5-μm sections were cut and placed on slides. The samples were stained with hematoxylin and eosin (H&E) and then observed at ×400 magnification.

2.15.5. Statistical Analysis. SPSS version 19.0 statistical software was used to analyze all the data using a one-way ANOVA. Data are represented as mean ± S.E.M. Differences between groups were considered significant at $p < 0.01$ and $p < 0.05$ levels.

3. Results

3.1. Evaluation of the Dio-NS Preparation. The results of stabilizer screening showed that different stabilizers had a considerable influence on the average particle size, polydispersity index, and system storage stability of drug suspensions [29](Table 4). On the premise of maintaining the same total amount, the combined use of different types of stabilizers effectively reduced the 3 qualitative indexes of drug suspension. In this study, we found that when the combined application of soybean lecithin and SDS was used as a stabilizer for the suspension system, the average size of the drug particles was small, the distribution was narrow, and the physical stability of the system was good. Therefore, we used soybean lecithin and SDS as stabilizers for Dio-NS. An SDS : lecithin ratio of 1 : 1 proved to be the optimal combination.

As shown in Figure 3, it is clear that temperature has little effect on emulsification. We also established that the minimum particle size and polydispersity index are obtained under the following conditions: a shear speed of 19,500 rpm, a shear time of 2 min, a homogeneous pressure of 800 bar, and 7 cycles of homogenization. We thus obtained the optimal operation parameters (Table 5). Table 6 shows the results of 20-run experiments designed on the basis of 3 factors and 4 levels using Design-Expert 8.0.6 software. The results of a regression analysis are shown in equations (2) and (3):

$$\begin{aligned} Y &= +0.66 - 0.095A - 0.023B - 0.065C + 0.10AB - 0.033AC \\ &\quad + 2.375E - 003BC - 0.13A^2 + 0.030B^2 + 0.047C^2, \\ R &= 0.9411, P < 0.0001. \end{aligned} \tag{2}$$

$\mathrm{OD} = (d1, d2, \ldots, dk)1^K$, where K is the number of indices.

$$\begin{aligned} d_{\min} &= (Y_{\max} - Y_i)(Y_{\max} - Y_{\min}), \\ d_{\max} &= (Y_i - Y_{\min})(Y_{\max} - Y_{\min}). \end{aligned} \tag{3}$$

Figure 4 shows the results of the interaction between 2 groups. For Dio-NS preparation with a content of 26.67% (w/w) dioscin, 20% (w/w) SDS, and 53.33% (w/w) soybean lecithin, we obtained a maximum OD of 0.868, which was close to that predicted. As shown in Table 1, the diameter of Dio-NS dry powder particles, polydispersity index, and zeta potential were less than those obtained using other freeze-drying protection agents. Furthermore, the powder showed no collapse or shrinkage, the color and luster were more uniform, and the preparation had good dispersion, and therefore, soybean lecithin and SDS were selected as the protectants for the dioscin freeze-dried powder.

It can be seen from Table 2 that the particle size obtained using mannitol in the aqueous phase was 7%, and values for the polydispersity index and the zeta potential were the smallest recorded.

The size, zeta potential, and polydispersity index of the Dio-NS formulations are shown in Table 7. A particle size diagram and zeta potential are shown in Figures 5(a) and 5(b), respectively. A sharp peak of Dio-NS, which represents its size, was identified at approximately 106.72 ± 8.90. Furthermore, the zeta potential of Dio-NS was −34.27 ± 2.91 mV, indicating the reasonable stability of the preparation.

3.2. Characterization of Dio-NS

3.2.1. Particle Size and Zeta Potential. The particle size and zeta potential of the optimum Dio-NS are given in Table 7.

3.2.2. Surface Morphology and Particle Size of Dio-NS. Transmission and scanning electron microscopy were applied to analyze the morphology and structure of the Dio-NS formulations. Dioscin has a tubular crystal structure (Figure 6(a)). Figure 6 shows that Dio-NS has a near-spheroid particle structure with a particle size of approximately 106 nm. Figure 6(b) shows that the redispersibility of Dio-NS powder in purified water was also nearly globoid and that the particle size is somewhat larger at approximately 173 nm.

The scanning electron microscopy images shown in Figure 7 show that dioscin raw material (A) is acicular with a larger particle size, whereas that with mannitol B is an irregular prism, that with soybean lecithin (C) shows irregular lumps, and that with twelve alkyl sodium sulfate (D) is irregular spherical and loose with pores. Dio-NS nanoparticles (E) show the same shape as seen under transmission electron microscopy, and the morphology changes. As described above, these features indicate that the freeze-drying process has significant effect on particle size [30].

3.2.3. Physical Status of Dioscin in the Dio-NS. DSC thermograms of pure dioscin, SDS, soybean lecithin, mannitol, physical mixture, and freeze-dried and dry powder of Dio-NS are shown in Figure 8. The DSC thermograms of raw dioscin, mannitol, and SDS show a sharp endothermic peak at approximately 294–296°C, 166°C, and 204–207°C, respectively. A peak similar to that of pure dioscin was also observed in the thermogram of the physical mixture, indicating a weak or negligible influence. However, this peak was not present in the freeze-dried and dry Dio-NS preparations, which indicates that dioscin occurs in an amorphous form in Dio-NS.

The diffraction intensity and distribution of each crystal will have a special rule [31]. By using X-ray diffraction, we can analyze whether the crystalline form has changed in the preparation process. The diffraction peak of dioscin raw powder shown in Figure 9 indicates that it has a strong crystalline structure, whereas the diffraction peak of the excipient soybean lecithin indicates that its structure is essentially amorphous. The peaks of dioscin in the physical

Table 4: Screening of stabilizers.

Type	Content	MPS	PDI	Macrostability of the system
F-68	0.5%	145.17	0.227	The suspension is white and opaque, producing flocculent precipitates and deepening the color of the system.
SDS	0.5%	125.47	0.196	The suspension is white and opaque and easy to precipitate. It can be dispersed into an original emulsion.
PVP K30	0.5%	91	0.301	The suspension is white and opaque, and it produces microprecipitates, which can be dispersed into an original emulsion.
Tween-80	0.5%	108.8	0.316	The suspension is white and opaque. It is easy to precipitate. It cannot be dispersed into an original emulsion.
Soybean lecithin	0.5%	201	0.269	The suspension is white and opaque, and it produces microprecipitates, which can be dispersed into an original emulsion.
Sodium cholate	0.5%	89.43	0.298	The suspension is white and opaque. It is easy to precipitate. It cannot be dispersed into an original emulsion.
F-68 + SDS	0.25% + 0.25%	175.23	0.294	The suspension is white and opaque, and it produces microprecipitates, which can be dispersed into an original emulsion.
PVP K30 + SDS	0.25% + 0.25%	128.57	0.265	The suspension is white and opaque, and it produces microprecipitates, which can be dispersed into an original emulsion.
Tween + SDS	0.25% + 0.25%	160.5	0.530	The suspension is white and opaque, producing flocculent precipitates and deepening the color of the system.
Lecithin + SDS	0.25% + 0.25%	99.84	0.228	The suspension is white and opaque, and it produces microprecipitates, which can be dispersed into an original emulsion.
F-68 + PVP K30	0.25% + 0.25%	124.2	0.247	The suspension is white and opaque, and it produces microprecipitates, which can be dispersed into an original emulsion.

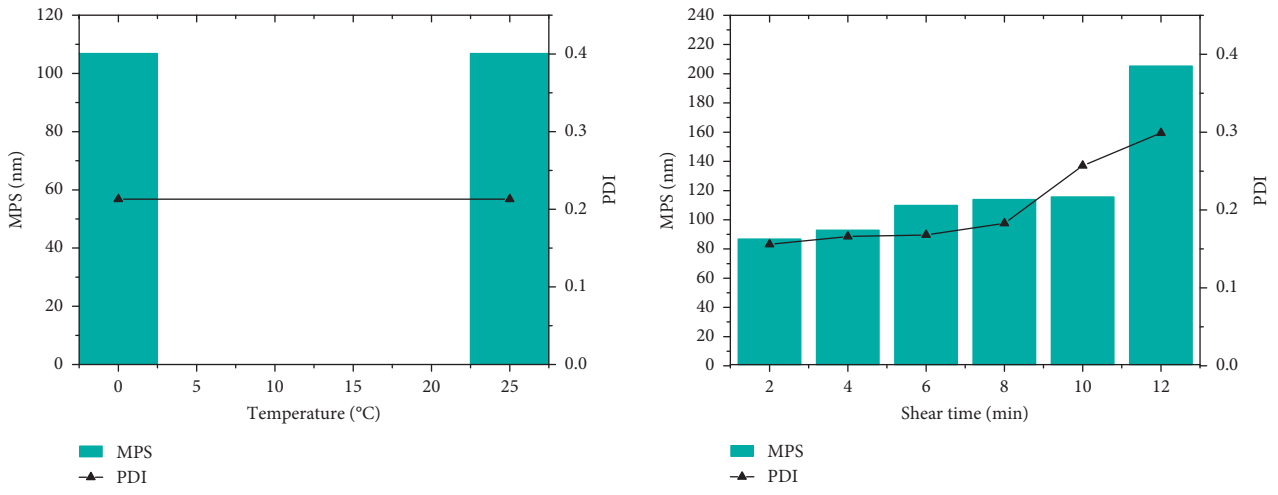

(a) (b)

Figure 3: Continued.

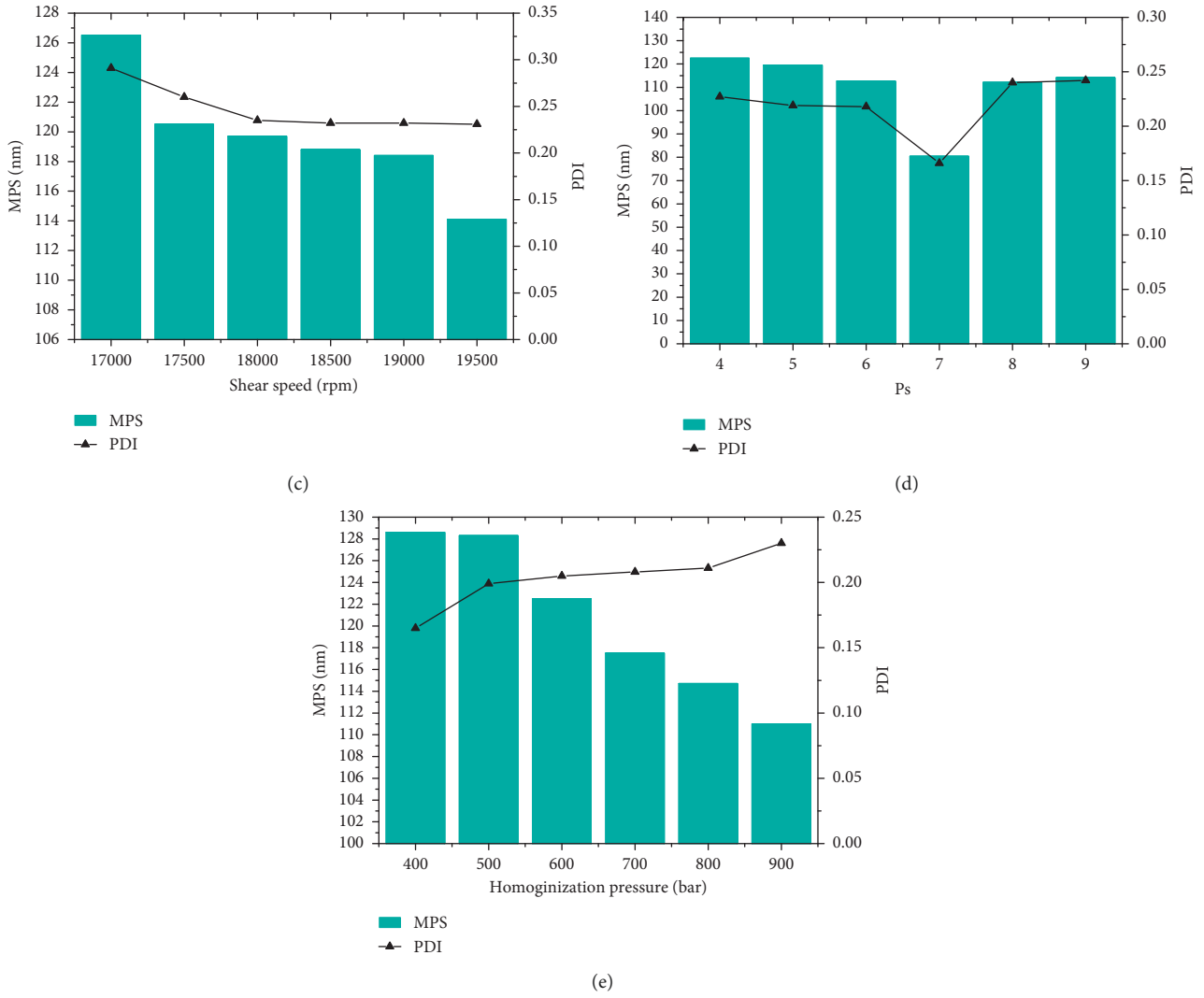

Figure 3: The influences of temperature (a), number of homogenization cycles (b), shear speed (c), shear time (d), and homogenization pressure (e) on the particle size and polydispersity index of Dio-NS preparations.

Table 5: Variables and levels in the star design.

Variables	Levels				
	−1.68	−1	0	+1	+1.68
Dio (A)%	0.02	0.03	0.04	0.05	0.06
Sph (B)%	0.03	0.05	0.08	0.10	0.12
SDS (C)%	0.03	0.05	0.08	0.10	0.12

mixture and dry powder are both in the crystal form of the carrier. The structure did not change, and the crystalline peak of the drug in the Dio-NS freeze-dried powder essentially disappeared, indicating that the drug occurs in an amorphous state and the freeze-drying process has an effect on the crystalline structure of the drug.

3.2.4. In Vitro Dissolution and Stability. As shown in Figure 10, the dissolution rate of dioscin can be significantly improved after the preparation of nanosuspensions. In PBS (pH 7.4), the dissolution rate of Dio-NS during the initial 2 h was close to 30%, whereas the release rate at 12 h was close to 90%. The dissolution rate of the physical mixture group was slightly faster than that of the raw material group, which can be attributed to the solubilization effect of the twelve alkyl sulfate and soybean lecithin used in the formulation. However, the dissolution rate was considerably less than that of Dio-NS. It is suggested that the dissolution rate of nanosuspensions is not only caused by the solubilization of excipients but is also mainly due to the reduction of particle size after the formation of nanoscale suspensions.

Table 6: Response value of the formulation using a central composite design ($n = 3$).

Run	A	B	C	MPS	PDI	OD
1	0	0	0	97.98	0.250	0.661
2	+1	−1	+1	131.45	0.203	0.39
3	0	0	0	97.98	0.250	0.661
4	0	0	0	97.99	0.250	0.661
5	+1	+1	+1	104.9	0.267	0.55
6	−1	−1	−1	85.49	0.226	0.841
7	0	+1.68	0	96.9	0.25	0.67
8	−1	−1	+1	90.29	0.235	0.772
9	−1	+1	+1	106.4	0.27	0.53
10	+1	−1	−1	102.4	0.261	0.59
11	0	0	+1.68	98.23	0.253	0.65
12	0	0	0	97.98	0.250	0.661
13	0	0	0	97.98	0.250	0.661
14	+1.68	0	0	141.6	0.345	0
15	+1	+1	−1	92.93	0.24	0.74
16	−1.68	0	0	108.24	0.274	0.5
17	0	−1.68	0	91.56	0.239	0.75
18	0	0	0	98.97	0.250	0.661
19	0	0	−1.68	74.88	0.238	0.868
20	−1	+1	−1	101.57	0.263	0.59

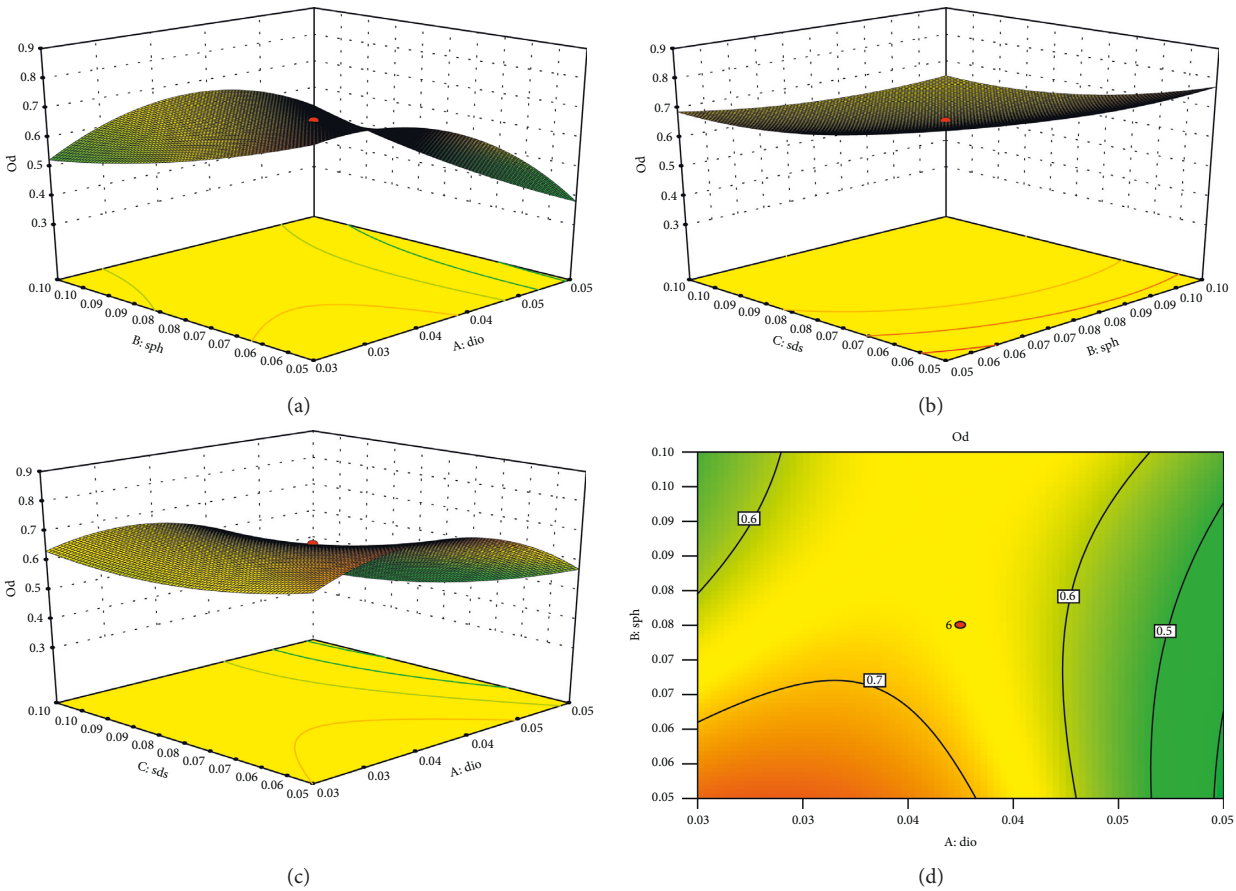

(a) (b) (c) (d)

Figure 4: Continued.

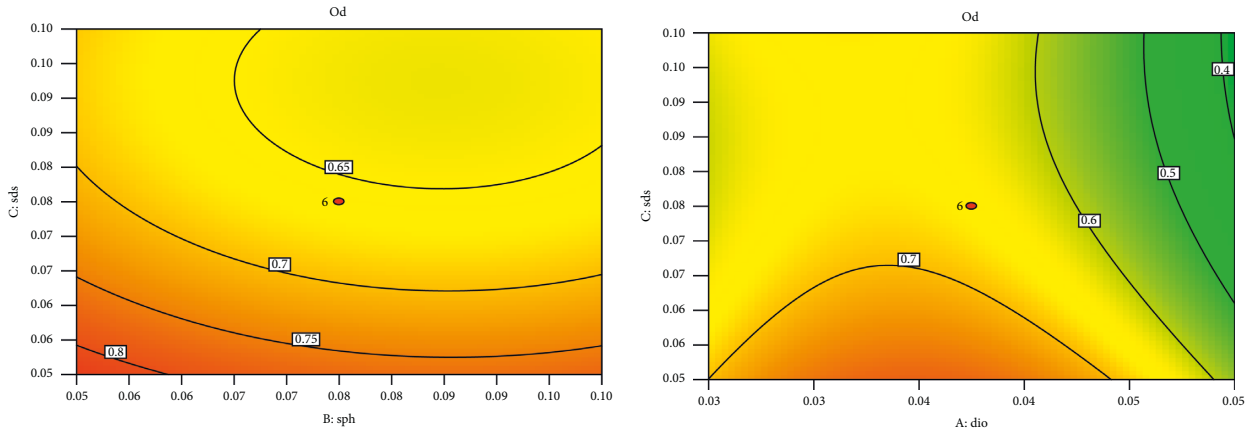

(e) (f)

Figure 4: The response surface model of the reciprocal action among the concentrations of dioscin% (A), soybean lecithin (B), and SDS (C) on OD.

Table 7: Particle size and zeta potential of the optimum Dio-NS ($n = 3$, $x \pm s$).

Batch no.	Particle size (nm)	PDI	ZP (mV)
VAL1001	106.5 ± 0.50	0.177 ± 0.02	−32.13 ± 2.35
VAL1002	115.73 ± 0.76	0.231 ± 0.002	−33.1 ± 5.26
VAL1003	97.93 ± 1.26	0.254 ± 0.02	−37.6 ± 2.53
Mean value	106.72 ± 8.90	0.221 ± 0.04	−34.27 ± 2.91

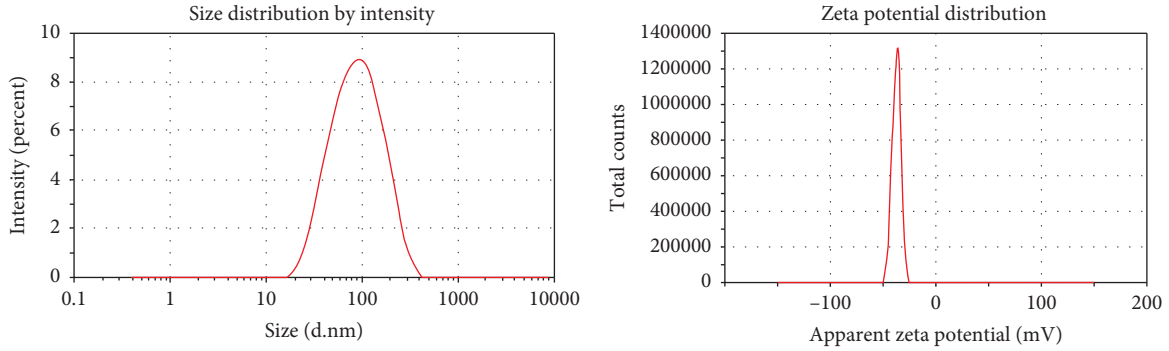

(a) (b)

Figure 5: Particle size and zeta potential distribution of Dio-NS formulations.

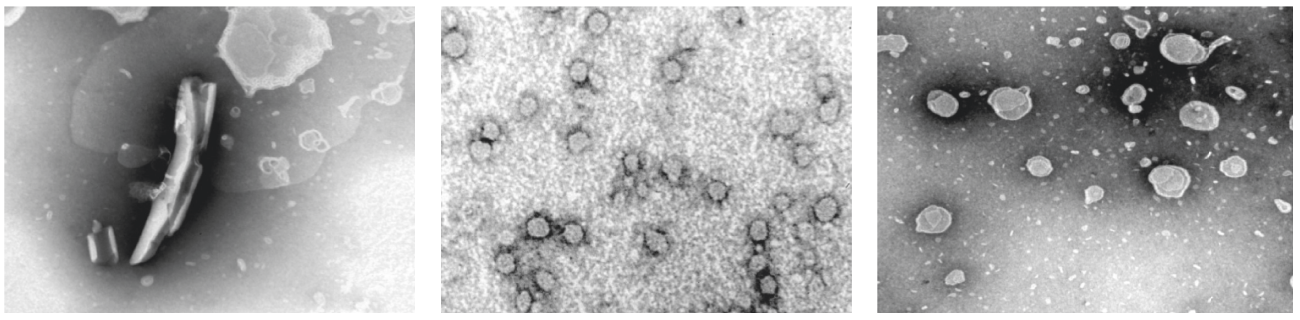

(a) (b) (c)

Figure 6: Transmission electron micrographs of samples dispersed in water. (a) Dioscin. (b) Dio-NS. (c) Dio-NS powder.

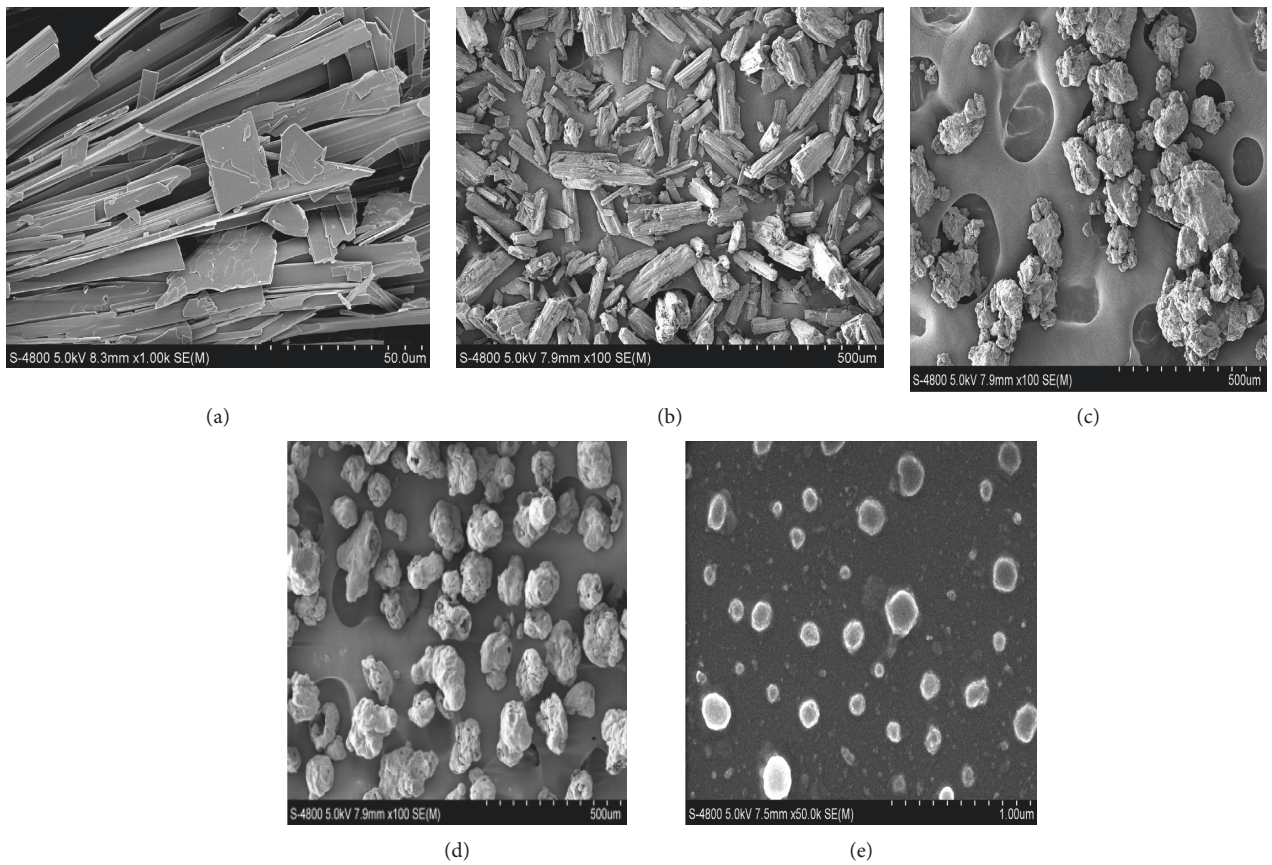

Figure 7: Scanning electron micrographs of (a) dioscin raw material, (b) with mannitol, (c) with soybean lecithin, (d) with twelve alkyl sulfates, and (e) Dio-NS lyophilized powder.

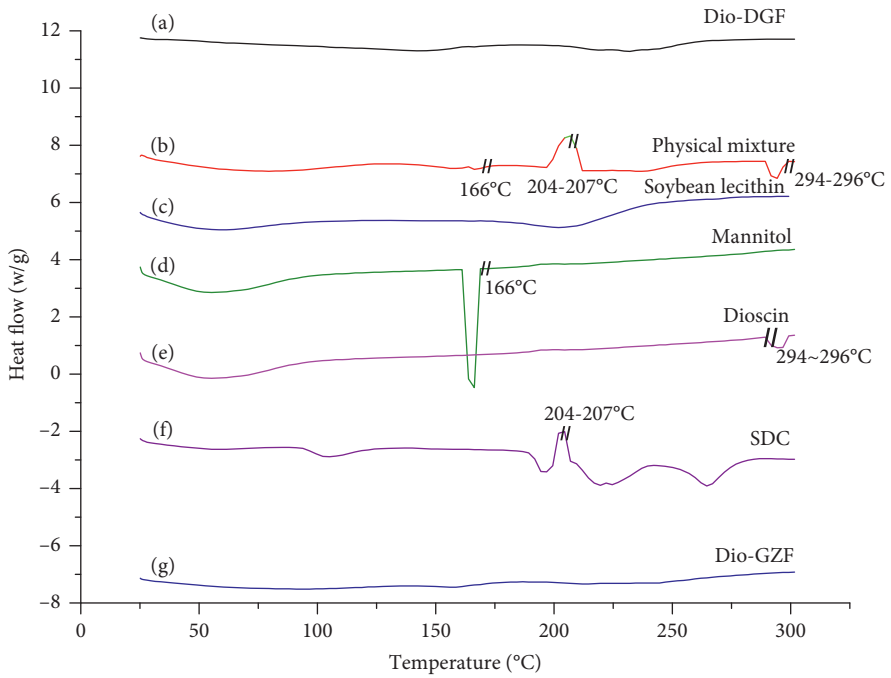

Figure 8: DSC patterns of freeze-dried Dio-NS (a), physical mixture (b), soybean lecithin (c), mannitol (d), raw dioscin (e), SDS (f), and dry Dio-NS (g).

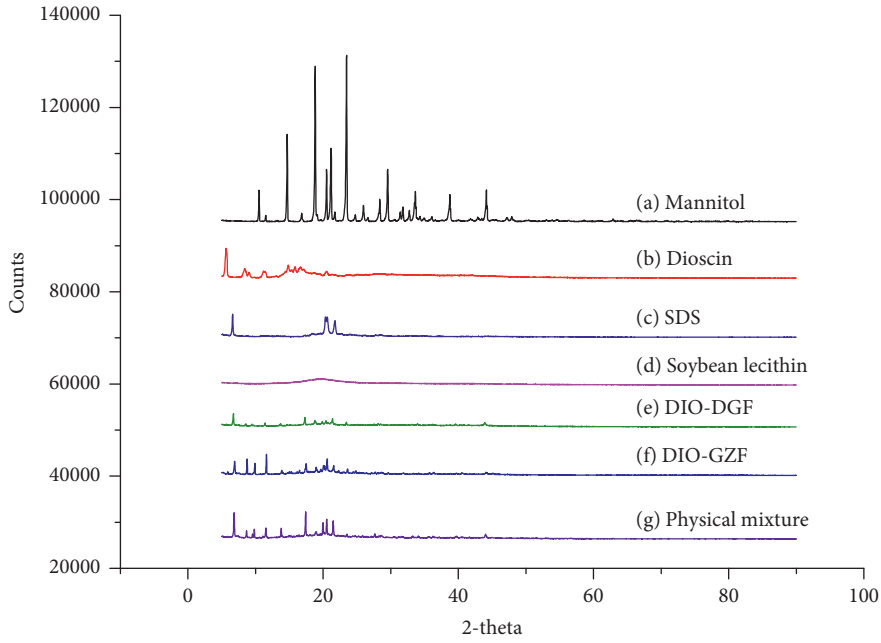

Figure 9: X-ray diffraction patterns of mannitol (a), raw dioscin (b), SDS (c), soybean lecithin (d), freeze-dried Dio-NS (e), dry Dio-NS (f), and physical mixture (g).

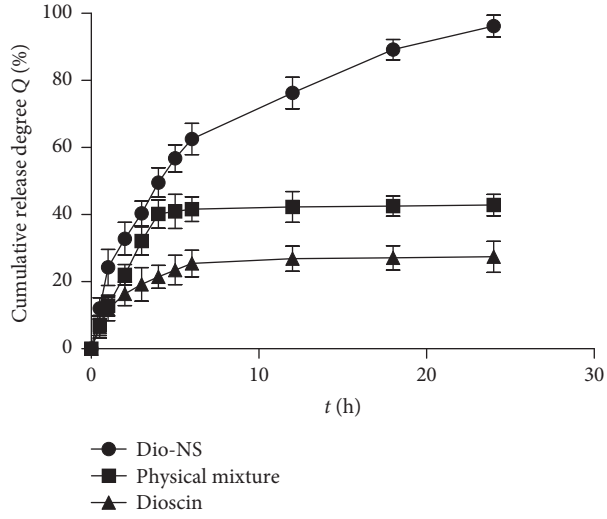

Figure 10: *In vitro* dissolution of dioscin nanosuspensions.

The results showed that although the non freeze-dried Dio-NS had poor stability at room temperature (Figures 11 and 12), the freeze-dried powder remained stable for 2 months (Table 3).

3.3. The Effects of Dio-NS on Liver Preservation

3.3.1. Serum Biochemistry and Hepatic Lipid Peroxidation Assays. In order to assess the influence of Dio-NS on CCl_4-induced liver damage, the activities of ALT, AST, TNF-α, IL-1β, and IL-6 in the serum were monitored (Figure 13). The results indicate that our model is successful, given that the model groups show significant difference compared with the control ($p < 0.01$). Compared with the model groups, there were significant differences in groups with different Dio-NS and silymarin doses ($p < 0.01$ and $p < 0.05$).

The results of our analysis of liver lipid peroxidation showed that the activity of GSH-Px and SOD in different dose groups of Dio-NS were markedly increased, compared with those of the model control ($p < 0.01$ and $p < 0.05$) (Figure 13). In contrast, the level of MDA was significantly reduced ($p < 0.01$ and $p < 0.05$). In the different drug groups, the liver index was reduced to some extent. Consequently,

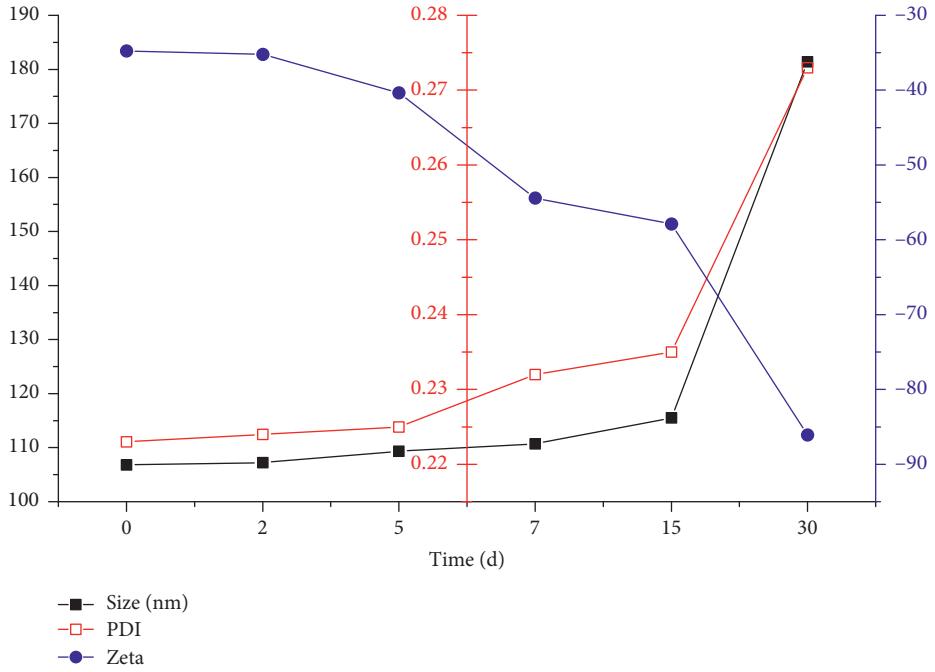

Figure 11: Particle size, polydispersity index, and zeta potential of dioscin nanoscale suspension NS-B at 25°C.

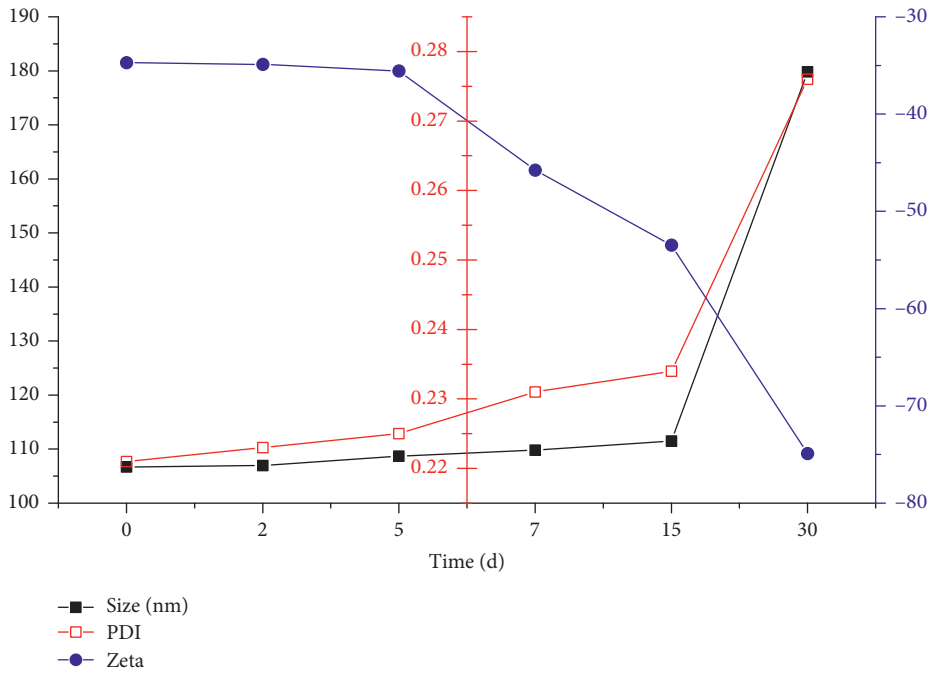

Figure 12: Particle size, polydispersity index, and zeta potential of dioscin nanoscale suspension NS-B at 4°C.

there was an equivalent or even better effect from the high-dose group (100 mg/kg) of Dio-NS compared with that of silymarin (the positive control drug).

HE staining showed that the liver cells in the blank control group were arranged normally, the cytoplasm was uniform, the nucleus and nucleolus were obvious, the central vein was clearly visible, and the cells had local edema (Figure 14). In the model group, a large number of necrotic hepatocytes were observed in the tissue, as indicated by a more intense staining or disintegration of liver cells. Furthermore, cytoplasmic eosinophilia was enhanced, accompanied by infiltration of inflammatory cells, and a small amount of white blood cells were seen in the veins. In the silymarin group and the high-dose group

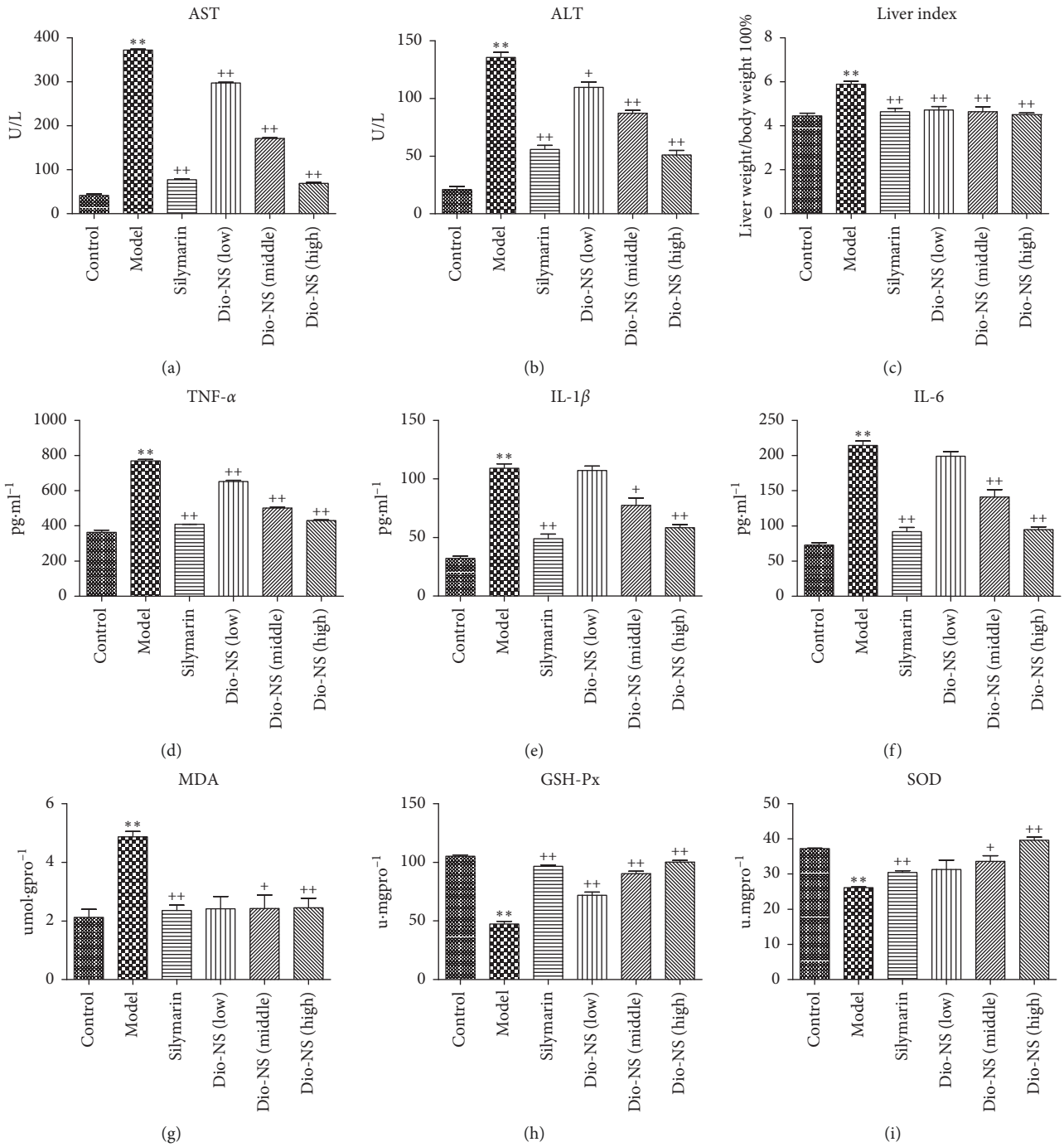

Figure 13: Effect of Dio-NS on CCl4-induced hepatotoxicity. (a) The activities of ALTin the serum. (b) The activities of ASTin the serum. (c) The liver index. (d) The activities of TNF-a in the serum. (e) The activities of IL-1β in the serum. (f) The activities of IL-6 in the serum. (g) The levels of MDA in the liver. (h) The levels of GSH-px in the liver. (i) The levels of SOD in the liver. $^{**}P < 0.01$ vs control, $+P < 0.05$, and $++P < 0.01$ vs. model.

of Dio-NS, the structure of hepatocyte was more complete with few inflammatory cells and little necrosis, and the pathological damage was clearly ameliorated. Compared with the model group, the low- and medium-dose groups of Dio-NS decreased the infiltration of inflammatory cells and reduced the degree of hepatocyte damage to a certain extent; however, the effect was not as conspicuous as in the silymarin and high-dose Dio-NS groups.

4. Discussion

It is well known that nanoparticle formulations improve the solubility of drugs to some extent because of their small size. However, in the process of drug preparation, excessive heat and solvent residues can adversely affect the production of good formulations. However, dioscin dissolves in ethanol, which has beneficial effects with regards to our preparation,

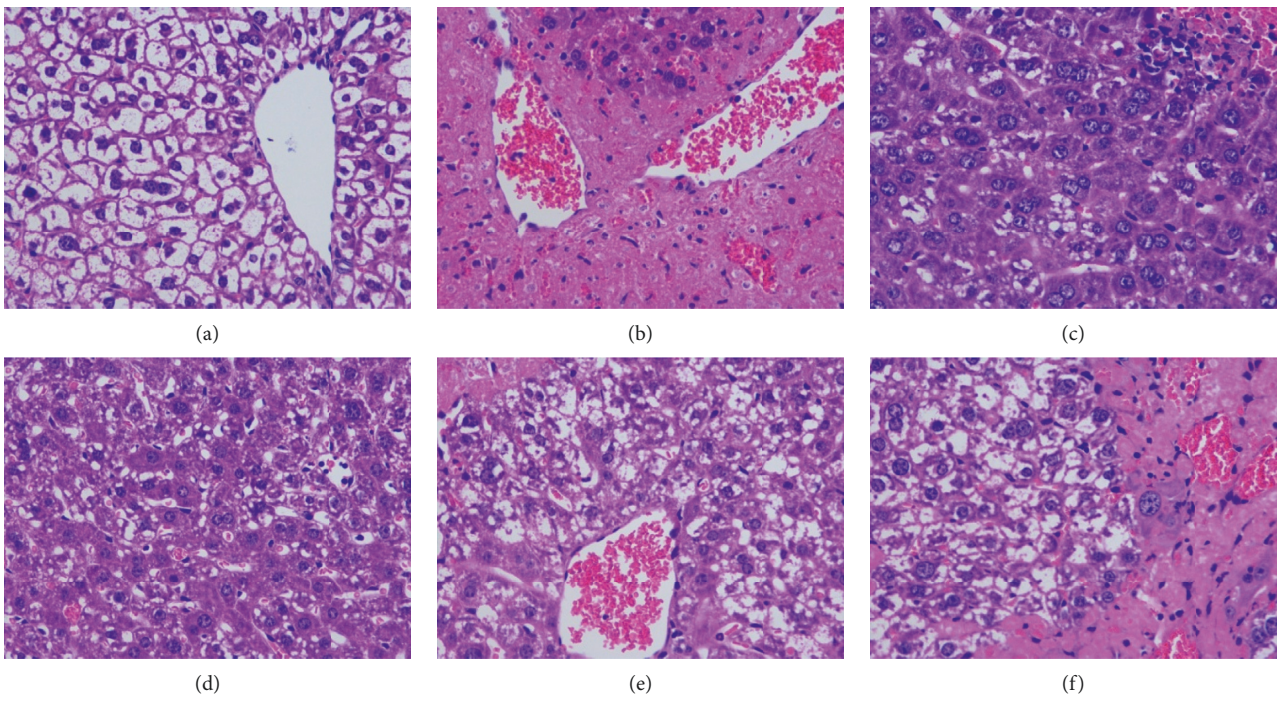

Figure 14: HE staining of liver cells: (a) control, (b) model, (c) silymarin, (d) Dio-NS (high), (e) Dio-NS (medium), and (f) Dio-NS (low).

as the rapid volatility of ethanol ensures low amounts of solvent residue.

In previous experiments, we used the reverse solvent preparation method and this method combined with high-pressure homogenization to prepare nanoemulsions. However, when using high-pressure homogenization, we found that the heat generated caused the production of excessive amounts of foam, which we believe may be attributable to the thermal decomposition of surfactants or dioscin. Moreover, using the reverse solvent preparation method alone, we were not able to obtain particles of the requisite size. Therefore, in the present study, we examined the applicability of using magnetic stirring and high-speed shearing combined with high-pressure homogenization to prepare the Dio-NS. Using this approach, the excessive heat generated by homogenization can be dissipated, thereby minimizing or eliminating foaming or degradation of the drug preparation.

Furthermore, we adopted a star design-response surface optimization method in order to determine the optimal formulation ratio. This enabled us to clearly assess each level of interaction. We were surprised to discover that the ratio of dioscin in the formulation was as high as 21.26%.

Through an evaluation of the physical and chemical properties and morphology of Dio-NS, we discovered that the nature of dioscin in the formulation had undergone changes. Observations indicated that the dioscin no longer retained a crystalline form, but instead occurred as spherical particles, as indicated by the disappearance of peaks on thermal analysis.

On the basis of an *in vitro* solubility test, we found that the solubility of dioscin was significantly increased in the Dio-NS formulations. This was confirmed by pharmacodynamic experiments. The possible reasons for these observed properties are as follows. Firstly, the particle size decreases, the adsorption surface is enlarged, the saturation solubility increases, the dissolution rate increases, the permeability of the biofilm increases, at the same time the retention time of the gastrointestinal tract is prolonged, the concentration of drug in the blood is enhanced, and thus the efficacy of the drug is enhanced. Secondly, when drug particles are less than 1 μm in size, the internal dissolution rate will suddenly increase.

However, we did not evaluate the bioavailability of Dio-NS. In this study, we examined the use of ultrahigh liquid phase and liquid mass in combination but were unable to detect any dioscin. On the one hand, dioscin exists in the body in the form of glycogen. On the other hand, there were impertinent methods on handling samples or the type of instruments. These problems will be difficult to solve in subsequent experiments.

5. Conclusion

We have demonstrated that nanosuspensions can be successfully prepared using an emulsification method in which high-speed homogenization is used in combination with high-pressure homogenization, which is better than previously prepared drug formulations [32, 33]. Dioscin is an effective component extracted from plants that belong to the family Dioscoreaceae. The present study shows that dioscin has protective effect against acute hepatic injury in mice induced by intraperitoneal injection of CCL_4. However, dioscin is difficult to dissolve in water, although it can be dissolved in the organic solvent ethanol [34]. Therefore, in

this study, we adopted the methods of reverse solvent precipitation and high-pressure homogenization [35] to prepare nanosuspensions. The particle size distribution of the resulting suspensions is between 70 and 120 nm. The suspensions also have a high specific surface area and increased solubility, which may promote their bioavailability.

Therefore, we performed various pharmacodynamic analyses to evaluate the bioavailability of our newly prepared nanosuspensions (Dio-NS). We accordingly found that, at a high dose, Dio-NS reduces the levels of ALT and AST, enhances SOD activity, reduces MDA content, and ameliorates liver pathology to some extent compared with silymarin (the positive control drug).

Thus, the results of the present study will provide a reference for the development and clinical application of dioscin formulations. Finally, in further studies, we intend to evaluate the bioavailability of our dioscin formulations and investigate the precise mechanisms underlying the hepatoprotection properties of these preparations.

Abbreviations

Dio: Dioscin
DSC: Differential scanning calorimetry
Dio-NS: Dioscin nanosuspension
E t: Emulsification time
HP: Homogenization pressure
HPH: High-pressure homogenization
HPLC: High-performance liquid chromatography
MPS: Mean particle size
OD: Overall desirability
PSD: Particle size distribution
P s: Passes
SEM: Scanning electron microscope
SDS: Sodium alkyl sulfate twelve
Tem: Transmission electron microscope
XRPD: X-ray powder diffraction
ZP: Zeta potential.

Data Availability

All relevant data are within the paper and its Supporting Information files.

Conflicts of Interest

There are no conflicts of interest.

Authors' Contributions

Xiao Song and Hongye Ju contributed equally to this work. Xiao Song conceived and designed the experiments. Hongye Ju, Kunxia Hu, Li-Zhu Han, and Guo-Wang Zhao performed the experiments. The rest of the authors were also involved in the different processes of the experiments. Xiao Song, Hongye Ju, Guo-Wang Zhao analyzed the data and wrote the paper. Xiao Song and Zhi-Shu Tang provided funding for scientific research.

Acknowledgments

The authors would like to acknowledge the financial support from the National Natural Science Foundation of China (nos. 81373944 and 81373978), the Department of Science and Technology of Shaanxi Province (2012KTCQ03-13), the Key Laboratory of the Basic and New Medicine Research of the Traditional Chinese Medicine in Shaanxi Province, the Special Subsidization of the Key Subjects of the Traditional Chinese Medicine Pharmacy in Shaanxi Province, and the Three Level Laboratory of the Chinese Medicine Preparation of the State Administration of Traditional Chinese Medicine (TCM).

Supplementary Materials

Supplementary Table S1-3: three experimental data during the preparation of nanosuspensions, which describe the effects of shear speed, shear time, temperature, homogenization times, and homogenization pressure on the particle size and polydispersity index of nanosuspensions, and the evaluation results *in vitro* and *in vivo*. The experimental results were plotted by origin 8.5 and GraphPad Prism 5. Supplementary Material 1: Animal Ethics Society approval document. (*Supplementary Materials*)

References

[1] C. Zhu, N. Bao, S. Chen, and J. Zhao, "Dioscin enhances osteoblastic cell differentiation and proliferation by inhibiting cell autophagy via the ASPP2/NF-κβ pathway," *Molecular Medicine Reports*, vol. 16, no. 4, pp. 4922–4926, 2017.

[2] H. Zeng, L. Yang, X. Zhang, Y. Chen, and J. Cai, "Dioscin prevents LPS-induced acute lung injury through inhibiting the TLR4/MyD88 signaling pathway via upregulation of HSP70," *Molecular Medicine Reports*, vol. 17, no. 5, pp. 6752–6758, 2018.

[3] Y. S. Zhang, Y. L. Ma, K. Thakur et al., "Molecular mechanism and inhibitory targets of dioscin in HepG2 cells," *Food and Chemical Toxicology*, vol. 120, pp. 143–154, 2018.

[4] S. Zhu, S. Tang, and F. Su, "Dioscin inhibits ischemic stroke induced inflammation through inhibition of the TLR4/MyD88/NFκB signaling pathway in a rat model," *Molecular Medicine Reports*, vol. 17, no. 1, pp. 660–666, 2018.

[5] L. Zheng, L. Yin, L. Xu et al., "Protective effect of dioscin against thioacetamide-induced acute liver injury via FXR/AMPK signaling pathway in vivo," *Biomedicine & Pharmacotherapy*, vol. 97, pp. 481–488, 2018.

[6] C. Li, Y. Lu, S. Du et al., "Dioscin exerts protective effects against crystalline silica-induced pulmonary fibrosis in mice," *Theranostics*, vol. 7, no. 17, pp. 4255–4275, 2017.

[7] L. Yin, Y. Qi, Y. Xu et al., "Dioscin inhibits HSC-T6 cell migration via adjusting SDC-4 expression: insights from iTRAQ-based quantitative proteomics," *Frontiers in Pharmacology*, vol. 8, p. 665, 2017.

[8] X. Tao, L. Yin, L. Xu, and J. Peng, "Dioscin: a diverse acting natural compound with therapeutic potential in metabolic diseases, cancer, inflammation and infections," *Pharmacological Research*, vol. 137, pp. 259–269, 2018.

[9] Y. Qin, X. Wu, W. Huang et al., "Acute toxicity and subchronic toxicity of steroidal saponins from Dioscorea

zingiberensis C.H.Wright in rodents," *Journal of Ethnopharmacology*, vol. 126, no. 3, pp. 543–550, 2009.

[10] X. J. Liang, Y. Z. Shang, H. R. Song, and W. J. Dong, "Acute toxicity study of whole saponin of Dioscorea nipponica Makino in mice," *Journal of Chengde Medical College*, vol. 27, pp. 117-118, 2010.

[11] T. Xu, S. Zhang, L. Zheng, L. Yin, L. Xu, and J. Peng, "A 90-day subchronic toxicological assessment of dioscin, a natural steroid saponin, in Sprague–Dawley rats," *Food and Chemical Toxicology*, vol. 50, no. 5, pp. 1279–1287, 2012.

[12] L. Padrela, M. A. Rodrigues, A. Duarte, A. M. A. Dias, M. E. M. Braga, and H. C. de Sousa, "Supercritical carbon dioxide-based technologies for the production of drug nanoparticles/nanocrystals—a comprehensive review," *Advanced Drug Delivery Reviews*, vol. 131, pp. 22–78, 2018.

[13] L. R. Zawar and S. B. Bari, "Preparation, characterization and in vivo assessment of repaglinide nanosuspension for oral bioavailability improvement," *Recent Patents on Drug Delivery and Formulation*, vol. 12, no. 3, pp. 162–169, 2018.

[14] A. G. Thombre, J. C. Shah, K. Sagawa, and W. B. Caldwell, "In vitro and in vivo characterization of amorphous, nanocrystalline, and crystalline ziprasidone formulations," *International Journal of Pharmaceutics*, vol. 428, no. 1-2, pp. 8–17, 2012.

[15] M. H. He, L. Chen, T. Zheng et al., "Potential applications of nanotechnology in urological cancer," *Frontiers in Pharmacology*, vol. 9, p. 745, 2018.

[16] N. Kamaly, J. C. He, D. A. Ausiello, and O. C. Farokhzad, "Nanomedicines for renal disease: current status and future applications," *Nature Reviews Nephrology*, vol. 12, no. 12, pp. 738–753, 2016.

[17] D. C. Snow-Lisy, M. K. Samplaski, V. Labhasetwar, and E. S. Sabanegh Jr, "Drug delivery to the testis: current status and potential pathways for the development of novel therapeutics," *Drug Delivery and Translational Research*, vol. 1, no. 5, pp. 351–360, 2011.

[18] P. J. Patel, B. Y. Gajera, and R. H. Dave, "A quality-by-design study to develop Nifedipine nanosuspension: examining the relative impact of formulation variables, wet media milling process parameters, and excipient variability on drug product quality attributes," *Drug Development and Industrial Pharmacy*, vol. 44, no. 12, pp. 1942–1925, 2018.

[19] A. N. Oktay, A. Karakucuk, S. Ilbasmis-Tamer, and N. Celebi, "Dermal flurbiprofen nanosuspensions: optimization with design of experiment approach and in vitro evaluation," *European Journal of Pharmaceutical Sciences*, vol. 15, no. 122, pp. 254–263, 2018.

[20] E. B. Basalious and M. A. Ahmed, "Phospholipid based self-nanoemulsifying self-nanosuspension (p-SNESNS) as a dual solubilization approach for development of formulation with diminished food effect: fast/fed in vivo pharmacokinetics study in human," *European Journal of Pharmaceutical Sciences*, vol. 109, pp. 244–252, 2017.

[21] H. Liu, Z. Zhang, H. Hu et al., "Protective effects of Liuweiwuling tablets on carbon tetrachloride-induced hepatic fibrosis in rats," *BMC Complementary and Alternative Medicine*, vol. 18, no. 1, p. 212, 2018.

[22] X. Jiang, H. Zhang, K. Mehmood et al., "Protective effects of Herpetospermum caudigerum extracts against liver injury induced by carbon tetrachloride in mouse," *Journal of Biological Regulators & Homeostatic Agents*, vol. 32, no. 3, pp. 699–704, 2018.

[23] J. Leng, Z. Wang, C.-L. Fu et al., "NF-kappaB and AMPK/PI3K/Akt signaling pathways are involved in the protective effects of Platycodon grandiflorum saponins against acetaminophen-induced acute hepatotoxicity in mice," *Phytotherapy Research*, vol. 32, no. 11, pp. 2235–2246, 2018.

[24] C. Ning, X. Gao, C. Wang et al., "Ginsenoside Rg1 protects against acetaminophen-induced liver injury via activating Nrf2 signaling pathway in vivo and in vitro," *Regulatory Toxicology and Pharmacology*, vol. 98, pp. 58–68, 2018.

[25] H. Zhao, Q. Han, N. Lu, D. Xu, Z. Tian, and J. Zhang, "HMBOX1 in hepatocytes attenuates LPS/D-GalN-induced liver injury by inhibiting macrophage infiltration and activation," *Molecular Immunology*, vol. 101, pp. 303–311, 2018.

[26] H. Lv, X. Fan, L. Wang, H. Feng, and X. Ci, "Daphnetin alleviates lipopolysaccharide/d-galactosamine-induced acute liver failure via the inhibition of NLRP3, MAPK and NF-κB, and the induction of autophagy," *International Journal of Biological Macromolecules*, vol. 119, pp. 240–248, 2018.

[27] P. Kanmani and H. Kim, "Protective effects of lactic acid bacteria against TLR4 induced inflammatory response in hepatoma HepG2 cells through modulation of toll-like receptor negative regulators of mitogen-activated protein kinase and NF-κB signaling," *Frontiers in Immunology*, vol. 9, p. 1537, 2018.

[28] B. Lu, Y. Xu, L. Xu et al., "Mechanism investigation of dioscin against CCl_4-induced acute liver damage in mice," *Environmental Toxicology and Pharmacology*, vol. 34, no. 2, pp. 127–135, 2012.

[29] Y.-J. Son, P. W. Longest, G. Tian, and M. Hindle, "Evaluation and modification of commercial dry powder inhalers for the aerosolization of a submicrometer excipient enhanced growth (EEG) formulation," *European Journal of Pharmaceutical Sciences*, vol. 49, no. 3, pp. 390–399, 2013.

[30] G. Pilcer, T. Sebti, and K. Amighi, "Formulation and characterization of lipid-coated tobramycin particles for dry powder inhalation," *Pharmaceutical Research*, vol. 23, no. 5, pp. 931–940, 2006.

[31] W. Yang, J. Tam, D. A. Miller et al., "High bioavailability from nebulized itraconazole nanoparticle dispersions with biocompatible stabilizers," *International Journal of Pharmaceutics*, vol. 361, no. 1-2, pp. 177–188, 2008.

[32] Y. Li, X. Zhao, Y. Zu, and Y. Zhang, "Preparation and characterization of paclitaxel nanosuspension using novel emulsification method by combining high speed homogenizer and high pressure homogenization," *International Journal of Pharmaceutics*, vol. 490, no. 1-2, pp. 324–333, 2015.

[33] S. E. Lee, S. F. Bairstow, J. O. Werling et al., "Paclitaxel nanosuspensions for targeted chemotherapy—nanosuspension preparation, characterization, and use," *Pharmaceutical Development and Technology*, vol. 19, no. 4, pp. 438–453, 2014.

[34] Y. Zhang, L. Jin, J. Liu et al., "Effect and mechanism of dioscin from Dioscorea spongiosa on uric acid excretion in animal model of hyperuricemia," *Journal of Ethnopharmacology*, vol. 214, pp. 29–36, 2018.

[35] G. Pilcer, F. Vanderbist, and K. Amighi, "Preparation and characterization of spray-dried tobramycin powders containing nanoparticles for pulmonary delivery," *International Journal of Pharmaceutics*, vol. 365, no. 1-2, pp. 162–169, 2009.

Hindawi
Evidence-Based Complementary and Alternative Medicine
Volume 2019, Article ID 4213928, 12 pages
https://doi.org/10.1155/2019/4213928

Research Article

Effect of Electroacupuncture at Different Acupoints on the Expression of NMDA Receptors in ACC and Colon in IBS Rats

Li-hua Tan,[1,2] Kai-ge Li,[1,3] Yan-ying Wu,[1,4] Meng-wei Guo,[1] Yin Lan,[1] Shan Wang,[1] Wen-lian Zhu,[1] and Xiao-xuan Ren [1]

[1] *College of Acupuncture and Massage, Beijing University of Chinese Medicine, Beijing, China*
[2] *Maternal and Child Health-Care Hospital of Yichang, Hubei, China*
[3] *Beijing Kang Yide Combination of Chinese Traditional and Western Medicine Lung Hospital, China*
[4] *Traditional Chinese Medicine of Huairou Hospital in Beijing, China*

Correspondence should be addressed to Xiao-xuan Ren; rxx7005@aliyun.com

Received 11 September 2018; Revised 5 December 2018; Accepted 17 January 2019; Published 3 February 2019

Guest Editor: Célia Cabral

Objective. To observe the effects of electroacupuncture (EA) at different acupoints on the expression of N-methyl-D-aspartate receptor (NMDA receptor) and behaviors in irritable bowel syndrome (IBS) rats. *Methods*. Wistar rats were randomly divided into blank control group (blank group, n=10) and model preparation group (n=50); experimental rat model of IBS was established by the "neonatal maternal separation and acetic acid enema" combined with "colorectal distension stimulation" method. A total of 50 IBS rats were randomly assigned to five groups of 10 each: model group, Yintang (GV29) group, Neiguan (PC6) group, Tianshu (ST25) group, and Zusanli (ST36) group. Rats in four treatment groups, aged 9 weeks old, were treated with EA by HANS with a sparse-dense wave with a frequency of 2/100 Hz, current of 0.1-0.3mA, and 20 min/stimulation, every other day for a total of 5 sessions. After treatment, the abdominal visceral sensitivity was evaluated by abdominal withdrawal reflex (AWR), and the psychological and emotional behavior of rats were evaluated by the open-field test (OFT). The expression of NMDA receptors in anterior cingulate cortex (ACC) was detected by Quantitative Real-time PCR, and the positive expression of NMDA receptors in colon was detected by immunohistochemistry. *Results*. The IBS rat's abdomen is more sensitive and irritable; NR1, NR2A, and NR2B in ACC and NR1 and NR2B in colon of rats significantly increased in the model group versus the normal group ($P<0.01$) and were inhibited in all treatment groups ($P<0.01$, $P<0.05$). Additionally, NR2A and NR2B in ACC reduced more in GV29 group ($P<0.01$) than in other treatment groups (P all<0.05) compared with the model group. The expression of NR2B in colon was significantly inhibited in ST36 group ($P<0.01$) and inhibited in GV29 group and ST25 group (P all <0.05) compared with the model group. And the expression of NR2B in colon was more inhibited in ST36 group than in PC6 group ($P<0.01$). *Conclusions*. EA at different acupoints could obviously relieve abdominal pain and abnormal behaviors in IBS rats in different degrees of effects. The effect of abdominal pain-relief, from greatest to least, is ST25, ST36, GV29, and PC6, while the effect of relieving abnormal behaviors caused by IBS, from greatest to least, is GV29, PC6, ST36, and ST25. There are significant differences in the expressions of NMDA receptors in ACC and colon among different acupoints. This difference should be related to the location distribution and indications of acupoints.

1. Introduction

Acupuncture and moxibustion believe that stimulating acupoints can specifically regulate the corresponding visceral organs, which is different from nonacupoints and other acupoints. This difference is the acupoint specificity [1]. The specificity of acupoint effect is one of the important bases for acupoint selection along meridians. Moreover, a large number of clinical practices [2–4] and experimental studies [5, 6] have confirmed that acupoint effect has specificity. Previous studies on the effect specificity of acupoints have been conducted to observe the therapeutic effects of different acupoints on the same symptoms of a disease [3, 7]; however, the curative effect of different points on different symptoms of a disease is rarely reported. In order to further verify the specificity of meridian effect, this experiment selected

different parts of acupoints with different functions by syndrome differentiation and acupoint selection along meridians to observe whether they have different regulating effects on abdominal pain and abnormal mental disorder in irritable bowel syndrome (IBS).

Irritable bowel syndrome (IBS) is a typical psychosomatic disease manifested as abdominal pain or discomfort, stool irregularities, and bloating, as well as other somatic, visceral, and psychiatric comorbidities [8]. As a multifactorial disease, the underlying pathogenesis of IBS is complex including mental disorders, brain-gut axis dysfunction, and visceral paresthesia. Different etiologies and pathogenesis can influence each other, and the brain-gut axis [9] plays a key role in the interaction of various factors.

N-methyl-D-aspartate receptor (NMDA receptor) is an important excitatory ionotropic glutamate neurotransmitter in the central nervous systemand is associated with mood disorders and psychosis-schizophrenia [10, 11]. NMDA receptor plays a critical role in the neuroplasticity of nociceptive networks, and there is evidence [12–14] proving its involvement in chronic stress-induced visceral hyperalgesia. It has also been reported that NMDA receptor was associated with the formation of high intestinal sensitivity of IBS [15]. Whether there is a close relation between intestinal sensitivity and mental disorders in the pathogenesis of IBS, or whether they play a key role in acupuncture regulation, is to be studied.

Based on the holistic review and syndrome differentiation in Traditional Chinese Medicine (TCM) acupoints with different functions should be selected according to the different diseases and syndromes, and then the curative effect is remarkable [16, 17]. In classical acupuncture, acupoints with effects of tranquilizing the mind, relieving pain, and regulating the functions of stomach and intestines all showed satisfied effect on IBS [18]. However, the specific effect of different acupoint on IBS and its underlying mechanism is still unclear. Therefore, this study selected four commonly used acupoints for IBS including Yintang (GV29), a sedative point, Tianshu (ST25), a point for regulating intestines and bowels, and Neiguan (PC6) and Zusanli (ST36), two points with satisfied effect for both physical and mental diseases, to compare the effects on the behavior and the expression of NMDA receptors in ACC and colon of IBS rats with abdominal pain and emotional disorder. The purpose of this study is to explore the effect and difference of acupoints distributed in head, trunk, and limbs with different therapeutic effects on different symptoms of physical and mental diseases.

2. Methods

2.1. Animals and Grouping. Eight cleaning Wistar pregnant rats were provided by Beijing Weitong Lihua Experimental Animal Technology Co. Ltd., certificate number: SCXK- (in 2012-004). The rats were fed in the room with temperature of 23±2°C and humidity of about 50%, 12h alternating between day and night, eating and drinking in free. The neonatal rats were randomly divided into blank control group (blank group (n=10)) and model preparation group (n=50).

2.2. Irritable Bowel Syndrome Model. The IBS model (n=50) was established by the "neonatal maternal separation and acetic acid enema" combined with the "colorectal distension stimulation" method. The neonatal rats were isolated with mother rats 3h/d from 2 to 21 days after birth. Stimulation was given to the colon by using 0.5% acetic acid from 8^{th} day to 21^{th} day; the central venous catheter (1 mm in diameter) lubricated with paraffin oil was inserted into the colon through the anus for 2 cm, and the perfusion volume increased from 0.2ml to 0.7ml with age, as shown in Table 1. Then, without any experimental operation until 6 weeks of age, a mechanical stimulation of colorectal distention (CRD) was performed to enhance the establishment success rate and the stability of the model. The model preparation group were randomly divided into model group (model group), GV29 group, PC6 group, ST25 group, and ST36 group after modeling.

2.3. Electroacupuncture (EA). Acupoint selection: GV29 (Yintang) is located at the middle point between two eyes [19], PC6 (Neiguan) about 3 mm to the wrist transverse stripe on the axopetal end, and ST36 (Zusanli) about 5 mm inferior of the capitulum fibulae and posterior-lateral to the hind-limb knee joint [20]; ST25 (Tianshu) [21] was approximately 5 mm away from the Shenque acupoint (the distance to subxiphoid area and pubic symphysis at a ratio of 8 : 5, 8 from the top and 5 from the bottom).

Acupuncture method: In addition to the blank group, rats in the model group were bound restraint 20min without acupuncture, and the treatment groups were routinely treated with EA at the age of 9 weeks. The rats in 4 EA groups were fixed by soft cloth sleeve, a needle was inserted into the acupoint area and connected with the positive pole, and another needle was inserted 1mm in the same area and connected with the negative pole of Han's acupoint nerve stimulator (HANS). The parameters of the HANS were as follows: sparse-dense wave with a frequency of 2/100 Hz and current of 0.1~0.3 mA. EA stimulation was performed 20 min per session, one treatment every other day, with a total of 5 sessions.

2.4. Abdominal Withdrawal Reflex (AWR). The abdominal withdrawal reflex was used to assess the visceral sensitivity of the rats. Rats were fasted for 12h before assessment. Abdominal withdrawal method was improved by referring to Al-Chaer [22], who, using BL-420S biological function experimental system, collected intestinal pressure signals through pressure channel to observe the sensitivity of colon under different pressure. The BL-420S, pressure transducer, and microinjection pump were connected with three-way piece, and the pipeline was kept airtight. The microinjection pump (injected with 2.0ml purified water) was connected to a self-made saccule, which was coated with paraffin oil and was slowly inserted into the anus to a depth of about 8 cm. When the microsyringe pump was opening, the saccule was dilated by injecting water at a speed of 1ml/min for 90 seconds. The pressure signals were showed in BL-420S' display screen. When the rat's colon was contracted by stimulation, the

Table 1: 0.5% acetic acid enema dose of colorectal in infancy rats.

Age (d)	8	9	10	11	12	13	14	15	16	17	18	19	20	21
Dose (ml)	0.2	0.2	0.2	0.3	0.3	0.3	0.4	0.4	0.5	0.5	0.6	0.6	0.7	0.7

pressure line would present a wave. The time before the first contraction wave appeared (latent period) and the number of contraction waves in 90s (contraction wave) was recorded. Each rat was detected 3 times, with each interval being at least 30 min, taking the average value.

2.5. Open-Field Test (OFT). The next day after AWR test, open-field test reflecting the mental state of rats was performed. After adaption to the experimental environment for about 10min, the rats were put into the box of autonomous behavior device. The number of horizontal and vertical movement (two forelegs are erected at the same time for 1 time) times of the rats in the box within 5min was recorded by software. The open box was cleaned after testing every time, without any foreign matter or odor. Horizontal activity reflects the excitability of animals and vertical activity reflects the animals' curiosity of risk and uncertainty in the surrounding environment. In this way, animal emotion and psychology were evaluated.

2.6. Specimen Collection and Processing. After the OFT, all rats were sacrificed to collect specimens. ACC brain tissue was taken from subcortical and anterior fontanelle and ground in the EP tube with 0.5ml Trizol for real-time quantitative polymerase chain reaction (PCR). The colon was collected 1 cm above the anus from 7^{th} cm to 8^{th} cm and fixed by 10% neutral formalin.

2.7. Real-Time PCR. Total RNA was extracted with Trizol from ACC brain tissues. Promega ImProm-II Reverse Transcription System kit (Promega) was used to reverse transcription: RNA template 4ul, Oligo(dT)15 0.5ul, random primers 0.5ul, run cycle 70°C 5min and then static on ice10min; adding nuclease free water 4.5ul, 5xbuffer 4ul, $MgCl_2$ 4ul, dNTP 1ul, RNasin ribonuclease inhibitor 0.5ul, ImProm-IITM reverse transcriptase 1ul, run cycle 25°C 5min, 42°C 1h, and 70°C 15min; $_C$DNA template 3ul, SYBR Green PCR Master Mix 10ul, Primer1(20) 0.5ul, Primer2(20) 0.5ul, RNase free H2O 11ul, 94°C 5min, 94°C 30s, 59°C 30s, 72°C 60s, 35 cycles to amplification. Gene expression levels were measured by qRT-PCR using the following primer sequences: NMDA receptor 1:sense: 5-GCTGTACCTGCTGGACCG-CT-3', antisense: 5-GCAGTGTAGGAAGCCACTATGATC-3', predicted size (bp): 219bp. NMDA receptor 2A: sense: 5'-TCCATTCTTCTGTCATCCTGC-3', antisense: 5'-AAG-ACCGTCTCTCACTCTTGC-3', predicted size (bp)225bp. NMDA receptor 2B: sense: TGCACAATTACTCCTCGACG-3', antisense: 5'-TCCGATTCTTCTTCTGAGCC-3', predicted size (bp): 222bp. The amplification curve and melting curve of real-time PCR were confirmed at the end of reaction. The Ct value of the sample was taken as the average value of three replicates. Relative quantification of target genes by ΔΔCt: the relative expression of the target gene = $2^{-\Delta\Delta Ct}$, ΔΔCt = experience group (target gene Ct- reference gene)- control group (target gene Ct- reference gene). The beta-actin was used as reference gene, group CON was used as control gene, and the relative quantity of each target gene was quantified.

2.8. Immunohistochemical Method. NR1 and NR2B in colon were detected using immunohistochemistry. The tissue sections were dewaxed and hydrated by xylene I, II and alcohol with different concentration and distilled water. Antigen retrieval was performed by heating samples in citric acid buffer in a microwave oven. After washing with PBS for 3 × 2min, specimens were treated with 3% H_2O_2 in the dark for 10 min to inactivate endogenous peroxidases and then washed with PBS solution 3 × 3min. Specimens were immersed in the diluted anti-NMDAR1 antibody or anti-NMDAR2B antibody and incubated at 4°C overnight. The specimens were placed at room temperature for 30min, washed with PBS solution 3 × 3min, and incubated with the secondary antibody at room temperature for 30min. After washing with PBS for 2 × 3min, DAB developing solution was added for observation under microscope. After the target indicated positive reaction, it was washed with distilled water to terminate the development. After being redyed with hematoxylin, differentiated with hydrochloric acid alcohol, and returned blue with ammonia liquor, they were dehydrated, mounted, and observed under a light microscope.

NMDAR immunoreactivity was determined in the mucosa and muscularis of the colon, and each tissue slice was photographed under a high power microscope with 2 visual fields randomly, with 12 eyes per group. The collected images were analyzed by using Image-Pro Plus 6 image analysis system; the positive expression of NMDAR immunoreactivity based on each area of view area (A) and integrated optical density (IOD) of the positive reaction were measured to calculate the average optical density (AOD, IOD/A) as the quantitative index level of NMDAR expression.

2.9. Statistical Analysis. Data were analyzed using the Statistical Package for the Social Sciences (SPSS) version 20.0, and all data were expressed as mean ± standard deviation ($\overline{X} \pm s$). If the data of each group are normal and the variance is homogeneous, they were analyzed by one-way analysis of variance (ANOVA), followed by LSD to compare between groups; if the groups were normal and the variance was not uniform, the Welch test was used; if each group did not obey the normal test, the nonparametric test was used, followed by the comparison between each 2 groups. A value of $P<0.05$ was considered to be statistically significant.

3. Experimental Results

3.1. Effects of EA on AWR. In AWR experiment, the time before the first contraction wave appeared (latent period) and the number of contraction wave in 90s (contraction wave) reflected the intestinal sensitivity of rats. As shown in Figure 1, the latent period of IBS rats was significantly shortened and the number of the contraction waves increased significantly ($P<0.01$). After EA, the latent period was significantly prolonged ($P<0.01$) and contraction wave significantly decreased ($P<0.01$) in all EA groups except PC6 group. Comparison between groups: the latent period in ST25 group was longer than those in PC6 and GV29 group ($P<0.05$), and the contraction waves in ST25 group were fewer than those in PC6 group ($P<0.01$).

3.2. Effects of EA on OFT. In OFT, the number of horizontal and vertical movement times could reflect depression or anxiety in rats. As shown in Figure 2, the number of horizontal and vertical movement times of IBS rats was significantly reduced ($P<0.01$) and increased after EA. Compared with the model group, in GV29 and PC6 group the number of horizontal movement times increased significantly ($P<0.01$) and vertical movement times increased ($P<0.05$); in ST36 group only horizontal movement times increased ($P<0.05$). Compared with the ST25 group, GV29 group has more number of horizontal movement times ($P<0.05$).

3.3. Expression of NR1, NR2A, and NR2B in ACC. The above experiments showed that the NR1, NR2A, and NR2B in ACC played important roles in the pathogenesis of visceral pain and pain-emotion. In Figure 3, NR1, NR2A, and NR2B in ACC of IBS rats increased significantly ($P<0.01$) and decreased with different degree after EA at different acupoints. Compared with the model group, NR1 in ACC of all groups significantly reduced ($P<0.01$), and NR2A and NR2B significantly reduced in GV29 group ($P<0.01$) and decreased in PC6 group and ST36 group ($P<0.05$), while, only NR2B reduced in ST25 group ($P<0.05$).

3.4. Expression of NR1 and NR2B in Colon. NR1 and NR2B in colon also played important roles in the pathogenesis of visceral pain. In Figures 4, 5 and 6, NR1 and NR2B in the colon of IBS rats were significantly increased ($P<0.01$). After EA, NR1 in colon of GV29 and ST36 group decreased significantly ($P<0.01$) and decreased in PC6 group and ST25 group ($P<0.05$); NR2B in ST25 group significantly decreased ($P<0.01$) and decreased in GV29 and ST36 group ($P<0.05$). Meanwhile, NR2B in colon of PC6 group was significantly more than that in the ST25 group ($P<0.01$).

4. Discussion

Irritable bowel syndrome (IBS) is a functional gastrointestinal disease closely related to mental health. It has both physical symptoms and mental disorders. Abdominal withdrawal reflex [23], which can reflect the pain tolerance threshold and sensitivity of rats by different stimuli, indicates the visceral sensitivity of IBS model rats.

Open-field test [24] was a classic experiment based on the characteristic of rats being naturally close to the edge field (haptotaxis) in a new environment. Exploratory behavior and spontaneous activity in a new environment can be used to test the excitement or depression state in central nervous system of animals. In this experiment, the latent period of IBS rats was significantly shortened and contraction wave increased showing that the intestinal sensitivity was enhanced, and the horizontal and vertical movements in the open-field test were significantly reduced indicating that the rats were prone to depression. It shows that the experimental model is successfully prepared.

N-methyl-D-aspartic acid receptor [10, 11] (NMDA receptor) is a kind of monosodium glutamate receptor involving in essential brain functions like learning, memory formation and consolidation, mood, and behavioral responses to exogenous stimuli depending on the activity of NMDA receptors. NMDA receptor includes three subunits: NR1, NR2, and NR3; NR1 is the basic subunit of NMDA receptor [25], which is related to pain perception, NR2 (in the ACC is mainly NR2A and NR2B) is a regulatory subunit, and a single NR2 combination has no response to agonists. The activation of NMDA receptor in ACC plays an important role in the production of pain-emotion [26]. Study [27] has shown that NMDA receptors preferentially participate in the processing of emotional dimensions of pain in ACC and are closely related to negative emotions especially in rACC [26, 28]. Studies by Liu Zong et al. [29] suggest that ACC is an important component of the visceral pain response pathway, and the upregulation and activity enhancement of NMDA receptor in ACC can regulate the pain-emotion. Ren [30] found that noxious stimulation can induce the expression of NR2A and NR2B in the anterior cingulate cortex of rats and activate the Gly loci in NR1 to activate the ERK-CREB signaling pathway to form pain-emotion. NMDA receptor also played a regulatory role in ACC's pain sensitization. Huang [31] found that NR2A and NR2B in ACC increased after inflammation and play an important role in the formation of visceral sensitivity. Hence, NMDA receptor is not only involved in the formation of visceral sensitivity, but also closely related to pain-emotion. It is the key factor of visceral pain and pain-emotion.

Different from ACC brain region, Valle-Pinero et al. [32] found that NMDA receptor existed in the colonic mucosa and muscularis. By identifying NMDA receptor in the intestinal nervous system, it was found that NR1 coexisted with NR2B, but no NR2A was found. Qi Qingqing [33] also successfully detected NR1 and NR2B in the colon and confirmed that activation of NMDA receptor could induce the formation of IBS visceral sensitivity. In this experiment, the expression of NMDA receptor in the IBS model rats increased in both ACC and colon, which was consistent with the previous experimental results.

Acupuncture has a long history of analgesia and has a good effect on all kinds of pain, about 43 indications of acupuncture and moxibustion recommended by the WHO in 1987; almost half of the symptoms were associated with

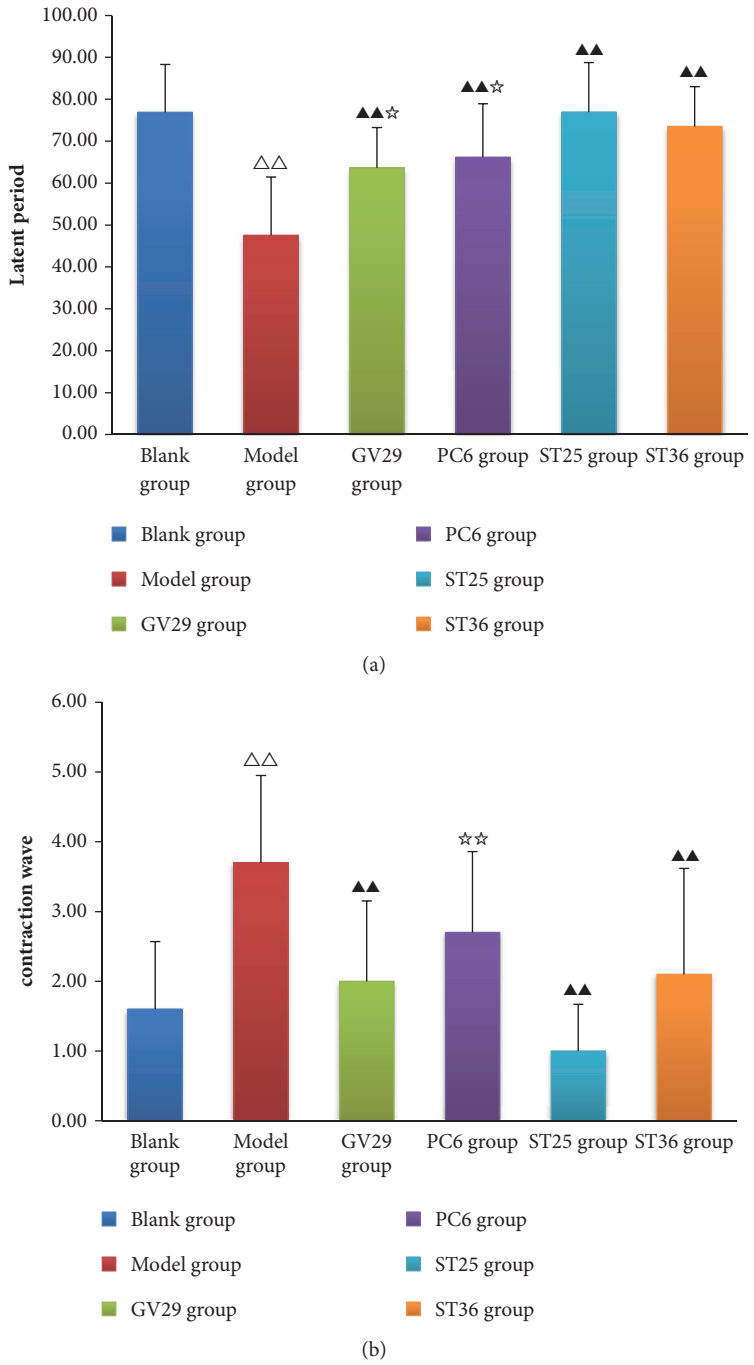

Figure 1: (a) Bar chart demonstrating the latent period, (b) bar chart demonstrating the contraction wave. Data are presented as mean ± SD (n=10). Note: $^{\triangle\triangle}P<0.01$, versus blank group; $^{\blacktriangle\blacktriangle}P<0.01$, versus model group; $^{\star\star}P<0.01$, $^{\star}P<0.05$, versus ST25 group.

pain. Consensus Development Conference on Acupuncture, held in November 1997 by the National Institutes of Health of the United States, believed that acupuncture is an effective treatment with scientific basis. Acupuncture not only has good curative effect on visceral pain [34], but also has a positive effect on the emotion induced by pain [35, 36]. In this study, the abdominal sensitivity of IBS rats was decreased after EA at different acupoints, the behaviors tended to be normal and the mental and psychological abnormality were improved. It is consistent with the previous research results [37, 38].

The results of this study showed that all acupoints were effective for IBS; however, each point had different effect on different IBS related symptoms. According to the classical theory of acupoints, GV29 (Yintang) is good at tranquilizing, ST25 (Tianshu) is mainly used for regulating bowel and relieving abdominal pain, and PC6 (Neiguan) and ST36 (Zusanli) are good for both physical and mental disease.

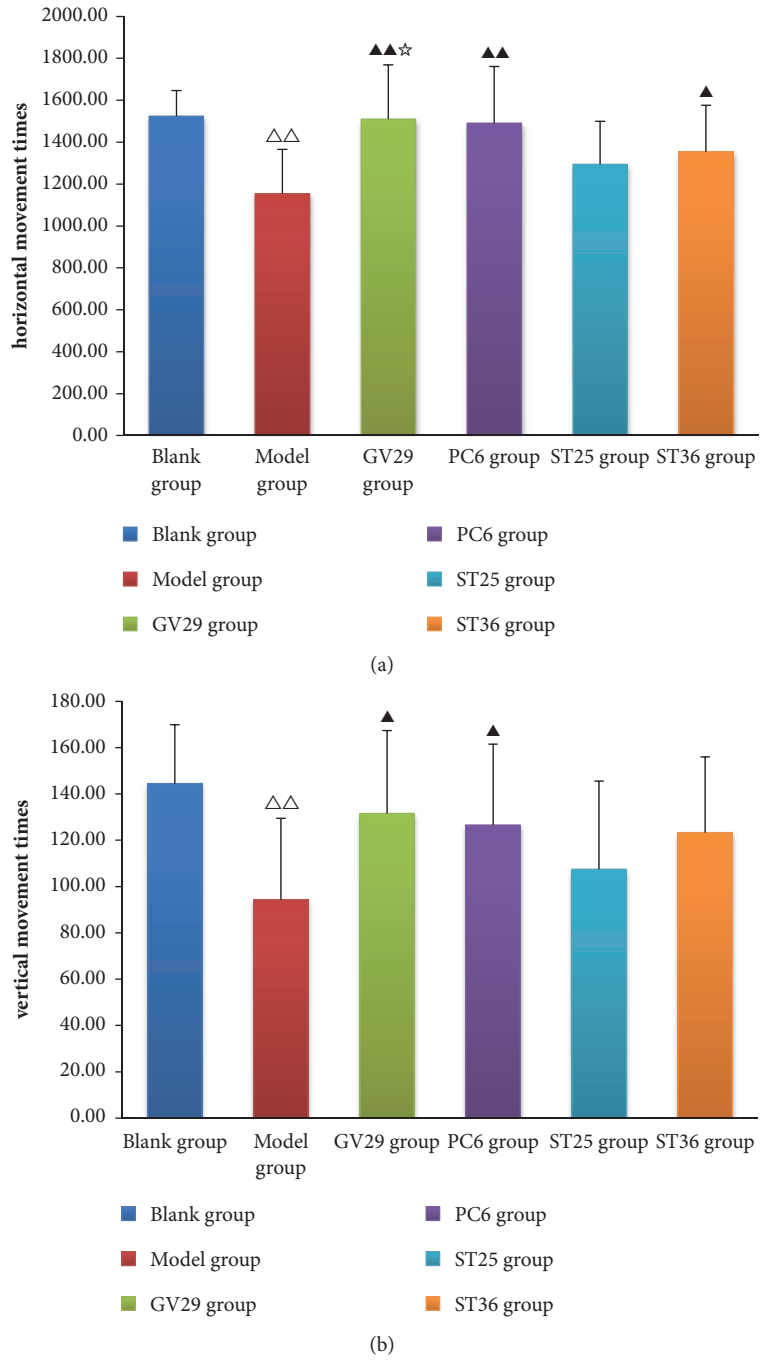

Figure 2: (a) Bar chart demonstrating the horizontal movement times, (b) bar chart demonstrating the vertical movement times. Data are presented as mean ± SD (n=10). Note: $^{\triangle\triangle}P<0.01$, versus blank group; $^{\blacktriangle\blacktriangle}P<0.01$, $^{\blacktriangle}P<0.05$, versus model group; $^{\star}P<0.05$, versus ST25 group.

GV29 belongs to Governor Vessel, which goes into the brain and its functions are closely related to the brain. The clinical studies [39, 40] found that "GV29" could regulate Governor Vessel and relieve the symptoms of insomnia, anxiety, and depression in patients with liver disease; meanwhile, GV29 also had certain curative effect on IBS [41]. Another study [42] has demonstrated that the psychiatric disorder-related cerebral functional regions, such as the frontal lobe, cingulate gyrus, and cerebellum, could be activated by stimulating GV29. The mechanism may be that acupuncture GV29 point after nerve impulses can be directly into the brain resulting in sedative effect caused by 5-TH, NE, BDNF, and other neurotransmitter release [43], thus creating a tranquilizing effect. PC6 has the effect of calming the mind due to the close relationship between the pericardium and the heart. Moreover, PC6 is the *Luo*-connecting point of pericardium meridian to connect triple energizer meridian, which could rectify Qi to regulate the function of intestine. Acupuncture

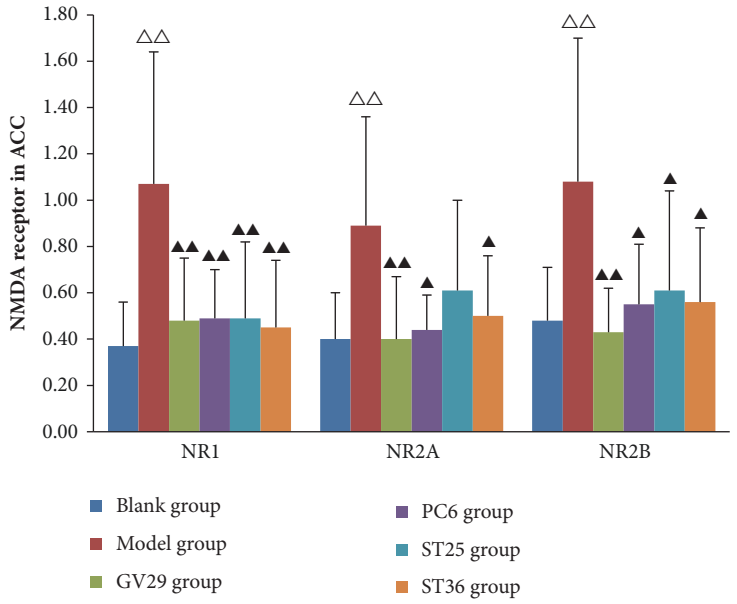

Figure 3: Bar chart demonstrating the NMDA receptor in ACC. Data are presented as mean ± SD (n=6). Note: $^{\triangle\triangle}P<0.01$, $^{\triangle}P<0.05$, versus blank group; $^{\blacktriangle\blacktriangle}P<0.01$, $^{\blacktriangle}P<0.05$, versus model group.

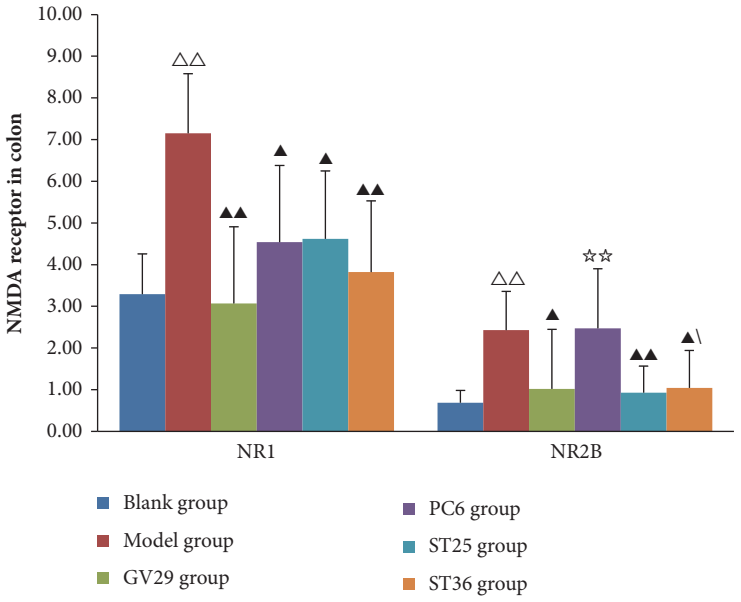

Figure 4: Bar chart demonstrating the NMDA receptor in colon. Data are presented as mean ± SD (n=6). Note: $^{\triangle\triangle}P<0.01$, versus blank group; $^{\blacktriangle\blacktriangle}P<0.01$, $^{\blacktriangle}P<0.05$, versus model group; $^{\star\star}P<0.01$, versus ST25 group.

on PC6 has a therapeutic effect on depression and anxiety [44] and can relieve the damage of astrocytes caused by chronic stress and play an antidepressant role possibly by upregulating the expression of GFAP in prefrontal cortex [45]. Li Wenwen et al. [46] found that the corresponding changes of brain waves occurred in the frontal lobe and cingulate cortex area of brain when stimulating PC6 point, and the central alpha wave energy was enhanced after stimulating PC6 point. Modern experimental research [47] had proved that acupuncture at PC6 can accelerate gastric emptying and improve dyspepsia and has an auxiliary therapeutic effect on IBS [48]. Therefore, applying EA at PC6 point not only can calm mind, but also can adjust the intestine, regulating the body and the psychic simultaneously. ST25, "the Front-Mu point" of large intestine is the main source of Qi and blood in the large intestine, and it is the first choice for treating intestinal diseases. Liu et al. [49] found that acupuncture at ST25 has bidirectional regulation effect on intestinal movement and has good curative effect on constipation and diarrhea. ST25 is one of the most commonly used acupoints to treat

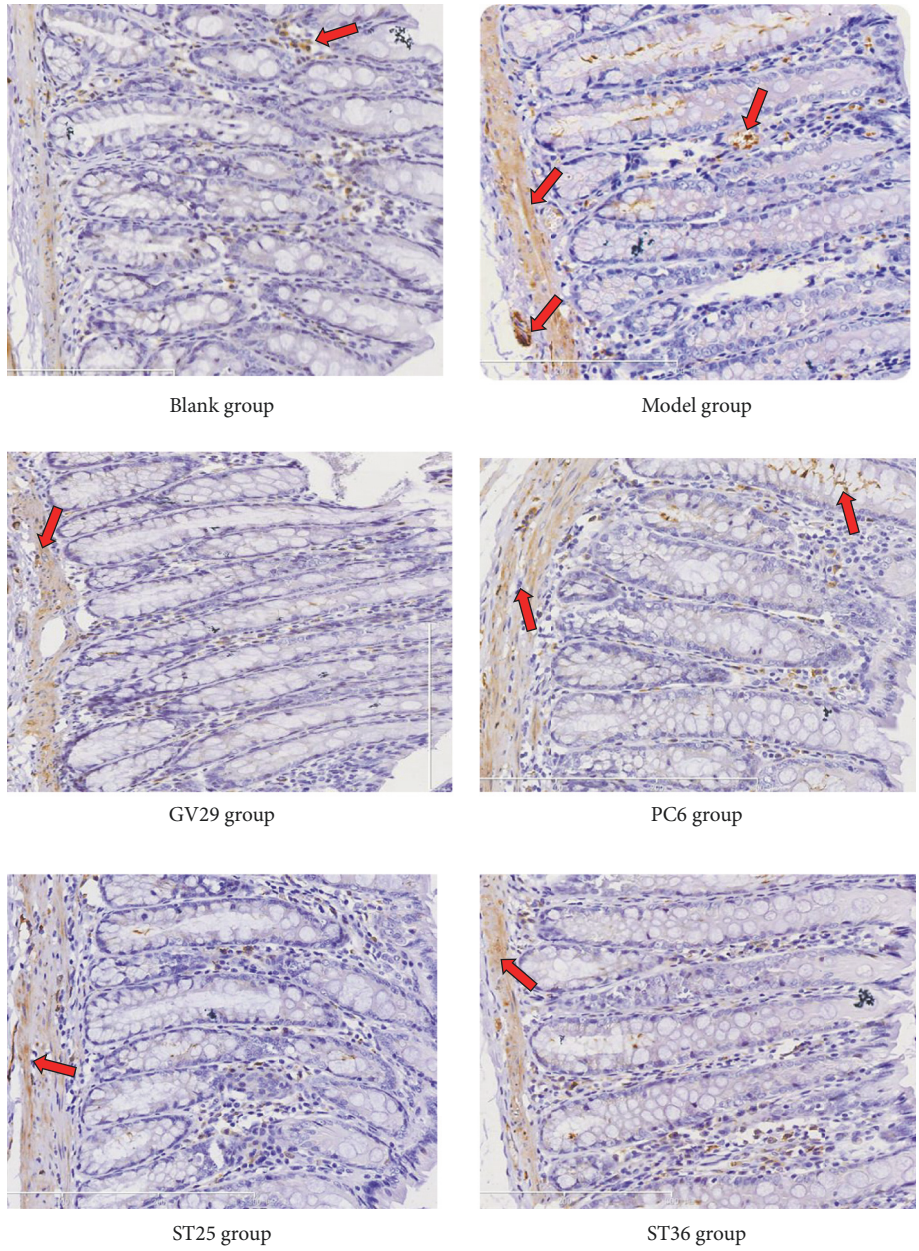

Figure 5: Representative photomicrographs showing immunohistochemical expression of NR2B (yellow or brown) in ACC (×200).

diarrhea-predominant IBS [50]. ST36 point is the "lower He-Sea point" of stomach and good at treating gastrointestinal diseases [51, 52]. EA at ST36 restores the rectal distension induced impairment in both colonic contraction and transit by enhancing vagal activity mediated via the cholinergic pathway [53]; EA ST36 also attenuates hemorrhage-induced intestinal inflammatory insult and protects the intestinal barrier integrity [54]. In addition, study found that EA at ST36 could relieve depression [55] and the effect of relieving the depressive behavior of rats was related to its pertaining meridian [56]. Wu et. al [56] found that electroacupuncture at ST36 can regulate the expression of βCaMKII in the lateral habenular nucleus and the protein of hippocampal brain derived neurotrophic factor (BDNF) to relieve depression.

Modern research [57] shows that the indication function of acupoints is related to the spinal segment of the acupoint and acupuncture has a reflex neuromodulation effect on viscera. Acupoints controlled by different spinal segments can regulate viscera, but their effects are different [58]. The upper nerve of the trochlear dominated the superficial skin and the temporal branch of the facial nerve dominated the muscle layer of GV29 in human body. Acupuncture at GV29 point can directly introduce impulses into hypothalamus, hippocampus, and prefrontal cortex, which are closely related to emotion [59]. Wang Jinjin et al. [60] observed the muscles distribution of acupoints in distal limbs of twelve meridians and found that PC6 is controlled by C7 ~ T1 nerves, ST36 mainly controlled by L4~S1 nerves, and ST25 controlled by

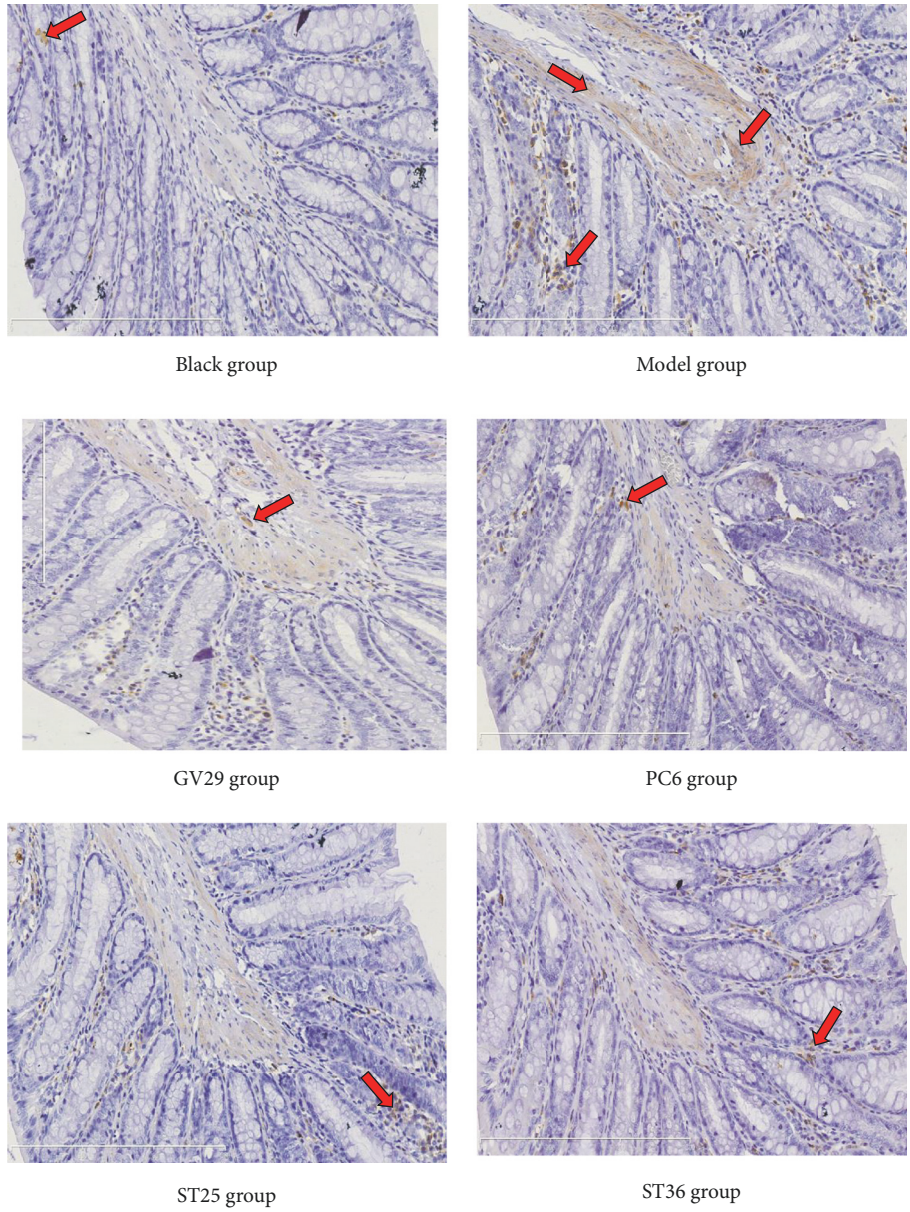

Figure 6: Representative photomicrographs showing immunohistochemical expression of NR2B (yellow or brown) in colon (×200).

T9~T11 nerves. The nerves derived from T10-L3 and the sacral plexus govern the large intestine. Thus, the spinal segment of the large intestine overlaps with that of ST25 and is adjacent to that of ST36. The study [61] demonstrates that the acupoint specificity existing in acupuncture relieves visceral hypersensitivity and the effects are more predominant at the acupoints on stomach meridian innervated by the same or adjacent spinal segments. Chen Xiaoman [62] found that the analgesic effect of local acupoint extraction on IBS abdominal pain is superior to distal acupoint, and the possible mechanism might be that there are more overlaps of spinal segments controlling viscera and nearby local points. After acupuncture, the regulating effect on gastrointestinal motility is achieved through the body surface-sympathetic reflex pathway [63]. Therefore, the analgesic effect of acupuncture at ST25 is more obvious. So according to the spinal segment domination of the acupoint, GV29, a point on the head, has better effect in regulating mood and ST25 located in the abdomen is better in relieving abdominal pain, while PC6 and ST36 have their own specific effects and indications. This is consistent with the results of this study.

The results show that the acupoint effect is specific, but this specificity is relative. Chinese medicine regards the human body as a whole. It believes that there is interaction between viscera and emotion, and the same among viscera. Which is consistent with "biopsychosocial" medicine mode [64], "psychosomatic disease", and "brain-gut axis" [65]. Due to the organism being considered as a whole, EA at acupoints located in different parts can alleviate IBS abdominal pain and relieve abnormal emotion by changing the internal

environment. However, the specificity of acupuncture effect is relative. The reason is that the regulatory intensity of the same neurotransmitter receptors is different in different tissues. The results of our study provide some experimental evidence for the specificity of acupuncture points, which is one of the important guiding principles for point selection in clinical treatment.

Data Availability

The data used to support the findings of this study are available from the corresponding author upon request.

Conflicts of Interest

The authors declare that they have no conflicts of interest regarding the publication of this paper.

Authors' Contributions

Li-hua Tan and Xiao-xuan Ren contributed equally to this work. Li-hua Tan performed the experiments and prepared the manuscript. Xiao-xuan Ren designed the study and revised the manuscript. Meng-wei Guo and Wen-lian Zhu supervised the experiments. Kai-ge Li and Yan-ying Wu performed the experimental work and data collection. Yin Lan and Shan Wang analyzed the data. All authors read and approved the final version of the manuscript accepted for publication.

Acknowledgments

This research was funded by the National Natural Science Foundation of China (NO-81473776): the specificity of acupoint effect based on the discharge of neurons in IBS rats.

References

[1] L. Zhao, J. Chen, C.-Z. Liu et al., "A review of acupoint specificity research in China: Status quo and prospects," *Evidence-Based Complementary and Alternative Medicine*, vol. 2012, Article ID 543943, 16 pages, 2012.

[2] D. Li, M. Yang, L. Zhao et al., "Acupuncture for chronic, stable angina pectoris and an investigation of the characteristics of acupoint specificity: study protocol for a multicenter randomized controlled trial," *Trials*, vol. 15, no. 50, 2014.

[3] M. Yang, J. Yang, F. Zeng et al., "Electroacupuncture stimulation at sub-specific acupoint and non-acupoint induced distinct brain glucose metabolism change in migraineurs: A PET-CT study," *Journal of Translational Medicine*, vol. 12, article 351, 2014.

[4] Y. Shan, J.-J. Wang, Z.-Q. Wang et al., "Neuronal specificity of acupuncture in alzheimer's disease and mild cognitive impairment patients: A functional MRI study," *Evidence-Based Complementary and Alternative Medicine*, vol. 2018, Article ID 7619197, 10 pages, 2018.

[5] X. Gao, Y. Zhao, Y. Su et al., "β1/2 or M2/3 receptors are required for different gastrointestinal motility responses induced by acupuncture at heterotopic or homotopic acupoints," in *PLoS ONE*, vol. 11, no 12, 2016.

[6] Q. Qin, X. Y. Gao, K. Liu et al., "Acupuncture at heterotopic acupoints enhances jejunal motility in constipated and diarrheic rats," *World Journal of Gastroenterology*, vol. 20, no. 48, pp. 18271–18283, 2014.

[7] B. Chen, S.-X. Hu, B.-H. Liu et al., "Efficacy and safety of electroacupuncture with different acupoints for chemotherapy-induced nausea and vomiting: study protocol for a randomized controlled trial," *Trials*, vol. 16, no. 1, article 212, 2015.

[8] P. Enck, Q. Aziz, G. Barbara et al., "Irritable bowel syndrome," *Nature Reviews Disease Primers*, vol. 2, article 16014, 2016.

[9] S. W. Tsang, K. K. W. Auyeung, Z. X. Bian, and J. K. S. Ko, "Pathogenesis, experimental models and contemporary pharmacotherapy of irritable bowel syndrome: Story about the brain-gut axis," *Current Neuropharmacology*, vol. 14, no. 8, pp. 842–856, 2016.

[10] M. Rodríguez-Muñoz, P. Sánchez-Blázquez, M. Merlos, and J. Garzón-Niño, "Endocannabinoid control of glutamate NMDA receptors: The therapeutic potential and consequences of dysfunction," *Oncotarget* , vol. 7, no. 34, pp. 55840–55862, 2016.

[11] S. Maeng and C. A. Zarate Jr., "The role of glutamate in mood disorders: Results from the ketamine in major depression study and the presumed cellular mechanism underlying its antidepressant effects," *Current Psychiatry Reports*, vol. 9, no. 6, pp. 467–474, 2007.

[12] S. Bradesi, V. Golovatscka, H. S. Ennes et al., "Role of astrocytes and altered regulation of spinal glutamatergic neurotransmission in stress-induced visceral hyperalgesia in rats," *American Journal of Physiology-Gastrointestinal and Liver Physiology*, vol. 301, no. 3, pp. G580–G589, 2011.

[13] A. Miranda, A. Mickle, M. Bruckert, P. Kannampalli, B. Banerjee, and J. N. Sengupta, "NMDA receptor mediates chronic visceral pain induced by neonatal noxious somatic stimulation," *European Journal of Pharmacology*, vol. 744, pp. 28–35, 2015.

[14] C. Lin and E. D. Al-Chaer, "Differential effects of glutamate receptor antagonists on dorsal horn neurons responding to colorectal distension in a neonatal colon irritation rat model," *World Journal of Gastroenterology*, vol. 11, no. 41, pp. 6495–6502, 2005.

[15] M.-X. Chen, Y. Chen, R. Fu et al., "Activation of 5-HT and NR2B contributes to visceral hypersensitivity in irritable bowel syndrome in rats," *American Journal of Translational Research*, vol. 8, no. 12, pp. 5580–5590, 2016.

[16] J.-J. Zhu, S. Liu, X.-L. Su et al., "Efficacy of chinese herbal medicine for diarrhea-predominant irritable bowel syndrome: a meta-analysis of randomized, double-blind, placebo-controlled trials," *Evidence-Based Complementary and Alternative Medicine*, vol. 2016, Article ID 4071260, 15 pages, 2016.

[17] H.-Y. Qin, H.-T. Xiao, F.-P. Leung et al., "JCM-16021, a chinese herbal formula, attenuated visceral hyperalgesia in TNBS-induced postinflammatory irritable bowel syndrome through reducing colonic EC cell hyperplasia and serotonin availability in rats," *Evidence-Based Complementary and Alternative Medicine*, vol. 2012, Article ID 239638, 12 pages, 2012.

[18] E. Manheimer, K. Cheng, L. S. Wieland et al., "Acupuncture for treatment of irritable bowel syndrome," *The Cochrane Database of Systematic Reviews*, vol. 5, Article ID CD005111, 2012.

[19] Y. Mo, H. Yao, H. Song et al., "Alteration of behavioral changes and hippocampus galanin expression in chronic unpredictable mild stress-induced depression rats and effect of electroacupuncture treatment," *Evidence-Based Complementary*

and Alternative Medicine, vol. 2014, Article ID 179796, 8 pages, 2014.

[20] Y. H. Gao, C. W. Li, J. Y. Wang et al., "Effect of electroacupuncture on the cervicospinal P2X7 receptor/fractalkine/CX3CR1 signaling pathway in a rat neck-incision pain model," *Purinergic Signalling*, vol. 13, no. 2, pp. 215–225, 2017.

[21] L. D. Wang, J. M. Zhao, R. J. Huang et al., "Study on the mechanism underlying the regulation of the NMDA receptor pathway in spinal dorsal horns of visceral hypersensitivity rats by moxibustion," *Evidence-Based Complementary and Alternative Medicine*, vol. 2016, Article ID 3174608, 11 pages, 2016.

[22] E. D. Al-Chaer, N. B. Lawand, K. N. Westlund, and W. D. Willis, "Pelvic visceral input into the nucleus gracilis is largely mediated by the postsynaptic dorsal column pathway," *Journal of Neurophysiology*, vol. 76, no. 4, pp. 2675–2690, 1996.

[23] J.-P. Yang, M. Yao, L.-N. Wang, and X.-H. Jiang, "Establishment of model of visceral pain due to colorectal distension and its behavioral assessment in rats," *World Journal of Gastroenterology*, vol. 12, no. 17, pp. 2781–2784, 2006.

[24] L. Prut and C. Belzung, "The open field as a paradigm to measure the effects of drugs on anxiety-like behaviors: a review," *European Journal of Pharmacology*, vol. 463, no. 1–3, pp. 3–33, 2003.

[25] G. C. Bird, L. L. Lash, J. S. Han, X. Zou, W. D. Willis, and V. Neugebauer, "Protein kinase A-dependent enhanced NMDA receptor function in pain-related synaptic plasticity in rat amygdala neurones," *The Journal of Physiology*, vol. 564, no. 3, pp. 907–921, 2005.

[26] T.-T. Li, W.-H. Ren, X. Xiao et al., "NMDA NR2A and NR2B receptors in the rostral anterior cingulate cortex contribute to pain-related aversion in male rats," *PAIN*, vol. 146, no. 1-2, pp. 183–193, 2009.

[27] L.-G. Lei, S. Sun, Y.-J. Gao, Z.-Q. Zhao, and Y.-Q. Zhang, "NMDA receptors in the anterior cingulate cortex mediate pain-related aversion," *Experimental Neurology*, vol. 189, no. 2, pp. 413–421, 2004.

[28] W.-H. Ren, J.-D. Guo, H. Cao et al., "Is endogenous D-serine in the rostral anterior cingulate cortex necessary for pain-related negative affect?" *Journal of Neurochemistry*, vol. 96, no. 6, pp. 1636–1647, 2006.

[29] L. Zong, G. Jun, W. Lei et al., "Changes of NR2A and NR2B expression in anterior cingulate cortex of visceral hypersensitivity rats after inflammation," *Gastroenterology*, vol. 15, no. 6, 331 pages, 2010.

[30] R. Wenhua, "Role of the NMDA receptor in the rostral cortex of the anterior cingulate cortex in pain aversion in rats," vol. 37, Fudan University, Shanghai, China, 2007.

[31] H. Junjing, J. Jinjin, and Z. Lin, "Changes in the expression of NR2A and NR2B in anterior cingulate cortex after enteritis in young rats," *Chinese Journal of Clinicians*, vol. 7, no. 6, pp. 2583-2586, 2013.

[32] A. Y. Del Valle-Pinero, S. K. Suckow, Q. Zhou, F. M. Perez, G. N. Verne, and R. M. Caudle, "Expression of the N-methyl-d-aspartate receptor NR1 splice variants and NR2 subunit subtypes in the rat colon," *Neuroscience*, vol. 147, no. 1, pp. 164–173, 2007.

[33] Q. Qingqing, *Colon N- Methyl -D- Aspartate Receptor Is Involved in The Pathogenesis of Visceral Hypersensitivity in Irritable Bowel Syndrome*, Shandong University, 2016.

[34] C. J. Wu, T. E. Ziea, L. Lao et al., "Effect of Electroacupuncture on visceral hyperalgesia, serotonin and fos expression in an animal model of irritable bowel syndrome," *Journal of Neurogastroenterology & Motility*, vol. 16, no. 3, pp. 306–314, 2010.

[35] Y. Wu, Y. Jiang, X. He et al., "5-HT in the dorsal raphe nucleus is involved in the effects of 100-Hz electro-acupuncture on the pain-depression dyad in rats," *Experimental and Therapeutic Medicine*, vol. 14, no. 1, pp. 107–114, 2017.

[36] F. Jianqiao and S. Xiaomei, "The new idea of Acupuncture Analgesia - the feasibility of acupuncture and moxibustion in the multidimensional regulation of pain," *Acupuncture Study*, vol. 01, pp. 85–89, 2017.

[37] Y. Huang, Y.-T. Yang, X.-X. Liu et al., "Effect of herbal-partitioned moxibustion at Tianshu (ST 25) and Qihai (CV 6) on pain-related behavior and emotion in rats with chronic inflammatory visceral pain," *Journal of Acupuncture and Tuina Science*, vol. 13, no. 1, pp. 1–8, 2015.

[38] G. Mengwei, Z. Yafang, W. Shun et al., "Effect of electroacupuncture at Baihui and Zusanli on behavior of IBS rats and expression of CGRP mRNA in thalamus," *Journal of Changchun University of Traditional Chinese Medicine*, vol. 33, no. 1, pp. 31–33, 2017.

[39] X. Yin, J. Xu, B. Dong et al., "Efficacy and safety of electroacupuncture on treating depression related sleep disorders: study protocol of a randomized controlled trial," *Evidence-Based Complementary and Alternative Medicine*, vol. 2016, Article ID 1069597, 7 pages, 2016.

[40] J. Xu, Y. She, N. Su et al., "Effects of electroacupuncture on chronic unpredictable mild stress rats depression-like behavior and expression of p-ERK/ERK and p-P38/P38," *Evidence-Based Complementary and Alternative Medicine*, vol. 2015, Article ID 650729, 8 pages, 2015.

[41] Z. D. Wei, S. Jianhua, X. L. Zhou et al., "Study on the acupoint mechanism of the treatment of diarrhea type irritable bowel syndrome by Shugan Jianpi acupuncture treatment," *Journal of Changchun University of Traditional Chinese Medicine*, vol. 28, no. 4, pp. 583–586, 2012.

[42] Y. Zheng, S. Qu, N. W. Wang et al., "Post-stimulation effect of electroacupuncture at *Yintang* (EX-HN3) and GV20 on cerebral functional regions in healthy volunteers: a resting functional MRI study," *Acupuncture in Medicine*, vol. 30, no. 4, pp. 307–315, 2012.

[43] W. Guanchao, W. Xiao, Z. Xianbao et al., "Tongdu method of treating melancholia needle after stroke in patients with depression of 5-HT, NE and BDNF levels in the study of effect of," *Journal of Gansu College of Traditional Chinese Medicine*, vol. 32, no. 2, pp. 58–62, 2015.

[44] H. Kim, H.-J. Park, S.-M. Han et al., "The effects of acupuncture stimulation at PC6 (Neiguan) on chronic mild stress-induced biochemical and behavioral responses," *Neuroscience Letters*, vol. 460, no. 1, pp. 56–60, 2009.

[45] U. L. Jun, S. Jin, W. Bao et al., "Effects of acupuncture on astrocytes in prefrontal cortex of chronic stress depression rats," *Journal of Traditional Chinese Medicine*, vol. 55, no. 15, pp. 1323–1326, 2014.

[46] L. Wenwen, X. Guizhi, C. Xiaogang et al., "The time-frequency analysis of electroencephalogram alpha wave based on the magnetic stimulation Neiguan point," *Beijing Biomedical Engineering*, vol. 30, no. 3, pp. 263–268, 2011.

[47] S. Xu, X. Hou, H. Zha et al., "Electroacupuncture accelerates solid gastric emptying and improves dyspeptic symptoms in patients with functional dyspepsia," *Digestive Diseases and Sciences*, vol. 51, no. 12, pp. 2154–2159, 2006.

[48] C. Xusheng and Z. Town, "Acupuncture treatment of diarrhea type irritable bowel syndrome of traditional Chinese medicine," *Shanxi*, vol. 33, no. 1, pp. 35-35, 2017.

[49] L. Lijuan, Z. Lili, and Z. Fang, "Tianshu point, clinical analysis of digestive system diseases," *Liaoning Journal of Traditional Chinese Medicine*, vol. 3, pp. 403-401, 2013.

[50] L. Chen, Z. Yiwen, and W. Jian, "Acupuncture points for treating diarrhea predominant irritable bowel syndrome," *Jilin Chinese Medicine*, vol. 7, pp. 737–739, 2016.

[51] H. Liu, L. Qi, L. Wu et al., "Effects of moxibustion on dynorphin and endomorphin in rats with chronic visceral hyperalgesia," *World Journal of Gastroenterology*, vol. 16, no. 32, pp. 4079–4083, 2010.

[52] X. Gao, Y. Qiao, B. Jia et al., "NMDA receptor-dependent synaptic activity in dorsal motor nucleus of vagus mediates the enhancement of gastric motility by stimulating ST36," *Evidence-Based Complementary and Alternative Medicine*, vol. 2012, Article ID 438460, 11 pages, 2012.

[53] H. Jin, J. Liu, R. D. Foreman, J. D. Z. Chen, and J. Yin, "Electrical neuromodulation at acupoint st36 normalizes impaired colonic motility induced by rectal distension in dogs," *American Journal of Physiology-Gastrointestinal and Liver Physiology*, vol. 309, no. 5, pp. G368–G376, 2015.

[54] S. Hu, Z.-K. Zhao, R. Liu et al., "Electroacupuncture activates enteric glial cells and protects the gut barrier in hemorrhaged rats," *World Journal of Gastroenterology*, vol. 21, no. 5, pp. 1468–1478, 2015.

[55] S.-C. Man, B. H. B. Hung, R. M. K. Ng et al., "A pilot controlled trial of a combination of dense cranial electroacupuncture stimulation and body acupuncture for post-stroke depression," *BMC Complementary and Alternative Medicine*, vol. 14, article 255, 2014.

[56] Y. Wu, Y. Jiang, X. He et al., "Effects of electroacupuncture with dominant frequency at SP 6 and ST 36 based on meridian theory on pain-depression dyad in rats," *Evidence-Based Complementary and Alternative Medicine*, vol. 2015, Article ID 732845, 10 pages, 2015.

[57] A. Sato, Y. Sato, and S. Uchida, "Reflex modulation of visceral functions by acupuncture-like stimulation in anesthetized rats," *International Congress Series*, vol. 1238, no. C, pp. 111–123, 2002.

[58] Z. Yucui, Y. Jun, M Qingling et al., "Effect of electroacupuncture at different ganglion segments on gastric intragastric pressure in rats with gastric dyskinesia model," *Journal of Hunan University of Chinese Medicine*, vol. 31, no. 11, pp. 65–68, 2011.

[59] Q. Yanming and S. Y. Jing, "Effect of electroacupuncture and Baihui on monoamine neurotransmitters in different brain regions of Acquired Helplessness rats," *Journal of Beijing University of Chinese Medicine*, vol. 25, no. 6, pp. 54–56, 2002.

[60] W. Jinjin, J. Songhe, L. Shasha et al., "Twelve Meridian in the distal limbs acupoint and the spinal segment dominated rule," *Relationship Between Chinese Medicine*, vol. 06, pp. 1272-1273, 2008.

[61] S. J. Wang, H. Y. Yang, F. Wang, and S. T. Li, "Acupoint specificity on colorectal hypersensitivity alleviated by acupuncture and the correlation with the brain–gut axis," *Neurochemical Research*, vol. 40, no. 6, pp. 1274–1282, 2015.

[62] C. Xiaoman, "Clinical study of acupoint injection therapy in the treatment of anal pruritus," *Guangzhou University of Chinese Medicine*, pp. 18-19, 2016.

[63] T. Takahashi, "Mechanism of acupuncture on neuromodulation in the gut—a review," *Neuromodulation: Technology at the Neural Interface*, vol. 14, no. 1, pp. 8–12, 2011.

[64] G. L. Engel, "The need for a new medical model: a challenge for biomedicine," *Science*, vol. 196, no. 4286, pp. 129–136, 1977.

[65] F. Shanahan, "The brain-gut axis and the mucosal immunoinflammatory responsen," in *Neuroendocrinology of Gastrointestinal Ulceration*, pp. 103–108, Springer, 1995.

Hindawi
Evidence-Based Complementary and Alternative Medicine
Volume 2018, Article ID 7370891, 8 pages
https://doi.org/10.1155/2018/7370891

Research Article

Gegen Qinlian Decoction Attenuates High-Fat Diet-Induced Steatohepatitis in Rats via Gut Microbiota

Yi Guo,[1] **Pang-hua Ding**,[2,3] **Li-juan Liu**,[4] **Lei Shi**,[2,3] **Tang-you Mao**,[2] **Jun-xiang Li**,[2] **and Yun-liang Wang**[2]

[1]*Gastroenterology Department, Dongzhimen Hospital, Beijing University of Chinese Medicine, Beijing, 100700, China*
[2]*Gastroenterology Department, Dongfang Hospital, Beijing University of Chinese Medicine, Beijing, 100078, China*
[3]*Beijing University of Chinese Medicine, Beijing, 100029, China*
[4]*Gastroenterology Department of Traditional Chinese Medicine, China-Japan Friendship Hospital, Beijing, 100029, China*

Correspondence should be addressed to Yun-liang Wang; yunliang_wang@sina.com

Received 6 June 2018; Revised 25 September 2018; Accepted 9 December 2018; Published 23 December 2018

Guest Editor: Flávio Reis

Gut microbiota play an important role in modulating energy contribution, metabolism, and inflammation, and disruption of the microbiome population is closely associated with chronic metabolic diseases, such as nonalcoholic fatty liver disease (NAFLD). Gegen Qinlian decoction (GGQLD), a well-known traditional Chinese herbal medicine (CHM), was previously found to regulate lipid metabolism and attenuate inflammation during NAFLD pathogenesis. However, the underlying mechanism of this process, as well as how the gut microbiome is involved, remains largely unknown. In this study, we investigated the effect of varying doses of GGQLD on the total amount and distribution of gut bacteria in rats fed a high-fat diet (HFD) for 8 weeks. Our analysis indicates that Oscillibacter and Ruminococcaceae_g_unclassified are the dominant families in the HFD group. Further, HFD-dependent differences at the phylum, class, and genus levels appear to lead to dysbiosis, characterized by an increase in the Firmicutes/Bacteroidetes ratio and a dramatic increase in the Oscillibacter genus compared to the control group. Treatment with GGQLD, especially the GGQLL dose, improved these HFD-induced changes in intestinal flora, leading to increased levels of Firmicutes, Clostridia, Lactobacillus, bacilli, and Erysipelotrichales that were similar to the controls. Taken together, our data highlight the efficacy of GGQLD in treating NAFLD and support its clinical use as a treatment for NAFLD/NASH patients.

1. Introduction

Nonalcoholic fatty liver disease (NAFLD) is a type of liver disease that includes simple hepatic steatosis, nonalcoholic steatohepatitis (NASH), and irreversible cirrhosis [1]. NAFLD affects both children and adults worldwide and its prevalence is rapidly increasing in parallel with the dramatic rise in obesity, diabetes [2, 3], hypertension [4], and dyslipidemia [5]. Indeed, the prevalence of NAFLD was estimated to be 20-30% in Western countries and 5-18% in Asia [6] and was reported to be as high as 80% in patients with obesity while being only 16% in individuals with a normal BMI and no metabolic risk factors [7].

Although NAFLD is a growing challenge worldwide, its pathogenesis is not fully understood and the therapeutic options for patients are limited [8]. Disease pathogenesis was initially explained by the "two-hit" hypothesis, but this theory failed to explain various NAFLD-related molecular changes, resulting in the adoption of the "multiple-hit" hypothesis, which takes into account the complex and multifactorial aspects of the disease [9]. Although a combination of "hits" is likely necessary, each of these risk factors is still ultimately related to the hepatic accumulation of lipids caused by a high-fat diet (HFD) in combination with a sedentary lifestyle [10]. This includes insulin resistance, hormonal changes, and altered genetic factors.

Interestingly, the human gut microbiome, which includes 10–100 trillion microorganisms, has also been shown to play an important role in NAFLD pathogenesis [11]. In fact, a recent study showed that patients with small intestinal bacterial overgrowth (SIBO) have an increased risk of hepatic steatosis [12]. Obesity, which is an independent NAFLD risk

factor, has also been associated with gut dysbiosis [13, 14]. Furthermore, the link between the gut microbiota and NASH development was also investigated in mice fed a methionine choline-deficient diet, and the mechanism appears to involve disruption of the NLRP3 or NLRP6 inflammasome which induces colonic inflammation and NASH [15]. SIBO observed in NASH patients is also associated with Toll-like receptor (TLR) 4 expression and the release of interleukin-8 [16].

Although bacteria such as Bacteroidetes and Firmicutes make up the bulk of the gut microflora, nonbacterial organisms such as resident archaeal, fungal, and viral populations might also play a significant function [17]. Moreover, obesity appears to be linked to a decline in microbial diversity in the gut that is accompanied by an increase in the ratio of Firmicutes to Bacteroidetes [18]. Taken together, these and other studies suggest that gut microflora dysbiosis may increase gut permeability and hepatic exposure to injurious substances. These changes could greatly affect NAFLD development and progression as well as the responsiveness of patients to therapeutic strategies.

The proposed NAFLD management strategies often include lifestyle modifications and pharmaceutical interventions [7, 19, 20]. However, compliance with long-term lifestyle modification is poor and most medicines have adverse effects, which limit their usage [21]. Although there are huge expectations regarding the use and effectiveness of probiotics in modulating gut microbiota, the lack of solid evidence precludes their implementation in the management of NAFLD/NASH [22, 23]. Thus, it is necessary to develop novel strategies with fewer side effects and high therapeutic efficiency.

Chinese herbal medicine (CHM) has been used in China and other Asian countries for thousands of years and its use is now spreading worldwide. A unique and basic feature of CHM is the use of multicomponent herbal formulas to ameliorate various abnormalities and diseases. For example, formulas like Linggui Zhugan [24], Yinchenhao [25], and Gegen Qinlian decoction (GGQLD) [26] have been used to treat NAFLD. GGQLD, a well-known traditional CHM from the Treatise on Febrile Diseases, consists of *Kudzu root*, *Rhizoma coptidis, Scutellaria baicalensis Georgi,* and *Glycyrrhizae Radix* and is widely used to clinically treat NASH. This formula has been used for thousands of years in clinic. Besides, we have not discovered specific side effects and contraindications of GGQLD in the process of document retrieval and our experiments. Therefore, GGQLD, which is under conventional dose, has been regarded as a kind of safe and potential treatment in treating NASH until now. In our previous studies, we found that GGQLD has an anti-inflammatory effect [27, 28], which could regulate lipid metabolism disorders and improve liver histology of the rats during NAFLD pathogenesis [26, 29]. In addition, the active components of GGQLD, including baicalin, glabridin, and berberine, have been shown to alleviate inflammation and oxidative stress in vivo and in vitro [30, 31]. Although gut microflora is considered a critical "organ" that participates in nutrient metabolism and immunity in the host [32–34], the effects of GGQLD on gut microflora have not been evaluated.

In the present study, we established a HFD-induced rat model of NASH and administered GGQLD in different dosages to examine its effects and underlying mechanisms, focusing on changes in gut microflora. This involved monitoring the total amount and distribution of bacteria in the gut as well as the relative abundance of different taxa and presence of specific harmful microorganisms in both untreated and GGQLD-treated NASH rats. To our knowledge, this is the first time the effects of GGQLD have been assessed with regard to gut microflora in NAFLD/NASH.

2. Materials and Methods

2.1. Preparation of GGQLD and Glutamine. GGQLD granules were provided by the Pharmacy Department of Dongfang Hospital, Beijing University of Chinese Medicine (Beijing, China). The granules consisted of the following ingredients: *Kudzu root* (24 g), *Rhizoma coptidis* (9 g), *Scutellaria baicalensis Georgi* (9 g), and *Glycyrrhizae Radix* (6 g). Glutamine (GLU) was purchased from AMRESCO Co., Ltd. (Missouri, TX, USA).

2.2. Animals, Treatment, and Sample Collection. Male Sprague-Dawley (SD) rats (7 weeks old) were supplied by SPF Biotechnology Co. Ltd. (Beijing, China). All experimental procedures were approved by the Animal Ethics Committee of Beijing University of Chinese Medicine (No. 2015BZHYLL0201) and followed the Regulations for Laboratory Animal Management. SD rats were maintained on a 12 h light/dark cycle at 22 ± 2°C with ad libitum access to a standard chow diet (n = 10) or a HFD (34% fat, 19% protein, and 47% carbohydrate by energy composition) for 8 weeks to induce NAFLD. Animals were randomly divided into the following experimental groups (each n = 10): control group, fed a standard chow diet and oral saline (10 mL/kg/day); HFD model group, fed a HFD and oral saline (10 mL/kg/day); GLU group, fed a HFD and oral GLU (1.5 g/kg/day); GGQLL group, fed a HFD and low dose GGQLD (1.26 g/kg/day); GGQLS group, fed a HFD and solid dose GGQLD (2.52 g/kg/day); and GGQLH group, fed a HFD and high dose GGQLD (5.04 g/kg/day). The GGQLD granules and GLU were dissolved in 100 mL of distilled water and kept at 2–8°C until use. Feedings occurred daily during the 8-week experimental period. Fresh stool samples were collected at the end of the eight-week treatment and stored at −80°C until further analysis.

2.3. Sequencing Analysis of Microbial Diversity. We followed the methods of Shin et al. (2017) [35]. DNA was extracted from the fecal samples by standard, published protocols. Three relatively conserved variable regions (V1, V2, and V3) of 16S rRNA were performed using a C1000 Touch thermal cycler (Bio-Rad, Hercules, CA, USA).

The obtained sequence data were sorted by their unique barcodes in a demultiplexing step, and low-quality reads (average quality score <25 or read length <300 bp) were not considered for analysis. Operational taxonomic units (OTUs) were defined at a cutoff of 97%. Sequences were assigned

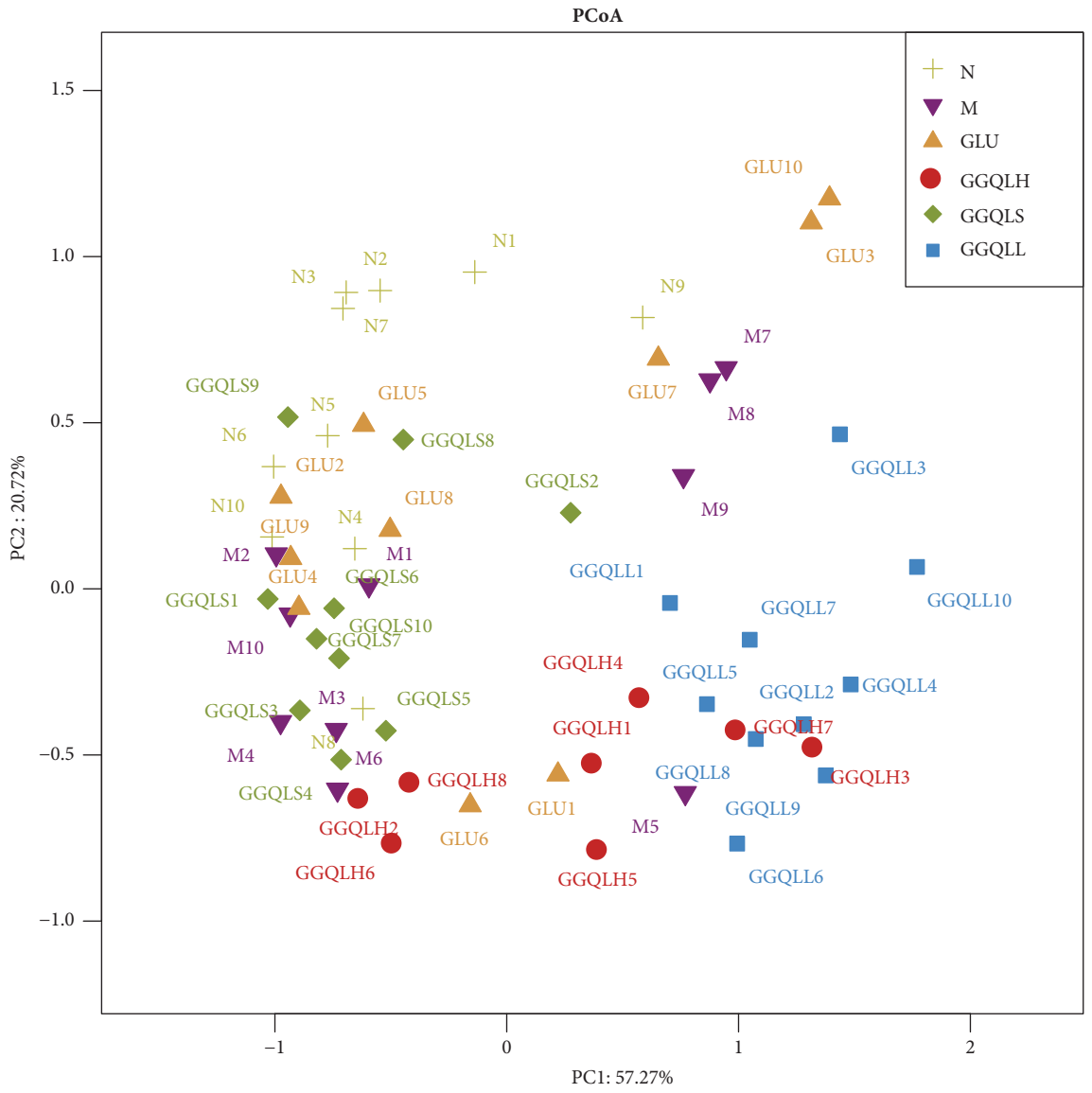

FIGURE 1: Principal component analysis (PCoA) score plot calculated from the operational taxonomic unit (OUT) levels with QIIME software and unweighted UniFrac analysis.

to OTUs (Greengenes Database: http://greengenes.lbl.gov) followed by the selection of the representative sequence using the Quantitative Insights into Microbial Ecology (QIIME) software package. Phylogenetic Investigation of Communities by Reconstruction of Unobserved States (PICRUSt) was performed to identify functional genes in the sampled microbial community on the basis of the data in the Kyoto Encyclopedia of Genes and Genomes (KEGG) pathway database.

To identify taxa with differential relative abundance in each experimental group, the linear discriminant analysis (LDA) effect size (LEfSe) method was used. For this analysis, a web-based program was employed with the following conditions: the alpha value of the factorial Kruskal-Wallis test among classes was set to <0.05 and the threshold of the logarithmic LDA score for discriminative features was set to >2.0.

3. Results

To profile the effect of GGQLD on gut microbial structure and composition in NAFLD rats, stool samples were sequenced for the 16S rRNA gene. According to our principal component analysis (PCoA), which divided the microbiome according to species composition, the gut composition of the HFD group was easily distinguished from the control, GGQLH, and GGQLL groups (Figure 1). Furthermore, the distance between the HFD and GGQLL groups was greater than that between the HFD group and both the GGQLH and GGQLS groups.

The microbial composition for each group was further analyzed at the phylum and genus levels. A heatmap analysis of 150 OTUs showed that the gut microbiome composition of the GGQLL group was closely related to that of the control group, both of which were different from the HFD group

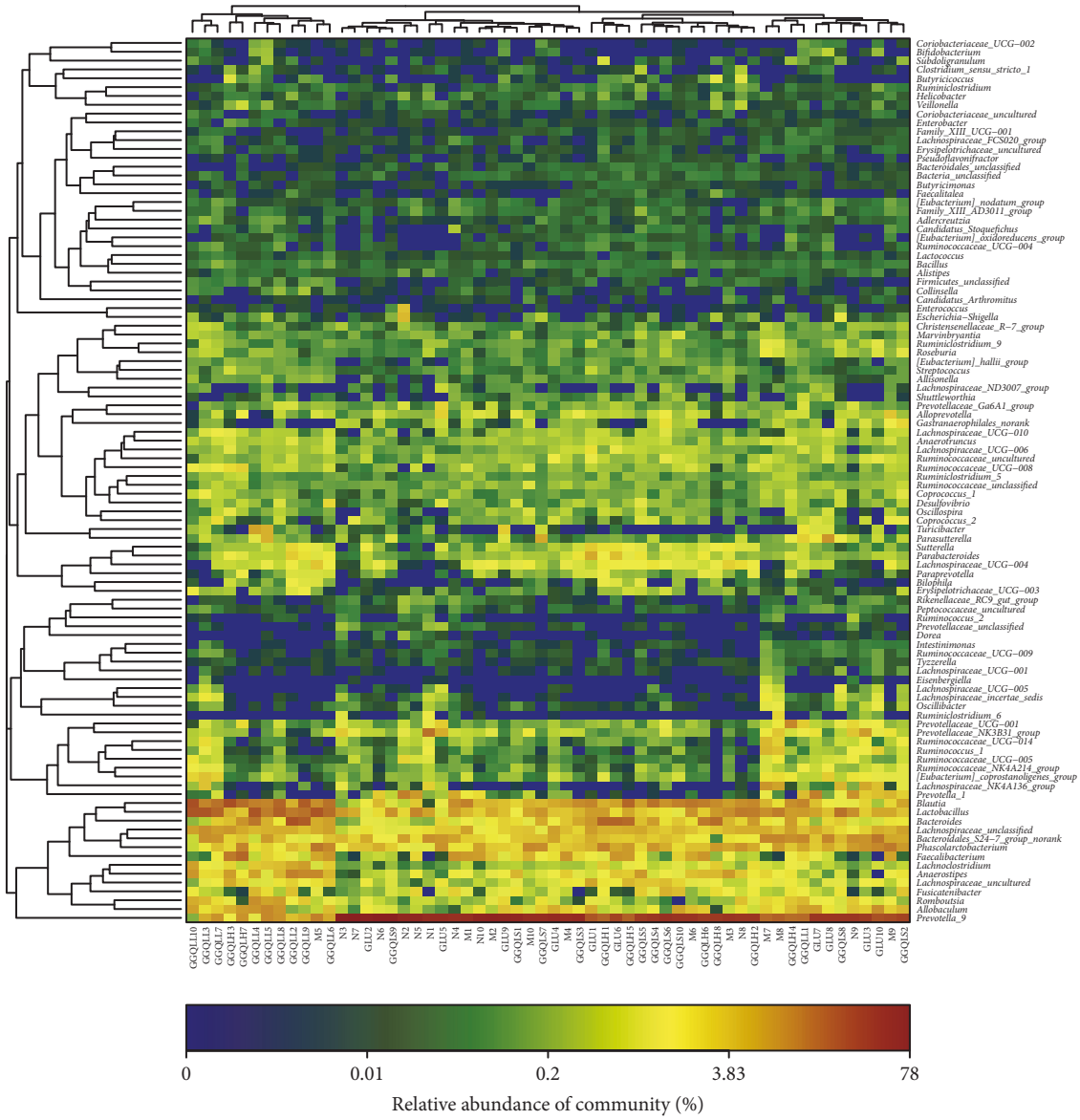

Figure 2: Heatmap and clustering of individual gut microbiota for 150 operational taxonomic units (OTUs).

(Figure 2). Bacteroidetes was the dominant class in the control, GLU, and GGQLS groups, contributing to 69.6%, 57.7%, and 56.2% of the total fecal microbial population, respectively. In contrast, Firmicutes was the dominant class in the HFD, GGQLH, and GGQLL groups, contributing to 50.9%, 57.1%, and 74.7% of the total fecal microbial population, respectively. Like phylum, microbial family also varied greatly among the experimental groups. The dominant family was Prevotella_9 in Bacteroidetes contributing to 56.1%, 35.7%, 40.8%, 21.4%, and 45.6% of the total fecal microbial population in the control, HFD, GLU, GGQLH, and GGQLS groups (Figure 3). The only exception was the GGQLL group, whose dominant family was Lactobacillus contributing to 15.8%.

Next, the LEfSe method was used to determine the differentially abundant microbial taxa between the experimental groups. The cladogram from the LEfSe results revealed that, compared with the other groups, two taxa were increased in the HFD group (Figure 4). In the control, GLU, GGQLS, GGQLL, and GGQLH groups, a total of 19, 8, 7, 42, and 17 taxa were increased, respectively. Collectively, these results indicate that the gut microbial composition was differentially modulated in GGQLL rats in response to being fed HFD.

4. Discussion

It is important to note that there are numbers of studies that have investigated microbiota composition in patients with simple steatosis or NASH, However, the results are controversial. Indeed, changes in the *Bacteroidetes*, *Lachnospiraceae,* and *Ruminococcaceae* families show completely opposite tendencies in different studies [21, 36, 37]. Therefore,

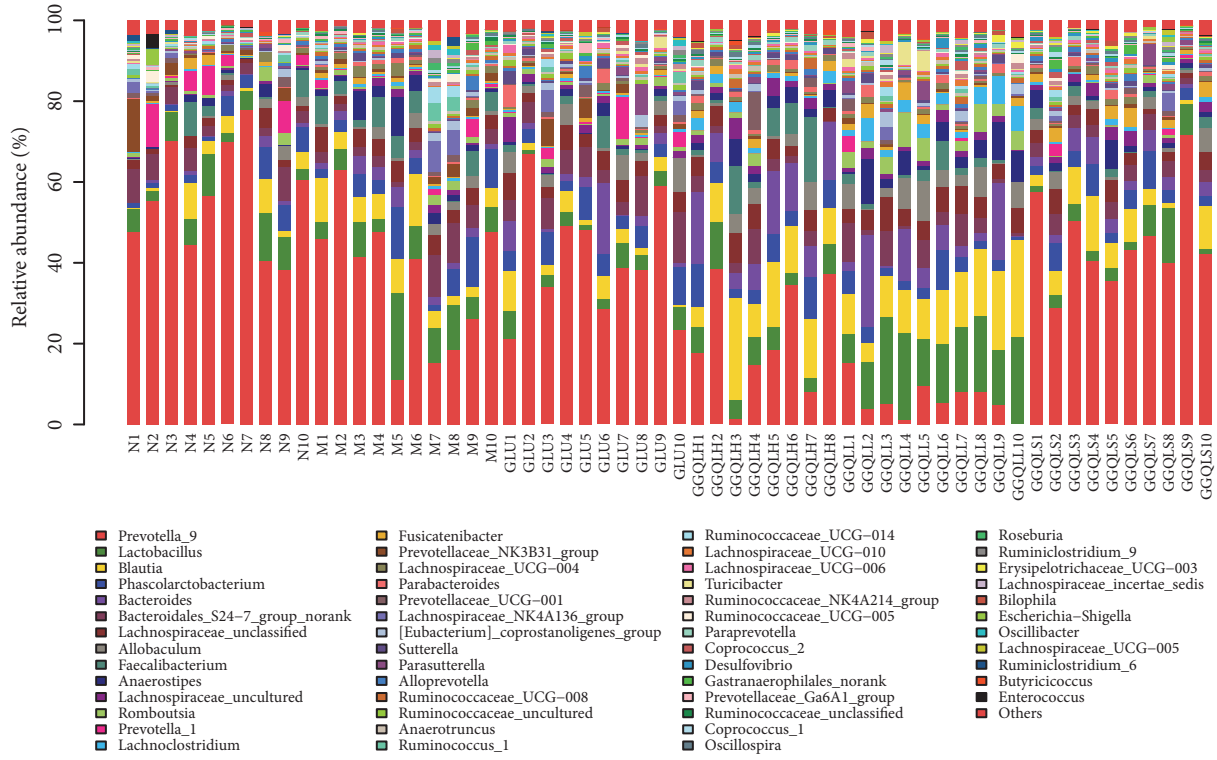

Figure 3: Relative abundance of various microbial families in each gut microbiota sample.

further evaluation of these changes in the gut microbiome during NAFLD is essential. Nowadays, the 16S rRNA method has been widely used for gut microbiome. Shin et al. set for us a good example of CHM research for treating NAFLD via gut microflora [35].

The mechanisms by which gut bacteria affect the symptoms of NAFLD are still largely unknown. However, some complicated processes have been indicated to be involved. Microbial populations of NASH patients have been proven to have a strong ability to produce ethanol [38] and some components of the gut microbiota can transform choline to trimethylamine, both of which can result in liver injury leading to hepatic steatosis and steatohepatitis [39, 40]. Furthermore, dysbiosis of gut microflora has been suggested to be related to changes in the level of serum metabolites, such as branched-chain amino acids (BCAAs) and aromatic amino acids (AAAs). Furthermore, BCAAs are increased in individuals with IR, which is regarded as the main risk factor of NASH [41].

In the present study, we utilized a HFD to induce NAFLD in rats. HFD feeding is extensively used in rodents to model obesity, steatosis, and insulin resistance. In fact, these models are considered more relevant to human metabolic diseases than other models of gene inactivation. By exploiting the close connection between intestinal permeability and the gastrointestinal microbiome, which represent the biological barrier in the gut, we investigated the relative abundance of different taxa in this HFD model. In our analysis, we observed HFD-dependent differences at the phylum, class, and genus levels that resulted in dysbiosis. These changes were characterized by an increase in the Firmicutes/Bacteroidetes ratio and a dramatic increase in the Oscillibacter genus compared to the control group.

Interestingly, studying the gut microbiome not only highlights disease-related changes, but the composition of the flora can also reflect the effectiveness of treatment. Although The proposed NAFLD is typically treated with lifestyle modifications and/or pharmaceutical intervention [7, 19, 20], these are associated with issues that limit their effectiveness. Furthermore, probiotic treatments to modulate the gut microbiome specifically still require further investigation before they can be recommended as a treatment for NAFLD [22, 23]. In the present study, we evaluated the effectiveness of GGQLD, a CHM that is commonly prescribed to treat NAFLD/NASH. We focused on the ability of this herbal formula to modulate the gut microbiome. In our analysis, GGQLD improved the HFD-induced changes in the intestinal flora, especially in the GGQLL group, which had increased levels of Firmicutes, Clostridia, Lactobacillus, bacilli, and Erysipelotrichales. These data are supported by other studies reporting similar results [42].

In a previous study, we found that GGQLD treatment reduced serum sIgA levels in this HFD-induced NASH rat model in addition to increasing zonula occludens-1 (ZO-1) expression and reducing prostaglandin E2 (PGE2) expression in the gut [29]. ZO-1 is a tight junction protein that is closely related to gut function, while PGE2 is a bioactive lipid that mediates inflammation. These data indicate that GGQLD may enhance the barrier function of the gut, while also suppressing inflammation. Furthermore, we also found that

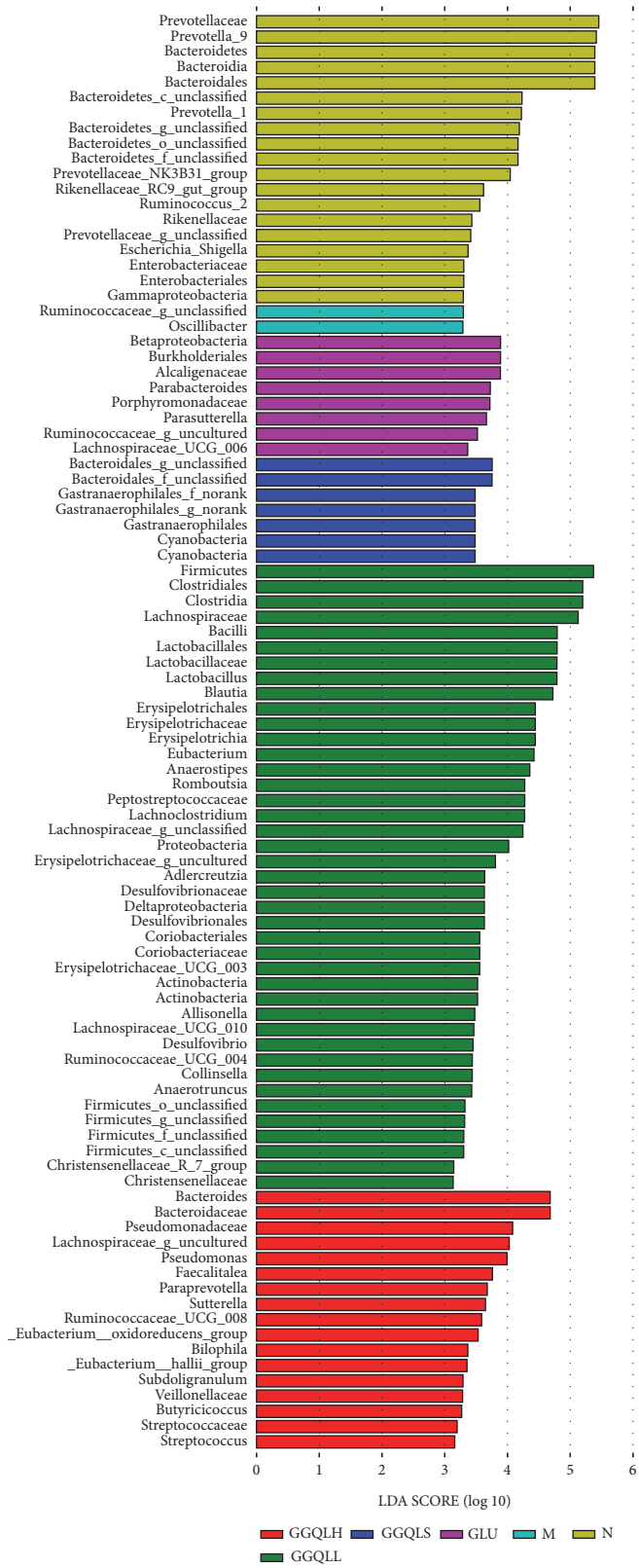

Figure 4: Cladogram showing the differentially abundant gut microbial taxa between experimental groups.

GGQLD regulated lipid aggregation and improved hepatic peroxisome proliferator-activated receptor-gamma (PPAR-γ) and insulin-resistance (IR) expression in vivo and in vitro [27], further highlighting the anti-inflammatory function of this CHM. Indeed, these changes appear to be modulated via the Sirt1 pathway. Sirt1, a regulator of PPAR-γ coactivator-1 alpha (PGC-1α), induces the transcription of metabolically relevant genes involved in the oxidation of mitochondrial fatty acids [43]. This cascade has a negative regulatory effect on inflammatory processes. Although some previous studies suggest that SIRT1 might prevent intestinal inflammation by regulating the gut microbiota [44], a theory that is supported by the present study, the interaction between the Sirt1 pathway and gut flora requires further investigation. Besides, some experiments suggest a potentially causal role of the gut microbiome and gut-microbiome-derived metabolites in the development of NAFLD such as phenylacetic acid, a novel microbial metabolite involved in AAA metabolism, which was identified as a key gut-microbiome-derived metabolite associated with hepatic steatosis. Therefore, we will explore the interaction between the gut microbiome, the liver, and metabolism under the effect of GGQLD through metabonomics.

In conclusion, we have shown that GGQLD treatment is effective in treating NAFLD/NASH via modulation of the gut microbiome. Indeed, the disease-related changes in abundance and distribution of different taxa in the gut microbiome that were observed in the HFD-induced NAFLD/NASH model were largely remedied following treatment with GGQLD, particularly GGQLL, which returned the microbiome to a similar composition as that of the untreated controls. To our knowledge, this is the first time the effects of GGQLD have been assessed with regard to gut microflora in NAFLD/NASH. Taken together, our data highlight the efficacy of GGQLD in treating NAFLD and support its clinical use as a treatment for NAFLD/NASH patients.

Data Availability

The data used to support the findings of this study are available from the corresponding author upon request.

Conflicts of Interest

The authors declare that there are no conflicts of interest regarding the publication of this paper.

Authors' Contributions

Yi Guo and Pang-hua Ding contributed equally to this work.

Acknowledgments

This study was supported by the Youth Fund of the Natural Science Foundation of China (grant no. 81503407).

References

[1] D. A. Sass, P. Chang, and K. B. Chopra, "Nonalcoholic fatty liver disease: a clinical review," *Digestive Diseases and Sciences*, vol. 50, no. 1, pp. 171–180, 2005.

[2] M. Charlton, "Nonalcoholic fatty liver disease: a review of current understanding and future impact," *Clinical Gastroenterology and Hepatology*, vol. 2, no. 12, pp. 1048–1058, 2004.

[3] R. Vuppalanchi and N. Chalasani, "Nonalcoholic fatty liver disease and nonalcoholic steatohepatitis: selected practical issues in their evaluation and management," *Hepatology*, vol. 49, no. 1, pp. 306–317, 2009.

[4] J.-H. Ryoo, Y. J. Suh, H. C. Shin, Y. K. Cho, J.-M. Choi, and S. K. Park, "Clinical association between non-alcoholic fatty liver disease and the development of hypertension," *Journal of Gastroenterology and Hepatology*, vol. 29, no. 11, pp. 1926–1931, 2014.

[5] N. Katsiki, D. P. Mikhailidis, and C. S. Mantzoros, "Non-alcoholic fatty liver disease and dyslipidemia: An update," *Metabolism - Clinical and Experimental*, vol. 65, no. 8, pp. 1109–1123, 2016.

[6] M. Masarone, A. Federico, L. Abenavoli, C. Loguercio, and M. Persico, "Non alcoholic fatty liver: epidemiology and natural history," *Reviews on Recent Clinical Trials*, vol. 9, no. 3, pp. 126–133, 2014.

[7] C. Eckard, R. Cole, J. Lockwood et al., "Prospective histopathologic evaluation of lifestyle modification in nonalcoholic fatty liver disease: a randomized trial," *Therapeutic Advances in Gastroenterology*, vol. 6, no. 4, pp. 249–259, 2013.

[8] J. K. Dowman, J. W. Tomlinson, and P. N. Newsome, "Pathogenesis of non-alcoholic fatty liver disease," *QJM: An International Journal of Medicine*, vol. 103, no. 2, pp. 71–83, 2010.

[9] E. Buzzetti, M. Pinzani, and E. A. Tsochatzis, "The multiple-hit pathogenesis of non-alcoholic fatty liver disease (NAFLD)," *Metabolism*, vol. 65, no. 8, pp. 1038–1048, 2016.

[10] W. Peverill, L. W. Powell, and R. Skoien, "Evolving concepts in the pathogenesis of NASH: beyond steatosis and inflammation," *International Journal of Molecular Sciences*, vol. 15, no. 5, pp. 8591–8638, 2014.

[11] L. K. Ursell, J. C. Clemente, J. R. Rideout, D. Gevers, J. G. Caporaso, and R. Knight, "The interpersonal and intrapersonal diversity of human-associated microbiota in key body sites," *The Journal of Allergy and Clinical Immunology*, vol. 129, no. 5, pp. 1204–1208, 2012.

[12] A. Fialho, A. Fialho, P. Thota, A. J. McCullough, and B. Shen, "Small intestinal bacterial overgrowth is associated with non-alcoholic fatty liver disease," *Journal of Gastrointestinal and Liver Diseases*, vol. 25, no. 2, pp. 159–165, 2016.

[13] M. Aguirre and K. Venema, "Challenges in simulating the human gut for understanding the role of the microbiota in obesity," *Beneficial Microbes*, vol. 8, no. 1, pp. 31–53, 2017.

[14] I. Węgielska and J. Suliburska, "The role of intestinal microbiota in the pathogenesis of metabolic diseases," *ACTA Scientiarum Polonorum Technologia Alimentaria*, vol. 15, no. 2, pp. 201–211, 2016.

[15] J. Henao-Mejia, E. Elinav, C. Jin et al., "Inflammasome-mediated dysbiosis regulates progression of NAFLD and obesity," *Nature*, vol. 482, no. 7384, pp. 179–185, 2012.

[16] A. A. Shanab, P. Scully, O. Crosbie et al., "Small intestinal bacterial overgrowth in nonalcoholic steatohepatitis: association with toll-like receptor 4 expression and plasma levels of

interleukin 8," *Digestive Diseases and Sciences*, vol. 56, no. 5, pp. 1524–1534, 2011.

[17] V. Tremaroli and F. Bäckhed, "Functional interactions between the gut microbiota and host metabolism," *Nature*, vol. 489, no. 7415, pp. 242–249, 2012.

[18] S. Softic, D. E. Cohen, and C. R. Kahn, "Role of dietary fructose and hepatic de novo lipogenesis in fatty liver disease," *Digestive Diseases and Sciences*, vol. 61, no. 5, pp. 1282–1293, 2016.

[19] D. B. Andrews and J. E. Lavine, "Medical therapy for nonalcoholic fatty liver disease in children and adolescents," *Expert Review of Gastroenterology & Hepatology*, vol. 6, no. 1, pp. 1–3, 2012.

[20] G. F. Watts, "Nutrition and metabolism: nutritional therapy for disordered triglyceride metabolism and nonalcoholic fatty liver disease," *Current Opinion in Lipidology*, vol. 21, no. 6, pp. 545–547, 2010.

[21] M. Raman, I. Ahmed, P. M. Gillevet et al., "Fecal microbiome and volatile organic compound metabolome in obese humans with nonalcoholic fatty liver disease," *Clinical Gastroenterology and Hepatology*, vol. 11, no. 7, pp. 868–875, 2013.

[22] M. Rahimlou, Z. Yari, A. Hekmatdoost, S. M. Alavian, and S. A. Keshavarz, "Ginger supplementation in nonalcoholic fatty liver disease: A randomized, double-blind, placebo-controlled pilot study," *Hepatitis Monthly*, vol. 16, no. 1, Article ID e34897, 2016.

[23] A. Sepideh, P. Karim, A. Hossein et al., "Effects of multistrain probiotic supplementation on glycemic and inflammatory indices in patients with nonalcoholic fatty liver disease: a double-blind randomized clinical trial," *Journal of the American College of Nutrition*, vol. 35, no. 6, pp. 500–505, 2016.

[24] M. Tang-you, G. Kang-li, and Z. Wei-han, "Experimental study of 'Wenyun Qingli' method on DAG-PKCƐ signal pathway in liver tissue of NASH rats," *Journal of Traditional Chinese Medicine*, vol. 9, no. 8, pp. 908–913, 2016.

[25] H. Dong, F.-E. Lu, and L. Zhao, "Chinese herbal medicine in the treatment of nonalcoholic fatty liver disease," *Chinese Journal of Integrative Medicine*, vol. 18, no. 2, pp. 152–160, 2012.

[26] Y. Guo, J.-X. Li, T.-Y. Mao, W.-H. Zhao, L.-J. Liu, and Y.-L. Wang, "Targeting sirt1 in a rat model of high-fat diet-induced non-alcoholic fatty liver disease: Comparison of Gegen Qinlian decoction and resveratrol," *Experimental and Therapeutic Medicine*, vol. 14, no. 5, pp. 4279–4287, 2017.

[27] Y.-l. Wang, L.-j. Liu, W.-h. Zhao, and J.-x. Li, "Intervening TNF-α via PPARγ with gegenqinlian decoction in experimental non-alcoholic fatty liver disease," *Evidence-Based Complementary and Alternative Medicine*, vol. 2015, Article ID 715638, 10 pages, 2015.

[28] W. Zhao, L. Liu, Y. Wang, T. Mao, and J. Li, "Effects of a combination of puerarin, baicalin and berberine on the expression of proliferator-activated receptor-γ and insulin receptor in a rat model of nonalcoholic fatty liver disease," *Experimental and Therapeutic Medicine*, vol. 11, no. 1, pp. 183–190, 2016.

[29] Y. Guo, J. Y Li, and T. Y Mao, "Protection of Gegen Qinlian Decoction on Gut Barrier in the Rats of NASH Induced by High-Fat Diet," *World Journal of Integrated Traditional and Western Medicine*, vol. 12, no. 9, pp. 1225–1229, 2017.

[30] L. Cui, L. Feng, Z. H. Zhang, and X. B. Jia, "The anti-inflammation effect of baicalin on experimental colitis through inhibiting TLR4/NF-κB pathway activation," *International Immunopharmacology*, vol. 23, no. 1, pp. 294–303, 2014.

[31] F. Yan, L. Wang, Y. Shi et al., "Berberine promotes recovery of colitis and inhibits inflammatory responses in colonic macrophages and epithelial cells in DSS-treated mice," *American Journal of Physiology-Gastrointestinal and Liver Physiology*, vol. 302, no. 5, pp. G504–G514, 2012.

[32] D. Compare, P. Coccoli, A. Rocco et al., "Gut-liver axis: the impact of gut microbiota on non alcoholic fatty liver disease," *Nutrition, Metabolism & Cardiovascular Diseases*, vol. 22, no. 6, pp. 471–476, 2012.

[33] E. A. Lin, G. M. Barlow, and R. Mathur, "The microbiome in non-alcoholic fatty liver disease: associations and implications," *Annals of Gastroenterology: Quarterly Publication of the Hellenic Society of Gastroenterology*, vol. 27, no. 2, pp. 181–183, 2014.

[34] C. Leung, L. Rivera, J. B. Furness, and P. W. Angus, "The role of the gut microbiota in NAFLD," *Nature Reviews Gastroenterology & Hepatology*, vol. 13, no. 7, pp. 412–425, 2016.

[35] N. R. Shin, S. Bose, J. Wang et al., "Flos lonicera combined with metformin ameliorates hepatosteatosis and glucose intolerance in association with gut microbiota modulation," *Frontiers in Microbiology*, vol. 8, 2017.

[36] T. le Roy, M. Llopis, P. Lepage et al., "Intestinal microbiota determines development of non-alcoholic fatty liver disease in mice," *Gut*, vol. 62, no. 12, pp. 1787–1794, 2013.

[37] M. Mouzaki, E. M. Comelli, B. M. Arendt et al., "Intestinal microbiota in patients with nonalcoholic fatty liver disease," *Hepatology*, vol. 58, no. 1, pp. 120–127, 2013.

[38] L. Zhu, S. S. Baker, C. Gill et al., "Characterization of gut microbiomes in nonalcoholic steatohepatitis (NASH) patients: a connection between endogenous alcohol and NASH," *Hepatology*, vol. 57, no. 2, pp. 601–609, 2013.

[39] Y.-M. Chen, Y. Liu, R.-F. Zhou et al., "Associations of gut-flora-dependent metabolite trimethylamine-N-oxide, betaine and choline with non-alcoholic fatty liver disease in adults," *Scientific Reports*, vol. 6, Article ID 19076, 2016.

[40] M. D. Spencer, T. J. Hamp, R. W. Reid, L. M. Fischer, S. H. Zeisel, and A. A. Fodor, "Association between composition of the human gastrointestinal microbiome and development of fatty liver with choline deficiency," *Gastroenterology*, vol. 140, no. 3, pp. 976–986, 2011.

[41] H. K. Pedersen, V. Gudmundsdottir, H. B. Nielsen et al., "Human gut microbes impact host serum metabolome and insulin sensitivity," *Nature*, vol. 535, no. 7612, pp. 376–381, 2016.

[42] D. Zhou, Q. Pan, F.-Z. Xin et al., "Sodium butyrate attenuates high-fat diet-induced steatohepatitis in mice by improving gut microbiota and gastrointestinal barrier," *World Journal of Gastroenterology*, vol. 23, no. 1, pp. 60–75, 2017.

[43] Y. Zhao, F. Ling, T. M. Griffin et al., "Up-regulation of the sirtuin 1 (Sirt1) and peroxisome proliferator-activated receptor γ Coactivator-1α (PGC-1α) genes in white adipose tissue of id1 protein-deficient mice: Implications in the protection against diet and age-induced glucose intolerance," *The Journal of Biological Chemistry*, vol. 289, no. 42, pp. 29112–29122, 2014.

[44] A. S. Wellman, M. R. Metukuri, N. Kazgan et al., "Intestinal Epithelial Sirtuin 1 Regulates Intestinal Inflammation During Aging in Mice by Altering the Intestinal Microbiota," *Gastroenterology*, vol. 153, no. 3, pp. 772–786, 2017.

Hindawi
Evidence-Based Complementary and Alternative Medicine
Volume 2018, Article ID 4821821, 9 pages
https://doi.org/10.1155/2018/4821821

Research Article

Regulation Effect of a Chinese Herbal Formula on Flora and Mucosal Immune Secretory Immunoglobulin A in Rats

Tian-hao Liu,[1,2] Xiao-mei Zhang,[1] Ni-ping Han,[1] Yang Liu,[1] Yue-ying Wu,[1] Xiao-ya Li,[1] Zhong-shan Yang ,[1] and Jia-li Yuan [1]

[1]*School of Basic Medical Sciences, Yunnan University of Traditional Chinese Medicine, Yuhua Road, No. 1024, Kunming, Yunnan 650500, China*
[2]*College of Traditional Chinese Medicine, Jinan University, No. 601 West of Whampo Avenue, Guangzhou, Guangdong 510632, China*

Correspondence should be addressed to Zhong-shan Yang; yangzhongshan@ynutcm.edu.cn and Jia-li Yuan; yjl20182018@126.com

Received 10 June 2018; Revised 22 September 2018; Accepted 22 October 2018; Published 8 November 2018

Guest Editor: Jose Boga

Flora and mucosal immunity are considered to be the barrier, which is associated with multiple respiratory diseases, including recurrent respiratory tract infection (RRTI). Fei-Xi-Tiao-Zhi-Fang (FTF) is a traditional Chinese herbal formula used in the treatment of RRTI. However, the mechanism is little known. This study aims to identify the function of FTF in flora and mucosal immune secretory immunoglobulin A (sIgA) in the model of RRTI rats. The samples of intestine and lung were collected to detect sIgA, short chain fatty acids (SCFAS), and flora with enzyme-linked immunosorbent assay (ELISA), gas chromatography, and 16S rDNA sequencing. The body weight and viscera index were increased dynamically in RRTI rats after the administration of FTF. Furthermore, the types and proportions of aboriginal flora were significantly changed in the model group, whereas the altered flora was rescued in the FTF administration group. *Desulfovibrio* increased in the intestinal microflora and *Ralstonia* and *Blautia* decreased in the pulmonary microflora at the genus level, similar to that in the normal group. In addition, the expressions of sIgA in pulmonary and intestinal tissues were significantly upregulated and the level of SCFAS was increased in FTF group compared to the RRTI model group. Our study suggests that FTF can alleviate the symptoms of RRTI by increasing sIgA and SCFAS, recovering flora, and improving the immunity.

1. Introduction

Recurrent respiratory tract infection (RRTI) is considered to be a chronic respiratory disease, which is characterized by flora infection and immune dysregulation. The disease is manifested in the respiratory tract and intestine and the changes of intestinal flora can also affect respiratory diseases [1–3]. According to the theory in traditional Chinese medicine, the relationship between the lung and the large intestine is the interior-exterior corresponding relationship and the lung and intestine axis have confirmed the obvious connection between the gut and the respiratory tract [4–6]. Many scholars have also explained it in many aspects. We can prevent respiratory diseases by changing the intestinal microenvironment, adjusting the respiratory environment, and affecting intestinal functions. Therefore, according to the famous ancient Chinese medicine decoction "Yupingfengsan" and "Cangerzisan" (both are important decoction for treating respiratory diseases), Chinese medicine experts created FTF, which could change the intestinal microenvironment and adjust the respiratory tract infection [7–9]. When FTF is used in clinic, it has an obvious curative effect and can alleviate the respiratory tract infection and intestinal symptoms.

Flora is closely related to mucosal immunity. The bacteria can act on the mucous membrane, which can also affect the flora. Intestinal flora can metabolize short chain fatty acids (SCFAS), which can act on the intestinal mucosa, thereby affecting the body [10, 11]. Pulmonary and intestinal mucosae are attached to a large number of bacteria and the microflora and immunity of lung and intestine may be considered as the biological basis of the lung-intestinal correlation. The

changes in the composition and structure of bacterial flora can be considered as the changes in the bacterial flora of the lung and intestine and the change in mucosal secretory immunoglobulin A (sIgA) may represent the level of mucosal immunity in the lung and intestine [12]. All the results suggest that FTF may play a role in the prevention and treatment of RRTI by regulating the flora and mucosal immunity. However, the direct evidence demonstrating the mechanism of FTF in the prevention and treatment of RRTI was seldom reported. In this study, we observed the changes in the flora and immunity in the lung and intestine of rats in order to illustrate the underlying mechanisms and provide scientific evidences for the role of FTF in the prevention and treatment of RRTI.

2. Materials and Methods

2.1. Animals. A total of 63 SPF Wistar rats (130±10 g, 3-4 weeks old, male) were purchased from Chengdu Dashuo Experimental Animal Co., Ltd. The rats were housed in standard environmental conditions and could freely access to diet and water. All groups were fed adaptively for seven days before the study. The study was approved by Committee on Animal Experimental Ethics of Yunnan University of Traditional Chinese Medicine and all the experimental methods were performed in accordance with the relevant guidelines and regulations.

2.2. Grouping. The animals were randomly divided into seven groups: normal control group (K), model control group (MX), high-dose FTF group (HZ), medium-dose FTF group (MZ), low-dose FTF group (LZ), FTF atomization group (AD), and positive medicinal control group (YZ) and each group contained 9 rats.

2.3. Immunosuppression and Dysbacteriosis in Rats and the Treatments. The study was divided into four phases. From the first to the sixth day, the rats were fed adaptively. From the seventh to fourteenth day, the rats were treated with the mixture of antibiotics and hormone every 24 h. From the fifteenth to the twenty-first day, the rats were treated with different drugs every 24 h. All the rats were killed on the twenty-second day.

2.4. Construction of the Model. Cefradine capsules (Shijiazhuang Pharmaceutical Group Ouyi Pharma Co., Ltd.), gentamycin sulfate (Shanghai Shenguang Company), and dexamethasone sodium phosphate injection (Shanxi, Ruicheng Kelon Veterinary Medicine Co., Ltd.) were combined to obtain a mixture of 22.6 g/L in the proportion of 1:5:6, which was administered intraperitoneally to rats (2 mL per day). From the seventh day, the mixed suspension was injected to the groups for 8 consecutive days except the normal control group once a day. Meanwhile, normal saline was injected to the normal control group in the same way.

2.5. Preparation of FTF. The FTF was prepared by Yunnan Hongxiang Yixintang Pharmaceutical Limited Ltd. FTF herbs include huangqi (astragalus), fangfeng (windbreak), baizhi (angelica root), cangerzi (cocklebur), xinyihua (magnolia flower), xingren (almond), tinglizi, and gancao (licorice). Firstly, after adding 800 mL of deionized water, FTF herbs were soaked for 1 h and then decocted over a low flame for 40 min after boiling. Then the filtrate was collected with gauze. Secondly, 600 mL of deionized water was added to the dregs of a decoction and then decocted in the same way. Then the filtrate was collected with gauze. Thirdly, 600 mL of deionized water was added to the dregs of a decoction and then decocted in the same way. Then the filtrate was collected with gauze. Finally, all filtrates were combined together, made into extractum, and stored at 4°C. The dose of FTF for rats was calculated with body surface area. The medium dose was the equivalent dose (0.5 g/mL) and the ratio of low, medium, and high doses was 1:2:4 [13].

2.6. Chemical Composition Analysis of FTF Extract. The FTF extract was diluted by 10 times. Then 1 mL of diluted FTF extract was added into a 2-mL centrifuge tube, centrifuged at 13,000 r/min for 10 min, filtered through 0.22-μm microporous membrane, and then loaded into a 1.5-mL automatic sampling bottle to obtain the covering liquid sample. Blank control samples were obtained under the same conditions. The samples were stored in the refrigerator at 4°C for analysis and the storage time should not exceed 24 h. The active components of FTF extract were analyzed qualitatively by ultrahigh performance liquid chromatography-time-of-flight high resolution mass spectrometry. The 20 components in the FTF extract with the response value greater than 100,000 are shown in Table 1.

2.7. Treatment Drugs. From the fifteenth to the twenty-first day, the rats in the HZ, MZ, and LZ groups were fed with different doses of FTF decoction orally every 24 h and the AD group was fed with atomized decoction with the equivalent dose every 24 h. Meanwhile, the YZ group was treated with Broncho-Vaxom with the equivalent dose and the MX and K groups were treated with the same amount of normal saline in the same way.

2.8. Index Detection. On the twenty-second day, all rats were sacrificed and tissue samples were collected under aseptic conditions.

2.9. Viscera Index. The thymus and spleen of all rats were collected and weighed and the viscera indexes were calculated according to the formula (viscera index = organ mass (mg) / body weight (g) $*$ 100%).

2.10. Enzyme-Linked Immunosorbent Assay (ELISA) for the Quantitative Detection of sIgA. The pulmonary and intestinal tissues of all groups were obtained. The grinding bowl was precooled with liquid nitrogen. Then, 400 mg of the tissue was put into the grinding bowl. Liquid nitrogen was added for grinding. The crushed tissue was poured into EP tube and 1 mL of phosphate buffer solution (pH 7.4) was added and centrifuged for 20 min with a cryogenic centrifuge at 3000

Table 1: 20 components in FTF extracts.

Components	Formula	Adduct	Found Mass	Adduct	RT	Intensity
Glycyrrhizic Acid	C42H62O16	-H	821.39266	-4.7	20.06	1555680
4'-O-beta-Glucopyranosyl-5-O-MethylviSamminol	C22H28O10	+H	453.17675	2.7	11.01	725986
Prim-O-glucosylcimifugin	C22H28O11	+H	469.17136	2	8.28	716074
S)-tetrahydrocolumbamine	C20H23NO4	+H	342.17112	3.3	6.81	471691
Corlumidine	C20H23NO4	+H	342.17112	3.3	6.81	471691
Cimifugin	C16H18O6	+H	307.11846	2.8	10.04	325644
Adenosine	C10H13N5O4	+H	268.10425	0.8	1.56	266516
Catechingallate	C22H18O10	-H	441.0832	2	0.93	216855
Scopoletin	C16H18O9	-H	353.08646	-3.8	5.03	201272
Episappanol	C16H16O6	+H	305.10251	1.8	14.25	200565
Oxypeucedanin hydrate	C16H16O6	+H	305.10251	1.8	14.25	200565
Monnieriside G	C21H26O10	+H	439.16081	2.1	15.09	152817
Liquiritigenin	C15H12O4	+H	257.08138	2.1	9.35	134270
4'-methoxy Daidzein	C22H22O9	+H	431.13467	2.3	13.19	109861
Ononin	C22H22O9	+H	431.13467	2.3	13.19	109861
3'-methoxypuerarin	C22H22O10	+H	447.1297	2.5	9.15	107116
Apigenin6-glucosyl-7-o-methylether	C22H22O10	+H	447.1297	2.5	9.15	107116
Glycitin	C22H22O10	+H	447.1297	2.5	9.15	107116
Calycosin-7-glucoside	C22H22O10	+H	447.1297	2.5	9.15	107116
Trifolirhizin	C22H22O10	+H	447.1297	2.5	9.15	107116

rpm. Finally, the expression of sIgA was detected according to the instructions of ELISA kit supplied by Nanjing Senbeijia Biological Technology Co., Ltd. (Nanjing, China).

2.11. High-Throughput Sequencing. The intestinal contents and lung tissues were taken under aseptic conditions and stored at -80°C. Three samples were randomly selected from each group of lung tissues and intestinal components (lung: FK, FMX, FMZ, FAD, FYZ; intestine: CK, CMX, CMZ, CAD, CYZ) for the sequence analysis of flora. The next-generation sequencing library preparations, Illumina MiSeq sequencing, and V3 and V4 hypervariable regions of 16S rDNA were provided by GENEWIZ, Inc. (Suzhou, China).

2.12. Expression of SCFAS Tested by Gas Chromatography. Three samples were randomly selected with 3 intestinal components of each group (K group, MX group, MZ group, AD group, and YZ group). After adding 2-mL of water, the samples (1 g) were homogenized for 2 min. Then 1 mL of ether was added for 10-min extraction and then centrifuged at 4000 rpm for 20 min. Then 1 mL of ether was added for 10-min extraction and then centrifuged at 4000 rpm for 20 min. The two extracts were combined and volatilized to the volume of less than 1 mL. Then 0.1 mL of 1000 mg/L ether internal standard solution was added and the volume was fixed to 1 mL. Further, the intermixture was transferred to be tested. SCFAS, including acetic acid (CAA), propionic acid (CPA), isobutyric acid (CIA), ethacetic acid (CEA), common valeric acid (CCVA), and pentanoic acid (CPEA), were tested by gas chromatography according to the operation process (GCMS ISQ LT). The experimental materials required in this section were provided by Qingdao Yixin Testing Technology Service Co., Ltd.

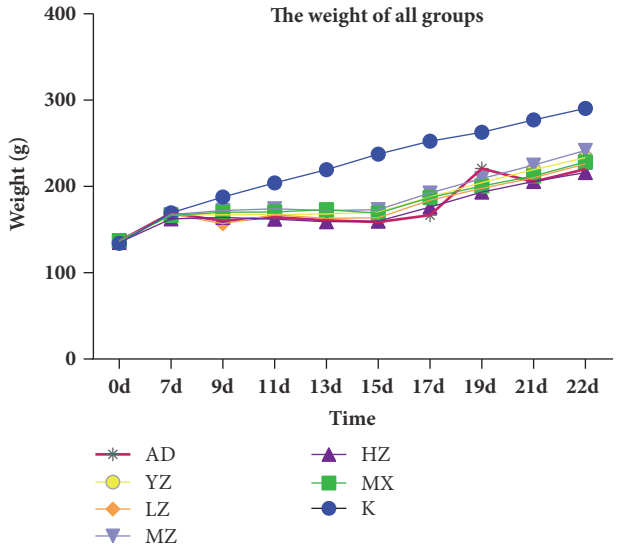

Figure 1: **Changes in the weight of rats during the experiment.** From Day 0 to Day 7, rats were naturally fed; from Day 8 to Day 15, rats were modeled; from Day 15 to Day 22, rats were treated. In the modeling process, the weight of the rats in the K group was significantly higher than that of the MX group; when the treatment was given, the MZ group rose significantly and the weight change of the AD group was tremendous at the beginning of the treatment.

2.13. Statistical Analysis. The 16S rDNA data analysis was performed with the QIIME package data and R programming

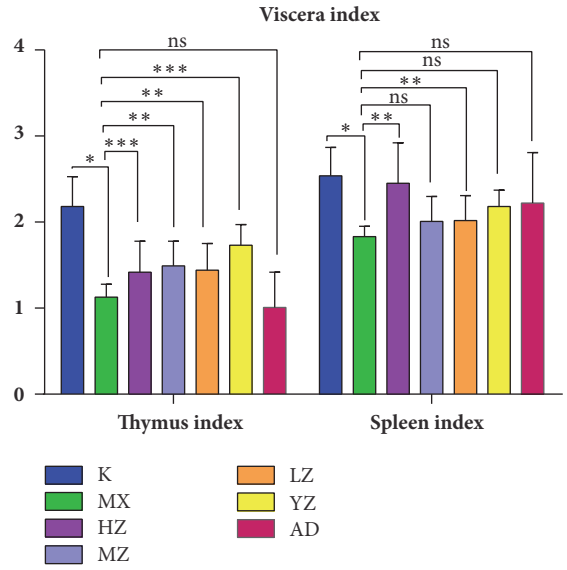

Figure 2: **FTF dynamically regulated viscera index.** The left side is the thymus index of each group (n=8) and the right is the spleen index of each group (n=8). Data are presented as mean ± SD. $^{*}P<0.05$ versus the K group; $^{**}P<0.05$ and $^{***}P<0.01$ versus the MX group.

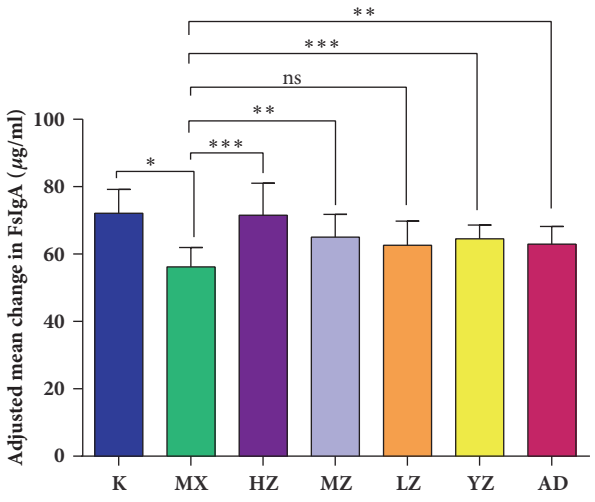

Figure 3: **FTF significantly improved the expression of sIgA in pulmonary tissues.** Data (n=8) are presented as mean ± SD. $^{*}P<0.05$ versus the K group; $^{**}P<0.05$ and $^{***}P<0.01$ versus the MX group.

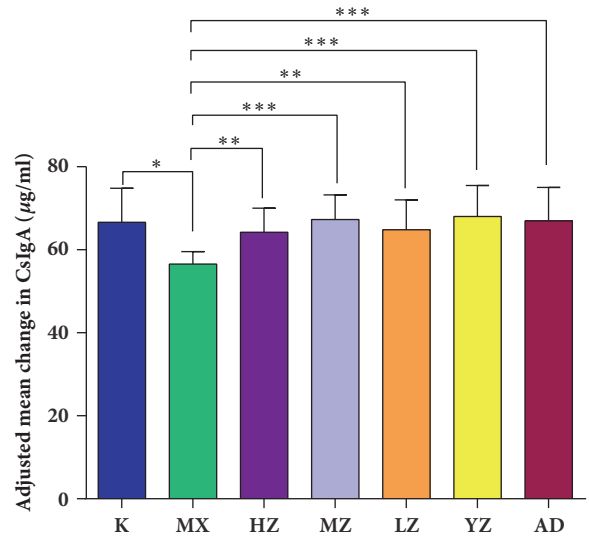

Figure 4: **FTF significantly improved the expression of sIgA in intestinal tissues.** Data (n=8) are presented as mean ± SD. $^{*}P<0.05$ versus the K group; $^{**}P<0.05$ and $^{***}P<0.01$ versus the MX group.

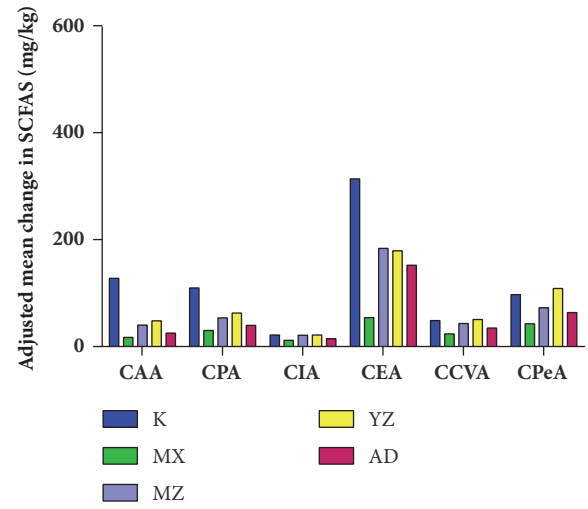

Figure 5: **Expression of SCFAS in rats of every group.** SCFAS, including acetic acid (CAA), propionic acid (CPA), isobutyric acid (CIA), ethacetic acid (CEA), common valeric acid (CCVA), and pentanoic acid (CPEA) were detected in every group (n=3).

language. Other results were presented as mean ± SD. The experimental data were analyzed by SPSS statistical software and GraphPad Prism 6. P<0.05 or P<0.01 was considered to be statistically significant or extremely significant.

3. Results

3.1. Weight Changes. In the seven days of adaptive feeding, the weight of all groups increased significantly. From Day 7 to Day 14, the weight of all the rats except the rats in the K group remained almost unchanged. From Day 14 to Day 21, the weights of the rats in the MZ and YZ group were higher than those in other groups except the K group. Meanwhile, the weight of the AD group increased obviously in the first several days (Figure 1).

3.2. FTF Dynamically Increased the Viscera Index. Compared with the K group, the thymus index of the MX group decreased significantly (P<0.05). Compared with the MX group, the thymus index of the HZ, MZ, and LZ groups significantly increased (P<0.05) and the thymus index of the AD group decreased slightly by aerosol (P>0.05), YZ>MZ>LZ>HZ>AD. There was no significant difference among the groups (P>0.05). Compared with the K group,

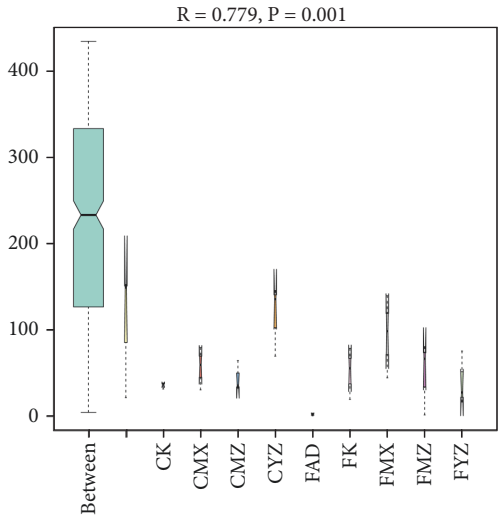

(a) **Results of Anosim analysis of all groups.** R value close to 1 indicates the differences between groups (n=3) more than differences in the group. P<0.05 indicates the statistical significance.

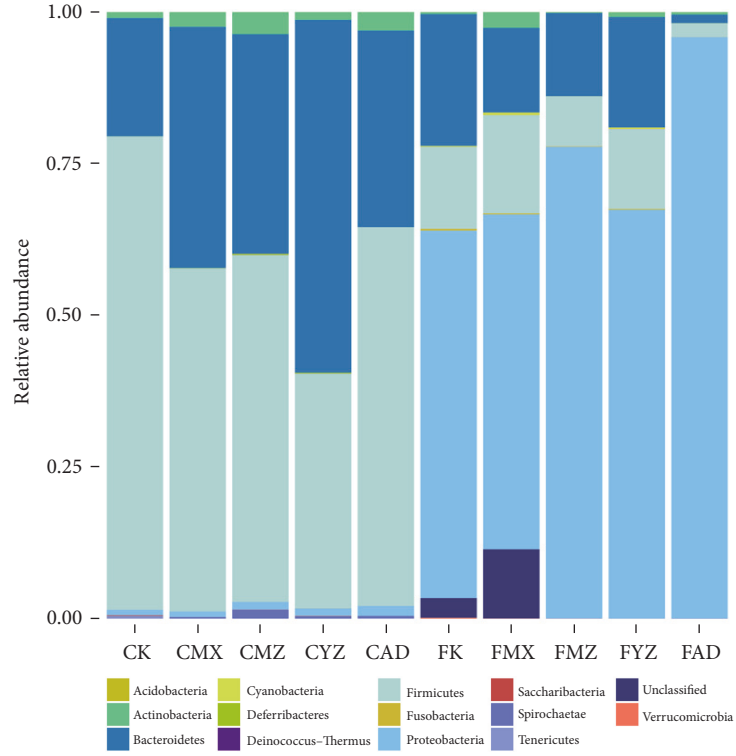

(b) **FTF significantly regulated the compositions and structures of the pulmonary and intestinal flora in the level of phylum.** The abscissa represents different groups (n=3) and the ordinate represents the relative abundance. Different colors correspond to different phyla.

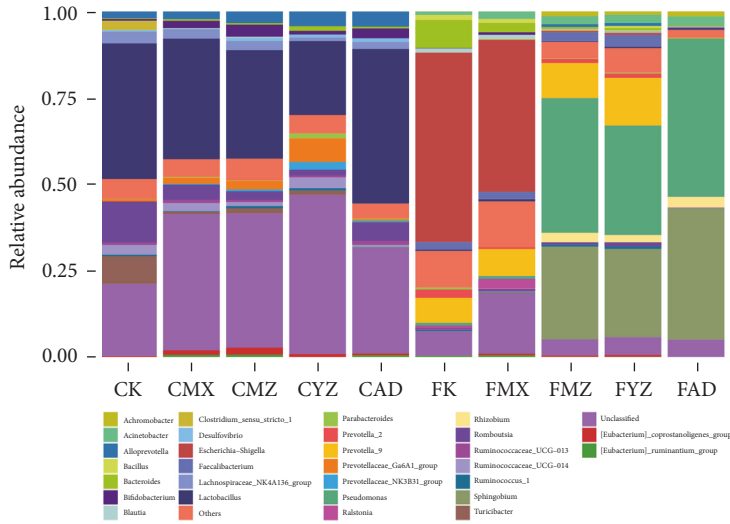

(c) **FTF significantly regulated the compositions and structures of the pulmonary and intestinal flora in the level of genus.** The abscissa represents different groups (n=3) and the ordinate represents the relative abundance. Different colors correspond to different genera.

Figure 6

the spleen index in the MX group rats decreased significantly (P<0.05); compared with the MX group, the spleen index of the HZ group significantly increased (P<0.05); the spleen index of the MZ and LZ group increased (P>0.05). There was no significant difference among the groups (P>0.05), HZ>AD>YZ>LZ>MZ (Figure 2).

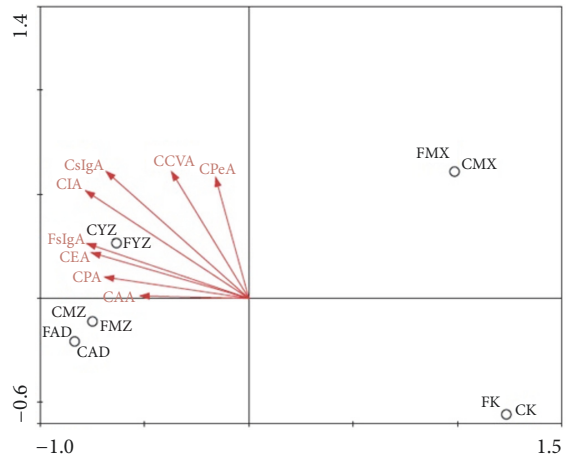

Figure 7: **Results of RDA/CCA analysis.** RDA/CCA is a ranking method based on correspondence analysis, which is mainly used to reflect the relationship between flora and environmental factors. The angles between environmental factors indicate positive and negative correlation between environmental factors (acute angle: positive correlation; obtuse angle: negative correlation; right angle: no correlation). As indicated by the vertical projection points of different samples on various environmental factors, the closer the distance between the vertical projection points is, the more similar the environmental factor among different samples is, indicating that the degrees of the influences of the environment factor on different samples are similar.

3.3. FTF Significantly Improved the Expression of sIgA in Pulmonary and Intestinal Tissues. Compared with the K group, the sIgA level in lung tissues of the MX group rats decreased significantly; compared with the MX group, the sIgA levels in lung tissues of the HZ group rats increased significantly ($P<0.01$) and the sIgA levels in lung tissues of MZ, YZ, and AD groups increased ($P<0.05$). The sIgA levels in the LZ group rats increased significantly ($P>0.05$), HZ>MZ>YZ>AD>LZ ($P>0.05$) (Figure 3).

Compared with the K group, the sIgA level in intestinal tissues of the MX group decreased significantly; compared with the MX group, the sIgA levels in lung tissues of the MZ, YZ, and AD groups increased significantly ($P<0.01$) and the HZ and LZ groups increased ($P<0.05$), YZ>MZ>AD>LZ>HZ. There was no significant difference among the groups ($P>0.05$) (Figure 4).

3.4. FTF Significantly Raised the Expression of SCFAS. SCFAS including cetic acid (CAA), propionic acid (CPA), isobutyric acid (CIA), ethacetic acid (CEA), common valeric acid (CCVA), and pentanoic acid (CPEA) were detected. All these acids in the MX group decreased compared with the K group. The SCFAS in MZ and AD groups was significantly increased compared with the MX group (Figure 5).

3.5. FTF Significantly Regulated the Compositions and Structures of the Pulmonary and Intestinal Flora. The result of 16S rDNA gene sequence (Figure 6(a)) indicated that there was a significant difference ($R = 0.779$, $P = 0.001$) among the groups. The changes in the phylum level showed that the intestinal flora in the K group was mainly composed of *Firmicutes*, *Bacteroidetes*, *Actinobacteria*, *Proteobacteria*, and *Spirochaetae*. Compared with the K group, the intestinal microflora in the rats of the MX group showed the decreased levels of *Firmicutes*, *Proteobacteria,* and *Spirochaetae* and the increased levels of *Bacteroidetes* and *Actinobacteria*. Compared with the MX group, the MZ group showed the increased levels of *Firmicutes*, *Spirochaetae,* and *Actinobacteria*, the decreased level of *Bacteroidetes*, and the unchanged level of *Proteobacteria*; the AD group showed the increased levels of *Firmicutes*, *Actinobacteria,* and *Proteobacteria*, the decreased level of *Bacteroidetes*, and the unchanged level of *Spirochaetae*; the YZ group showed the decreased levels of *Firmicutes* and *Actinobacteria* and the increased levels of *Proteobacteria*, *Spirochaetae,* and *Bacteroidetes*. Meanwhile, the pulmonary flora in K group was mainly composed of *Proteobacteria*, *Bacteroidetes*, *Firmicutes*, and *Actinobacteria*. The MX group showed the decreased levels of *Proteobacteria* and *Bacteroidetes* and the increased levels of *Firmicutes* and *Actinobacteria* compared with the K group. After the rats of the MZ, AD, and YZ groups were treated, the MZ group showed the increased levels of *Proteobacteria* and *Bacteroidetes* and the decreased levels of *Firmicutes* and *Actinobacteria*; the AD group showed the increased level of *Proteobacteria* and the decreased levels of *Bacteroidetes*, *Firmicutes,* and *Actinobacteria*; the YZ group showed the increased levels of *Proteobacteria* and *Bacteroidetes* and the decreased levels of *Firmicutes* and *Actinobacteria* (Figure 6(b)).

At the genus level, the intestinal microflora of rats was composed of *Bifidobacterium, Alloprevotella, Prevotellaceae_Ga6A1_group, Ruminococcaceae_UCG, Lachnospiraceae_NK4A136_group, Turicibacter-014, Romboutsia, Ruminococcus_1, [Eubacterium]_coprostanoligenes_group, Desulfovibrio, Ruminococcaceae_UCG, [Eubacterium]_ruminantium_group, Parabacteroides-013, Prevotellaceae_NK3B31_group,* and *Lactobacillus*.

The pulmonary flora was composed of *Pseudomonas, Sphingobium, Clostridium_sensu_stricto_1, Faecalibacterium, Prevotella_2, Achromobacter, Acinetobacter, Rhizobium, Ralstonia, Bacillus, Blautia, Escherichia* and *Shigella, Prevotella_9*, and *Bacteroides* (Figure 6(c)). Obviously, all these evidences showed that FTF could significantly regulate the compositions and structures of the pulmonary and intestinal florae.

3.6. Correlation Analysis of Flora and Mucosal Immune sIgA in Rats. According to the correlation analysis result, the six parts of SCFAS were positively correlated with sIgA of lung and intestine. At the same time, there was a significant positive correlation between sIgA of the lung and the intestine (Figure 7). After the analysis, we identified the positive and negative correlations of the first 30 OTUs between SCFAS and sIgA (Figure 8).

4. Discussion

Flora and immunity are important components of the body and play an important role in anti-inflammatory defense

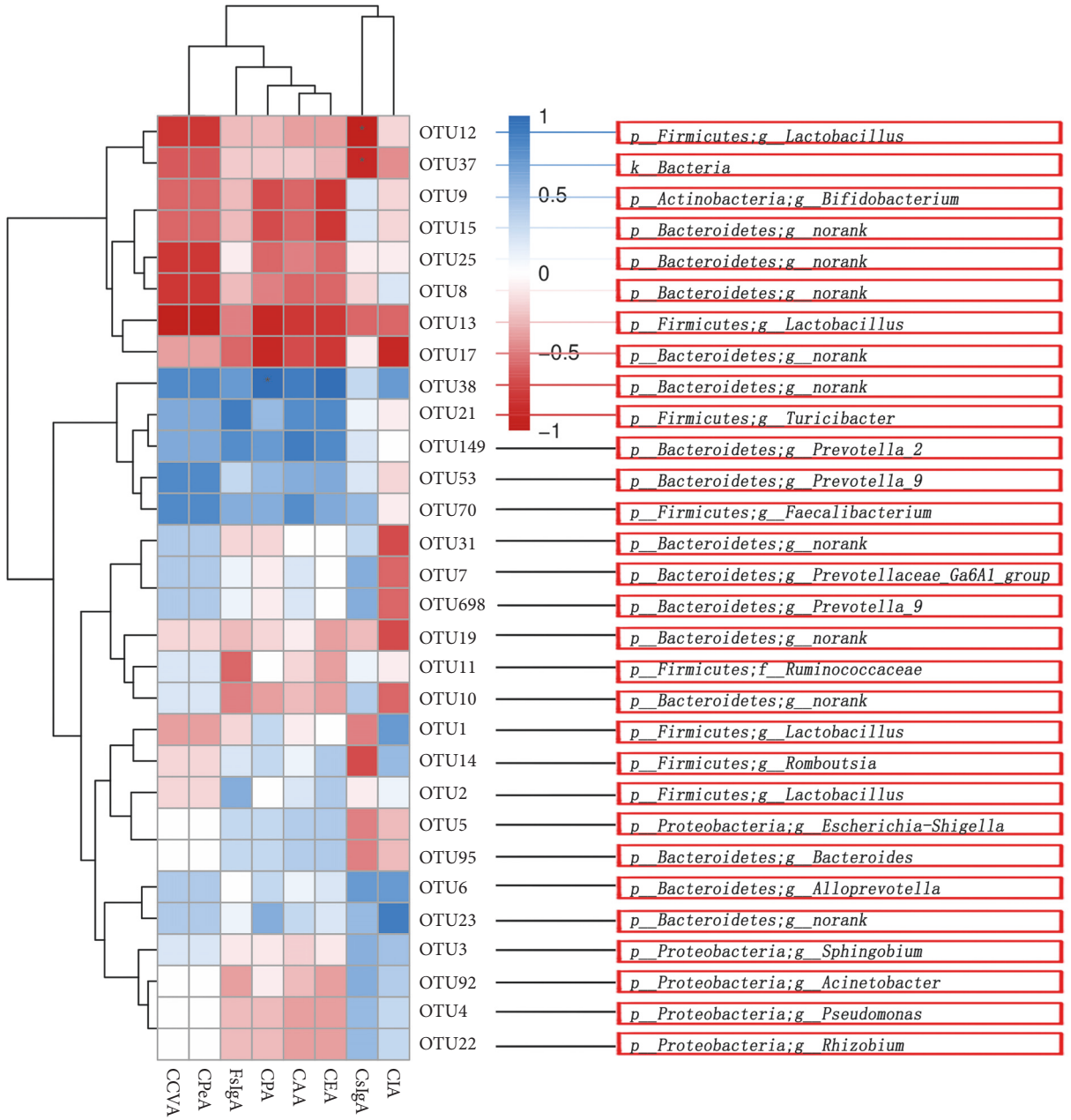

FIGURE 8: **Relationship between the environmental factors and community composition was intuitively displayed by Spearman using R language.** The data were based on OTU abundance or species richness and environmental factor data. The correlation coefficient r [-1~1], r>0 were positively correlated, and r<0 was negatively correlated. In significance tests, *P* values between 0.01 and 0.001 were marked as ∗∗; *P* values between 0.01 and 0.05 were marked as ∗.

against pathogens. Traditional Chinese medicine (TCM) has a long history and rich theory. A variety of useful chemical components have also been detected from Chinese medicine [14–16]. Many diseases have been cured with TCM nowadays in China, but many unknown mechanisms have restricted its widespread transmission in the world. Traditional Chinese medicine theories such as "lung intestine axis" and "the corresponding relationship between lung and large intestine" show that the respiratory tract is closely related to the intestinal tract. In our study, when the rats were stimulated by antibiotics and hormone, they were in a state of flora imbalance and immunosuppression. To our knowledge, this study was the first time to establish the model of immunosuppression and dysbacteriosis in rats on the basis of the immunosuppression and dysbacteriosis rats [17–19].

Viscera index is considered to represent the level of immune development [20–22]. sIgA can represent the level of mucosal immunity [23, 24]. The interaction between flora

and sIgA is significant [25]. SCFAS are confirmed to be the metabolites of intestinal flora, which also interacts with the gut [26, 27]. The changes in viscera index, the expressions of sIgA and SCFAS, and the changes in the pulmonary and intestinal flora in our study indicated that FTF could regulate the flora and mucosal immunity of the lung and intestine. The flora and mucosal immunity may be the scientific connotation of the lung-intestine correlation.

Aerosol inhalation of medicine has a significant effect on respiratory diseases [28, 29]. This study designed the AD group and found that atomized FTF controlled the disease quickly as indicated by the change in weight. The study may provide some ideas for the development of TCM atomization agent. Oral administration of FTF and aerosolized FTF both affect the lung and intestine simultaneously. Additionally, this study revealed that the specific bacterial community was associated with SCFAS and sIgA. We found that *g__Lactobacillus* was negatively correlated with intestinal mucosal sIgA, suggesting that *g__Lactobacillus* might inhibit intestinal mucosal immunity. The detailed mechanism between *g__Lactobacillus* and sIgA needs further study.

In conclusion, this study suggests that FTF can regulate the sIgA and the composition and structure of flora in the lung and intestine and increase SCFAS in intestinal microbiota metabolism. In addition, it reveals the possible biological basis of the connection of lung and intestine. Although the specific mechanisms that FTF directly acts on these indicators, as well as some specific bacterial communities and immune sIgA, are not clear, this study suggests a potential direction for the next research.

Abbreviations

RRTI: Recurrent respiratory tract infections
FTF: Fei-Xi-Tiao-Zhi-Fang
sIgA: Secretory immunoglobulin A
SCFAS: Short chain fatty acids
ELISA: Enzyme-linked immunosorbent assay
K: Normal control group
MX: Model control group
HZ: High-dose FTF group
MZ: Medium-dose FTF group
LZ: Low-dose FTF group
AD: FTF atomization group
YZ: Positive medicinal control group
CAA: Acetic acid
CPA: Propionic acid
CIA: Isobutyric acid
CEA: Ethacetic acid
CCVA: Common valeric acid
CPEA: Pentanoic acid.

Data Availability

The data used to support the findings of this study are included within the article and can be made freely available. Any questions of data will be considered to be answered by the corresponding author.

Conflicts of Interest

The authors declare that they have no conflicts of interest.

Acknowledgments

The authors thank all the scholars who have provided relevant guidance for the study. This study was supported by grants from National Natural Science Foundation of China (81460684, 81760819, 81503323, and 21662048).

References

[1] F. Dong, H. Yu, J. Ma et al., "Exploring association between gastrointestinal heat retention syndrome and recurrent respiratory tract infections in children: a prospective cohort study," *BMC Complementary and Alternative Medicine*, vol. 16, no. 1, pp. 1–8, 2016.

[2] S. Esposito, D. Rigante, and N. Principi, "Do children's upper respiratory tract infections benefit from probiotics?" *BMC Infectious Diseases*, vol. 14, no. 1, p. 194, 2014.

[3] K. Saad, M. G. Abo-Elela, K. A. El-Baseer et al., "Effects of bovine colostrum on recurrent respiratory tract infections and diarrhea in children," *Medicine*, vol. 95, no. 37, p. e4560, 2016.

[4] B. J. Marsland, A. Trompette, and E. S. Gollwitzer, "The gut-lung axis in respiratory disease," *Annals of the American Thoracic Society*, vol. 12, 2, pp. S150–S156, 2015.

[5] X. Zhong, F. Zheng, Y. Li, H. Xu et al., "Specific link between lung and large intestine: a new perspective on neuropeptide secretion in lung with herbal laxative stimulation," *Evidence-Based Complementary and Alternative Medicine*, vol. 2013, Article ID 547837, 2013.

[6] H. Y. C. Leung, P. K. Leong, J. Chen, and K. M. Ko, "Inter-Organ Relationships among Gut, Lung and Skin beyond the Pathogenesis of Allergies: Relevance to the Zang-Fu Theory in Chinese Medicine," *Chinese Medicine*, vol. 08, no. 03, pp. 73–81, 2017.

[7] M. Hauptmann and U. E. Schaible, "Linking microbiota and respiratory disease," *FEBS Letters*, vol. 590, no. 21, pp. 3721–3738, 2016.

[8] J. C. Madan, "Neonatal gastrointestinal and respiratory microbiome in cystic fibrosis: potential interactions and implications for systemic health," *Clinical Therapeutics*, vol. 38, no. 4, pp. 740–746, 2016.

[9] R. T. X. F. Zhang Dianrui, "GC-MS analysis of volatile components in Xanthium powder," *Chinese Journal of Traditional Chinese Medicine*, vol. 11, no. 28, pp. 1083–1086, 2003.

[10] J. Soldavini and J. D. Kaunitz, "Pathobiology and potential therapeutic value of intestinal short-chain fatty acids in gut inflammation and obesity," *Digestive Diseases and Sciences*, vol. 58, no. 10, pp. 2756–2766, 2013.

[11] H. Ohira, W. Tsutsui, and Y. Fujioka, "Are short chain fatty acids in gut microbiota defensive players for inflammation and atherosclerosis?" *Journal of Atherosclerosis and Thrombosis*, vol. 24, no. 7, pp. 660–672, 2017.

[12] N. J. Mantis, N. Rol, and B. Corthésy, "Secretory IgA's complex roles in immunity and mucosal homeostasis in the gut," *Mucosal Immunology*, vol. 4, no. 6, pp. 603–611, 2011.

[13] L. Yiku, *Experimental Methodology of Pharmacology of Chinese Materia Medica*, 2006.

[14] Q. D. Jiang, W. G. Yang, H. Cai et al., "Association between chemical composition of essential oil with penetration enhancement effect and drug properties of traditional Chinese medicine," *China Journal of Chinese Materia Medica*, vol. 41, no. 13, pp. 2500–2505, 2016.

[15] T. Li, S. Zhuang, Y. Wang et al., "Flavonoid profiling of a traditional Chinese medicine formula of Huangqin Tang using high performance liquid chromatography," *Acta Pharmaceutica Sinica B (APSB)*, vol. 6, no. 2, pp. 148–157, 2016.

[16] Q. Dong, L.-L. Qiu, C.-E. Zhang et al., "Identification of compounds in an anti-fibrosis Chinese medicine (Fufang Biejia Ruangan Pill) and its absorbed components in rat biofluids and liver by UPLC-MS," *Journal of Chromatography B*, vol. 1026, pp. 145–151, 2015.

[17] L. He, Y. Liu, Y. Guo, K. Shen, H. Hui, and Z. Tan, "Diversity of intestinal bacterial lactase gene in antibiotics-induced diarrhea mice treated with Chinese herbs compound Qi Wei Bai Zhu San," *3 Biotech*, vol. 8, no. 1, p. 4, 2017.

[18] Z. Xina, *Fuzheng Granule's Effect on Arterial Blood Lymphocyte Subsets in Immune Depression Rats*, Zhejiang University of Traditional Chinese Medicine, 2014.

[19] S. Ting, *Qidan Fugan Granule on The Intestinal Function of Children with Recurrent Respiratory Tract Infection and Immunosuppressive Mice*, Beijing University of Traditional Chinese Medicine, 2016.

[20] S. J. Hosseini-Vashan, A. Golian, and A. Yaghobfar, "Growth, immune, antioxidant, and bone responses of heat stress-exposed broilers fed diets supplemented with tomato pomace," *International Journal of Biometerology*, vol. 60, no. 8, pp. 1183–1192, 2016.

[21] A. Kowalska, Z. Zakeś, A. K. Siwicki, B. Jankowska, S. Jarmołowicz, and K. Demska-Zakeś, "Impact of Diets with Different Proportions of Linseed and Sunflower Oils on the Growth, Liver Histology, Immunological and Chemical Blood Parameters, and Proximate Composition of Pikeperch Sander Lucioperca (L.)," *Fish Physiology and Biochemistry*, vol. 38, no. 2, pp. 375–388, 2012.

[22] L. Liu, D. He, S. Zhang, W. Wang, and D. Fangling, "Effects of peanut peptides on immune function of mice," *Journal of the Chinese Cereals and Oils Association*, vol. 26, no. 1, pp. 79–82, 2011.

[23] O. Kornienko, D. R. Schaefer, S. D. Pressman, and D. A. Granger, "Associations between secretory immunoglobulin a and social network structure," *International Journal of Behavioral Medicine*, pp. 1–13, 2018.

[24] T. Zhang, J. Chen, C. Wang, W. Shi, and D. Li, "The therapeutic effect of Yinhuangerchen mixture on Avian infectious laryngotracheitis," *Poultry Science*, vol. 97, no. 8, pp. 2690–2697, 2018.

[25] G. P. Donaldson, M. S. Ladinsky, and K. B. Yu, "Gut microbiota utilize immunoglobulin A for mucosal colonization," *Science*, vol. 360, no. 6390SI, p. 795, 2018.

[26] Y. Zhang, K. Yu, H. Chen, Y. Su, and W. Zhu, "Caecal infusion of the short-chain fatty acid propionate affects the microbiota and expression of inflammatory cytokines in the colon in a fistula pig model," *Microbial Biotechnology*, vol. 11, no. 5, pp. 859–868, 2018.

[27] M. Sun, W. Wu, L. Chen et al., "Microbiota-derived short-chain fatty acids promote Th1 cell IL-10 production to maintain intestinal homeostasis," *Nature Communications*, vol. 9, no. 1, p. 3555, 2018.

[28] S. Ehrmann, J. Chastre, P. Diot, and Q. Lu, "Nebulized antibiotics in mechanically ventilated patients: a challenge for translational research from technology to clinical care," *Annals of Intensive Care*, vol. 7, no. 1, p. 78, 2017.

[29] A. E. Rajapaksa, J. J. Ho, A. Qi et al., "Effective pulmonary delivery of an aerosolized plasmid DNA vaccine via surface acoustic wave nebulization," *Respiratory Research*, vol. 15, no. 1, p. 60, 2014.